Ionization of helium in relativistic heavy-ion collisions

Inaugural-Dissertation
zur
Erlangung des Doktorgrades
der Naturwissenschaften
im Fachbereich 07
Fachrichtung Physik
der Justus-Liebig-Universität Gießen

vorgelegt von
Imre F. Barna
aus Budapest

Gießen, März 2002

D 26
Dekan: Prof. D. Albrecht Beutelspacher
I. Berichterstatter: Prof. Dr. Werner Scheid
II. Berichterstatter: Prof. Dr. Karl-Heinz Schartner
Tag der mündlichen Prüfung:

Contents

Chapter 1

Introduction

1.1 Motivation

Ionization of atoms and molecules is a fundamental process in nature. Ionization may happen through electron scattering, heavy ion collisions or electromagnetic wave interaction with matter. Ionization processes occur in the upper atmosphere, or in the sun corona and not at last in fusion-plasmas. Fusion research needs ionization cross sections for processes which can occur in plasmas e.g. highly charged ions enter the plasma from the wall as contamination.

The helium atom or two electron ions are the simplest systems, where the electron correlation plays an important role. A further experimental advantage of helium is its noble gas property.

The single-ionization by very fast, fully stripped projectile ions colliding with light atoms is well understood both theoretically [Inok71], [Inok78] and experimentally [Haug82]; for multiple ionization processes the level of knowledge is substantially lower. This is due to the fact that the electron-electron correlation can not be neglected. To handle the electron-electron correlation is still far from routine. The theory must go beyond the independent-electron model. The role of the wave function is essential as was shown in [Byr66].

In the following thesis we study collisions of heavy ions on helium with the coupled-channel method.

When a heavy ion (every charged particle which is equal or heavier than a proton will be called heavy ion in the following) collides with a helium atom the following processes in helium can happen:

- Excitation: one or both electrons 'jump' to a higher orbital, remaining bound to the nucleus.

- Single-ionization: one of the electrons becomes free and leaves the helium atom, the other electron remains bound.
- Double-ionization: both of the electrons become free and leave the helium atom.
- Single-transfer: one of the electrons leaves the proximity of the helium atom and is captured by the projectile, the other electron remains bound.
- Double-electron transfer: both bound electrons leave the helium atom and are captured by the projectile.

It is very important to classify the collisions in order to say which of the above mentioned process are important. There are three different cases: [Knu84]

- $$2\frac{Z_p}{v_p} < 0.1 \tag{1.1}$$

  (where v_p is the projectile velocity in atomic units and Z_p is the projectile charge). This is the perturbative region, which means that the Born approximation (or the lowest order perturbation theory) is valid to describe the process properly. In this case the projectile is a fast particle, and no electron transfer happens. (The cross section for transfer can be seven(!) orders of magnitude lower than the ionization cross sections [Ber92a].)
  The field of the projectile ion is so strong that the bound electron-electron interaction is negligible:

- $$0.1 \leq 2\frac{Z_p}{v_p} < 1. \tag{1.2}$$

  In the intermediate region, the projectile charge becomes higher and/or the velocity lower. The strength of the electron-electron interaction is comparable to the projectile-electron interaction. The results of the Born-approximation deviate from experimental data. The one-centre
  coupled-channel* calculation or other non-perturbative methods are needed to get acceptable results.

- $$2\frac{Z_p}{v_p} \geq 1 \tag{1.3}$$

*in the following 'coupled-channel' or 'close-coupling' means the same

In the strong interaction region, the field of the projectile exceeds the electron-electron interaction. When the impact-parameter b is in the magnitude of the atomic radius, $b \approx r_{Atom}$, than molecular orbitals can be formed. To describe this phenomena double-centre coupled-channel calculations must be used.

In the last two cases a further quantity is also needed to qualify whether electron transfer may occur or not. We define $\eta = \frac{2v_p}{v_e}$ where v_p is the velocity of the projectile, and v_e is the velocity of the bound electron. For slow collisions, $v_p \approx v_e$ and for small impact parameters $b \approx r_{atom}$ the capture process becomes relevant and the above mentioned two-centre calculation is needed. In our work we use only the one-centre model.

In the field of the ionization of helium in collisions with electrons or ions many experiments were done. Without completeness we mention some of them.
Electron-helium collision:
[Ada66], [Sch66], [Nag80], [Ste80] and some newer ones:
[Roes91], [Ull97], [Dor99], [Khe99]
Proton-helium collision:
[Knu84], [And86], [Sha85], [Ber99], [Mer97], [McG00]
Exotic projectiles such as antiproton on helium:
[And90], [And87], [Hve94], [Knu92]
Heavy ion-helium collisions:
[Hau81], [McG87] [Sha85], [Ber92a], [Ber92b], [Knu84].
We used the last four publications as experimental data for comparison with our calculations. There are several experimental publications on heavy-ion helium collisions, but only few of them contain total cross sections, sometimes only the double-to-single-ionisation ratio is measured e.g. [Heb90].

In the GSI in Darmstadt several experiments were done which are relevant for this study. The important ones are mentioned above. In the GSI not only total but differential cross sections can be measured. Nowadays the 'kinematically-complete' measurement is also available which gives further information about the outgoing electrons, all momentum components can be measured for both electrons. The method is called RIMS (Recoil-Ion-Momentum-Spectroscopy) [Mos94] where the ion beam crosses a supersonic 'cold' helium atom beam, ('cold' means that the temperature is about 10 mK). In this collision the out-coming particles are electrically and magnetically deflected and analyzed with a position sensitive Channel-Plate-Detector. With the help of the detected charge all the momentum components of the fragments can be derived from the time-of-flight.

There are monographs on ion-atom collisions including ionization. Now I will list some of them without completeness. At first I should mention [Bra83] 'The Brandsen Book' which is not the newest one but gives a overview on the atomic collision

theory. A newer one is [Bra92] from the same author, which concentrates on two centre coupled-channel calculations for charge transfer, 'simple' ionization is also discussed. The [McG97] gives methods and ideas used in atomic-collision theory. [Jan84] is the book which describes the physics of highly charged ions, different processes are described, not only ionization. All the books mentioned above are theoretical works with no respect to experimental methods. The book of [Stol97] Stolterfolth gives a small overview of the experimental methods and problems as well. The monograph of Lin [Lin93] gives an overview of fundamental processes in atoms and ions, new ideas methods and out-looks are presented. An example is the chaotic behavior of the atomic electrons in external electric and magnetic fields. The 'Relativistic Atomic Collisions' [Eich90] from Eichler concentrates on the fully relativistic description and uses the Dirac rather than the Schrödinger equation to describe the bound electrons. Ionization, electron-transfer, pair production and different recombination processes are also discussed.

In our further study we apply the one-center coupled-channel and the first order Born approximation models to calculate total cross sections for different heavy ion helium collisions. We concentrate much more on the coupled-channel description because we investigate systems where the projectile field is in the intermediate or in the strong interaction region.

Different studies were done to describe excitation, ionization or electron transfer with the help of different coupled-channel models. We mention some of them without completeness.
The stopping powers for intermediate-energy light ions penetrating atomic H and He targets were calculated with the coupled-channel model by [Sch90].
The hyper-spherical wave function was used in a coupled-channel calculation by [Mor91] to describe double-electron-excitation processes in the few MeV/amu projectile energy range.
For double-excitation there is a study from [Fri89] which uses the one-center atomic-orbital expansion in the coupled-channel model.
Ionization and electron-transfer were calculated by [Gra89] with a Gaussian basis set for the low energy He-He collision system.
In the first work of [Hil90] the low energy proton helium collision system was studied with Gaussian basis. Ionization and electron transfer cross sections were calculated in the 5-200 keV energy range.
In later works of [Hil94] or [Hil95] the $He^+ + He$ collision problem was examined with three active electrons. Ionization, excitation and electron transfer were calculated in the 3-1000 keV energy range. Gaussian orbitals were used as basis.
A newer coupled-channel study was done by [Bus96] for the $H^- - H^-$ collision system.
For heavier systems (Z=2-8) [Tos94] made two-center coupled-channel calculations

in the energy range 1 to 400 keV with Gaussian type orbitals. Ionization and transfer were calculated.
The two-coupled channel plane wave Born approximation was used by [Tir97] to calculate proton and antiproton on helium in the incident energy range of about 50 keV-20 MeV.
Ford and Reading [For94] used the Forced-Impulse Method (FIM), which is also a coupled-channel method and made many calculations for low energy proton helium and antiproton helium collision systems. The results agree well with the experimental data.
Slater wave functions were used as basis in the works of [Pfe96] and [Pfe99] to describe single- and double-ionization of helium in relativistic heavy ion collisions. All the above mentioned works approximate the continuum states with bound state wave functions.

As we know, there is only one coupled-channel calculation study for ionization of helium colliding with heavy ions (heavier than alpha particles) for energies higher than 5 MeV/amu.[Pfe99].

Our study is a further development of the last mentioned works [Pfe96] and [Pfe99]. We implemented the one-centre coupled-channel method and calculated the single- and double-ionization in various helium heavy-ion collision systems.

We describe the continuum states with Coulomb wave packages. The states created with the help of wave packages have a better physical interpretation as ionized states than the states approximated only with bound state functions. These new states have much larger spatial range and much more nodes than the states without packages. Coulomb wave functions in the continuum are characteristically much more complicated than bound state wave functions like Slater wave functions, which raises new problems.

The following work is divided into six larger chapters. The second one is a short overview of different theoretical methods, such as, the coupled-channel method, the Born Approximation, the forced-impulse and CTMC theories. The theory of coupled-channels will be discussed in details. In the third chapter the structure of the helium atom will be studied. The used basis and the calculated structure will also be presented. The fourth chapter presents the ionization calculations, and the technical details including different interaction operators. Our results will be presented and discussed in the fifth chapter. The whole study closes with a summary and outlook. A German summary ‘Zusammenfassung‘ is also given. The work ends with the bibliography and acknowledgements.

1.2 Units

In the whole study atomic units (a.u.) will be used. It means that the Planck's constant divided by two pi, the electron mass and the electron charge are equal to unity

$$\hbar = 1, \quad m_{\text{electron}} = 1, \quad e = 1, \quad 4\pi\epsilon_0 = 1. \tag{1.4}$$

With the help of this substitution the equations and the calculation become more transparent. The Schrödinger equation will lose all the electron masses and the $\hbar$s.

Using these three fundamental constants, every physical dimension can be expressed [Bet57]. The speed of light in this system is: $c \approx 137.036$ a.u.

At last I mention some useful conversion formulas which will be used below:

- to get the projectile velocity in a.u. when the collision energy is given in MeV: $v[a.u.] = 6.35\sqrt{E[MeV]/A}$ where A is the number of the nucleons. This is a non-relativistic formula.
- to get the relativistic gamma factor from collision energy given in MeV [Eic90]: $\gamma_p = 1 + E[MeV/A]/931.494$,
- to get the cross section in cm^2 instead of a.u.: $\sigma[cm^{-16}] = \sigma[a.u.] * 0.53^2$

Chapter 2

Theories for excitation and ionization

The ionization or excitation of helium atoms in heavy-ion collisions can be examined with different theoretical methods. The description can be quantum mechanical or even fully classical. In this chapter we mention four different models. The coupled-channel and the first order perturbation theory was used by us, and the CTMC and the forced-impulse methods were used by other authors to describe the same collision systems. This gives a good chance to test the validity of the different models. The discrepancies from experimental values are also discussed in the fifth chapter.

There are other theoretical models that we cannot present here, e.g.: Eikonal-Distorted-Wave- Born-Approximation (EDWBA) or Glauber-Approximation which can be found in [Hof93], [Ull94a], and in [Knu84]. The Magnus or (sudden) approximation is used in [Eic77]. The simplest model for ionization is the Independent Particle Model (IPM) which assumes that the electrons move independently. With this assumption the double ionization is traced back to a single electron problem. More on IPM can be found in [Knu84], [McG82].

2.1 Theory of coupled-channels

For a scattering system where the velocities of the bound electrons are much lower than the velocity of light, the Schrödinger equation is valid. We describe the electrons quantum mechanically and the projectile classically. The projectile is a classical point charge, without internal structure, moving on a straight line, which is the semi-classical approximation. The corresponding projectile-electron interaction is the classical time-dependent Liénard-Wiechert potential. To solve this

time-dependent Hamiltonian we make an expansion of the wave function with time dependent coefficients. This leads to the coupled-channel equations for the coefficients as will be shown later.

Contrary to this model when the projectile is for example an electron or a proton and the whole system can be described fully quantum mechanically, than the time independent close-coupling method which is described elsewhere, e.g. [Das97] can be applied.

Let's start now with the time dependent Schrödinger equation:

$$i\frac{\partial}{\partial t}\Psi(\vec{r}_1,\vec{r}_2,t) = (\hat{H}_{He}(\vec{r}_1,\vec{r}_2) + \hat{V}(\vec{r}_1,\vec{r}_2,\vec{p}_1,\vec{p}_2,t,b))\Psi(\vec{r}_1,\vec{r}_2,t) \tag{2.1}$$

where the $\hat{H}_{He}(\vec{r}_1,\vec{r}_2)$ is the operator of unperturbed helium atom, which will be specified in the next chapter. The $\hat{V}(\vec{r}_1,\vec{r}_2,\vec{p}_1,\vec{p}_2,t,b)$ is the time-dependent interaction between the target electrons and the projectile. In our case this is the so called Liénard-Wiechert potential. The term will be given in a more explicit form in Chapter 4.

The whole Hamiltonian is the following:

$$\begin{aligned}\hat{H}(\vec{r}_1,\vec{r}_2,\vec{p}_1,\vec{p}_2,t,b) = &\frac{(\vec{p}_1+\vec{A}(\vec{r}_1,t,b))^2}{2} + \frac{(\vec{p}_2+\vec{A}(\vec{r}_2,t,b))^2}{2} \\ &-\frac{2}{r_1} - \frac{2}{r_2} + \frac{1}{r_{12}} - \phi(\vec{r}_1,t,b) - \phi(\vec{r}_2,t,b).\end{aligned} \tag{2.2}$$

The first two terms contain the kinetic energy of the electrons and the vector potential of the projectile, the next three terms are the electron-target nucleon and the electron-electron interactions, and the last two are the time-dependent scalar potentials induced by the moving projectile. The whole form of the time dependent interaction will be shown later. The wave function can be expanded in terms of eigenstates of the $\hat{H}_{He}$, satisfying the stationary Schrödinger equation:

$$\hat{H}_{He}(\vec{r}_1,\vec{r}_2)\Phi_j(\vec{r}_1,\vec{r}_2) = E_j\Phi_j(\vec{r}_1,\vec{r}_2) \tag{2.3}$$

The solution of this equation (diagonalization) and all the related questions will be analyzed in the next chapter.
To solve the time-dependent equation the following ansatz is made:

$$\Psi(\vec{r}_1,\vec{r}_2,t) = \sum_{j=1}^{N} a_j(t)\Phi_j(\vec{r}_1,\vec{r}_2)e^{-iE_jt} \tag{2.4}$$

Our wave function $\Phi_j(\vec{r}_1,\vec{r}_2)$ is a configuration-interaction (CI) wave function which is a sum of properly symmetrized products of two single-electron orbitals. For single-electron orbitals we use Slater functions and regular Coulomb wave packages. The

concrete form will be shown in chapter 3.
The $a_j(t)$ are the so-called expansion coefficients. These are essential to get the total cross sections. Inserting this ansatz into the time-dependent Schrödinger equation (2.1) leads to:

$$i \cdot \sum_{j=1}^{N} \dot{a}_j(t)\Phi_j(\vec{r}_1,\vec{r}_2)e^{-iE_jt} + \sum_{j=1}^{N} a_j(t)\Phi_j(\vec{r}_1,\vec{r}_2)E_je^{-iE_jt} =$$
$$(\hat{H}_{He}(\vec{r}_1,\vec{r}_2) + \hat{V}(\vec{r}_1,\vec{r}_2,\vec{p}_1,\vec{p}_2,t,b)) \sum_{j=1}^{N} a_j(t)\Phi_j(\vec{r}_1,\vec{r}_2)e^{-iE_jt}. \tag{2.5}$$

With the help of the eigenvalue equation (2.3) we get the form:

$$i\sum_{j=1}^{N} \dot{a}_j(t)\Phi_j(\vec{r}_1,\vec{r}_2)e^{-iE_jt} = \sum_{j=1}^{N} \hat{V}(\vec{r}_1,\vec{r}_2,\vec{p}_1,\vec{p}_2,t,b)a_j(t)\Phi_j(\vec{r}_1,\vec{r}_2)e^{-iE_jt} \tag{2.6}$$

We multiply this equation from left with $\Phi_k^*(\vec{r}_1,\vec{r}_2)e^{iE_kt}$ to reach a system of first-order differential equations for the expansion coefficients $a_k(t)$:

$$i\sum_{j=1}^{N} \dot{a}_j(t)e^{i(E_k-E_j)t} \int_{\vec{r}_1}\int_{\vec{r}_2} \Phi_k^*(\vec{r}_1,\vec{r}_2)\Phi_j(\vec{r}_1,\vec{r}_2)d^3r_1d^3r_2 =$$
$$\sum_{j=1}^{N} a_j(t)e^{i(E_k-E_j)t} \int_{\vec{r}_1}\int_{\vec{r}_2} \Phi_k^*(\vec{r}_1,\vec{r}_2)\hat{V}(\vec{r}_1,\vec{r}_2,\vec{p}_1,\vec{p}_2,t,b)\Phi_j(\vec{r}_1,\vec{r}_2)d^3r_1d^3r_2. \tag{2.7}$$

With the help of

$$H_{kj}^{Int} = e^{i(E_k-E_j)t} \int_{\vec{r}_1}\int_{\vec{r}_2} \Phi_k^*(\vec{r}_1,\vec{r}_2)\hat{V}(\vec{r}_1,\vec{r}_2,\vec{p}_1,\vec{p}_2,t,b)\Phi_j(\vec{r}_1,\vec{r}_2)d^3r_1d^3r_2 \tag{2.8}$$

which is the coupling matrix (Int means interaction), we get the final form for the coupled-channel equations:

$$i \cdot \dot{a}_k(t) = \sum_{j=1}^{N} H_{kj}^{Int} \cdot a_j(t) \quad (k = 1, ..., N) \tag{2.9}$$

This is a differential equation system of first order, hence the vectorial notation can also be used:

$$\dot{\vec{a}}(t) = \frac{1}{i}\left(H_{kj}^{Int}\right) \cdot \vec{a}(t) \qquad (k = 1....N) \tag{2.10}$$

where $\vec{a}(t)$ forms a vector.

In practical calculations it is better to pull out the oscillating factor $e^{i(E_k-E_j)t}$ from the matrix elements. Let's define:

$$\tilde{a}_k(t) = a_k(t)e^{-iE_kt} \tag{2.11}$$

and

$$\tilde{H}^{Int}_{kj} = H^{Int}_{kj}e^{-i(E_k-E_j)t} \tag{2.12}$$

With these quantities the coupled-channel equations have a slightly different form:

$$i \cdot \dot{\tilde{a}}_k(t) = \sum_{j=1}^{N} \left(\tilde{H}^{Int}_{kj} + \delta_{kj}E_k \right) \tilde{a}_j(t) \tag{2.13}$$

This form is quicker to solve and enhances the accuracy of the calculations. To solve this equation system we need the following initial condition:

$$\tilde{a}_k\left(t \to -\infty\right) = \begin{cases} 1 \cdot e^{i\phi} & k = 1 \\ 0 & k \neq 1 \end{cases} \tag{2.14}$$

(ϕ is an arbitrary phase factor). This means that long before the collision only one state is populated, the helium atom is in the unperturbed (1^1S) ground-state ($k = 1$). The above condition can be slightly modified to simulate realistic ion sources where metastable states could also exist. In this cases some double excited states, e.g. (2s2s) are also populated.

The transformation (2.12) helps us to interpolate the coupling matrix without the oscillating energy factor. This coupling matrix has a simple decaying behavior in time and is easy to interpolate in contrast to the energy factor which is analytic and no problem to evaluate to any time point. This calculation trick helps us to save some time consuming integrals and to enhance the numerical accuracy. The practical solution of the coupled-channel equations will be discussed in Chapter 4. To solve the coupled-channel equations we use a five point Runge-Kutta-Fehlberg-Method.

The transition probabilities are the absolute squares of the coefficients at infinity:

$$P_k(b, t \to \infty) = \mid a_k(t \to \infty) \mid^2 \tag{2.15}$$

The coefficients have no explicit impact parameter dependence they depend on the impact parameter only through the coupling matrix. For a given channel the total cross section reads:

$$\sigma_k = 2\pi \int_0^\infty bP_k(b, t \to \infty)db. \tag{2.16}$$

This method is the so called "Impact Parameter-Method" and can be found in [Bra83]. The total cross section for single- or double-ionization is the sum of all the corresponding channels. The number and the properties of the channels used will be also discussed later on.

2.1.1 Conservation of the norm

The interpretation of the $|a_j(t)|^2$ as a population probability for the state j has only sense when the sum of all $|a_j(t)|^2$ is unity for any time during the collision, otherwise the norm conservation is violated. Let's calculate the time derivative of the coefficients:

$$\frac{d}{dt}[\vec{a}^+(t)\vec{a}(t)] = \left[\frac{d}{dt}\vec{a}^+(t)\right]\vec{a}(t) + \vec{a}^+(t)\left[\frac{d}{dt}\vec{a}(t)\right] = \left[\frac{d}{dt}\vec{a}(t)\right]^+ \cdot \vec{a}(t) + \vec{a}^+(t) \cdot \left[\frac{d}{dt}\vec{a}(t)\right], \tag{2.17}$$

where + means complex conjugation, the usage of (2.1) leads to:

$$\frac{d}{dt}[\vec{a}^+(t)\vec{a}(t)] = \left[-i\left(H_{kj}^{Int}\vec{a}(t)\right)\right]^+\vec{a}(t) + \vec{a}^+(t)\left[-i\left(H_{kj}^{Int}\vec{a}(t)\right)\right] = i\vec{a}^+(t)\left(H_{kj}^{Int}\right)^+\vec{a}(t) - i\vec{a}^+(t)\left(H_{kj}^{Int}\right)\vec{a}(t). \tag{2.18}$$

Now we prove that the coupling matrix H_{kj}^{Int} is hermitian. The energy of the whole collision system is a real measurable quantity hence it is hermitian. The unperturbed helium Hamiltonian is hermitian, the energy eigenvalues are real. Now the remaining coupling matrix also has to be hermitian $(H_{kj}^{Int})^+ = (H_{kj}^{Int})$. Using all this information gives

$$\frac{d}{dt}\left[\vec{a}^+(t)\vec{a}(t)\right] = 0 \tag{2.19}$$

or:

$$\sum_{j=1}^{N}\vec{a}^+(t)\vec{a}(t) = \text{const} \tag{2.20}$$

This criterion must be fulfilled during the whole collision. In our numerical calculations this quantity is continously observed, the norm conservation is always fulfilled better than 10^{-5}.

2.2 The Born Approximation

When the projectile-electron interaction is much larger than the electron-electron interaction in the target then the Born approximation is valid as was shown before. We apply this model parallel with the coupled-channel model to compare them and check their range of validity. The general Born approximation method has been described in detail elsewhere e.g. [McG97]. In the following we sketch the first-order calculations only. The transition amplitude for the electrons being ionized reads

$$a^{(1)} = -i \int_{-\infty}^{+\infty} dt e^{i(E_f - E_i)t} \langle \Phi_f | V(\vec{r}_1, \vec{r}_2, \vec{p}_1, \vec{p}_2, t, b) | \Phi_i \rangle, \tag{2.21}$$

where $|\Phi_i\rangle$, E_i and $\langle \Phi_f|$, E_f are the initial and the final states and energies respectively. The interaction operator is the same as for the coupled-channel model was. To evaluate the cross section for a channel the usual impact parameter integration (2.16) is needed. The single- or double-ionization cross section is a simple sum of all the corresponding channels.

For the description of the initial and final wave functions exist plenty of ways. Without the claim of completeness we mention some of them:

- For the initial wave function one can use correlated Hylleraas-type wave functions [Spi99]. These are wave functions which depend on the difference of the two electron coordinates, hence automatically include electron-electron correlation.
- For the final states $2C$ or $3C$ wave functions can be used. The $2C$ function consists of two incoming Coulomb waves and the $3C$ function contains a Coulomb distortion factor for the electron-electron repulsion. This wave function can be found in [Spi99] also.
- A new but complicated way to approximate the final state is the so called Φ_2 function. This function is a generalization of the ${}_1F_1(a, b; c; z)$ function for two variables and includes correlations obviously [Col98].

These kind of wave functions, in principle, can be used in our coupled-channel calculations as well. The only problem is how to build wave packages from the $2C$, $3C$ and Φ_2 functions to incorporate to a finite basis.

Our Born calculations are 'simplified' coupled-channel calculations which means that we use only the first row of the coupled-channel matrix. The coupled-channel

equations are given once again:

$$\frac{da_k(t)}{dt} = -i\sum_{j=1}^{N} V_{kj} e^{i(E_k - E_j)t} a_j(t) \qquad (k = 1....N), \tag{2.22}$$

where V_{kj} is the coupling matrix. When $N = 1$, no sum is considered. Then we have the 'normal' perturbation theory and the time integration can be formally written as in (2.21).

Our initial wave function (from its internal CI property) contains also ionized electron configurations that would not be needed. This configuration mixing is negligible.

The usage of the perturbation theory is a good help to find out the significant channels contributing to the cross section. Then we use the relevant channels in the coupled-channel calculation.

2.3 The Forced-Impulse Method (FIM)

J. F. Reading and A. L. Ford developed an *ab initio* method which is also a kind of coupled-channel calculation and includes the electron-electron correlation in an exact manner. The FIM method divides the collision time into sequential short segments. The electron-electron interaction is neglected and only the projectile-electron interaction acts. At the end of each segment the system is projected to fully correlated states which are the initial state of the next time segment. With this method a large number of states can be examined and the correlation can be fully included. With the help of this method more than a thousand channels can be included in a calculation. The above mentioned group has been developing their code more than a decade and angular correlated wave functions are already used. The physical idea and the mathematical details of the method are underlined in [Rea87]. As we know the method was predominately used to understand low energy proton helium and low energy antiproton helium collisions. A review article is [Knu92].

2.4 Classical Trajectory Monte Carlo (CTMC)

There is a completely different way to study ion-atom collisions purely classically. This method is the **C**lassical **T**rajectory **M**onte **C**arlo (CTMC) theory. The method is based on the solution of the classical Hamiltonian equations of motion for the four-body system which includes the incident ion, target nucleus and the two electrons initially bound to the target nucleus. The equations are solved for a variety of sets

of initial conditions, including impact parameters, relative velocities of projectile to target, and positions and momenta of electrons. For each set of initial conditions, the classical trajectories of the nuclei are calculated from a large internuclear separation to the distance of closest approach and out again to large internuclear separations. After each simulation the energies of the electrons are taken to decide weather ionization has occurred. For a good statistical distribution defining the cross sections more than ten thousand trajectories have to be calculated.

One of the basic dilemmas of any classical calculations is that it is impossible to correctly describe the bound initial two electron ground state. Different sophisticated conditions are needed to prevent the collapse of the helium atom as well as to impose the Heisenberg uncertainty principle. The angle between the two electron coordinate vectors has to remain 180° during the whole process; otherwise the atom falls apart without any outer perturbation. As we know more than two electron atoms or ions can not be hold together even in the ground state. A uniformly random number generator is essential [Hof93]. The theory itself can be learnt from the early works of Olson [Ols77] or [Ols78].

Chapter 3

The structure of the helium atom

3.1 The helium Hamiltonian

Before we begin the coupled-channel calculation the unperturbed helium Hamiltonian has to be diagonalized to get the spectrum and the wave functions. In this chapter we show how this procedure can be done. The main problem is now to solve the following eigenvalue equation (only the spatial part is presented, the spin comes later on):

$$H_{He}\Phi(\vec{r}_1, \vec{r}_2) = E\Phi(\vec{r}_1, \vec{r}_2) \tag{3.1}$$

where H_{He} is the non-relativistic, spin independent helium Hamiltonian, $\Phi(\vec{r}_1, \vec{r}_2)$ is the two-particle spatial wave function, and E is the energy of the whole system. The Hamiltonian H_{He} has the following form:

$$H_{He} = -\frac{1}{2\mu}\Delta_1 - \frac{1}{2\mu}\Delta_2 - \frac{1}{M}\vec{\nabla}_1\vec{\nabla}_2 - \frac{2}{r_1} - \frac{2}{r_2} + \frac{1}{r_{12}} \tag{3.2}$$

The first two terms are the kinetic energy operators of the two electrons, μ is the reduced mass of the electron with respect to the mass of the nucleus M.

$$\mu = \frac{m \cdot M}{m + M} \tag{3.3}$$

The third term with the two gradient operator stands for the mass-polarization. The precise derivation of this term can be found in [Bra83]. The next two terms are the electron-nucleon Coulomb interactions and the last is the electron-electron one. The figure (3.1) helps to understand the coordinates.

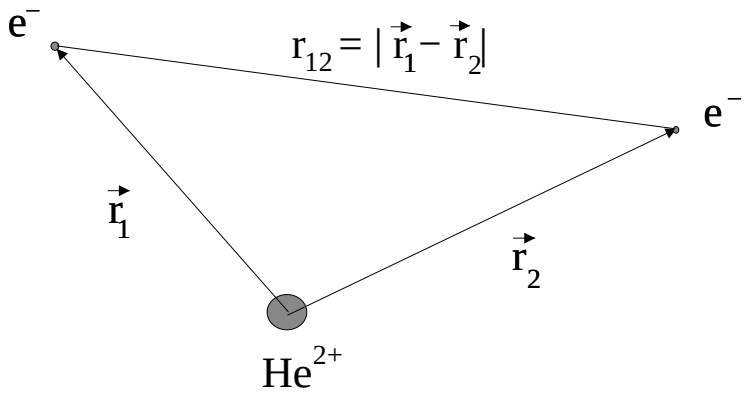

Figure 3.1: The schematic figure of the helium atom

The mass M is about 7300 larger then the mass of the electron. Due to this the electron mass can be used in the first two terms instead of the reduced mass. The mass polarization term can be neglected. The eigenvalue equation reads as follows:

$$\left[-\frac{1}{2m}\Delta_1 - \frac{1}{2m}\Delta_2 - \frac{2}{r_1} - \frac{2}{r_2} + \frac{1}{r_{12}}\right]\Phi(\vec{r}_1,\vec{r}_2) = E\Phi(\vec{r}_1,\vec{r}_2) \tag{3.4}$$

Having exchanged the two electrons the solution of the eigenvalue equation must not change. Let's introduce the electron exchange operator $\hat{P}_{12}$ in the following manner:

$$\Phi(\vec{r}_1,\vec{r}_2) = \hat{P}_{12}\Phi(\vec{r}_2,\vec{r}_1) \tag{3.5}$$

Now try to solve the eigenvalue equation of the previous operator.

$$\lambda\Phi(\vec{r}_2,\vec{r}_1) = \hat{P}_{12}\Phi(\vec{r}_2,\vec{r}_1) \tag{3.6}$$

Let's act the operator once again

$$\hat{P}_{12}\hat{P}_{12}\Phi(\vec{r}_1,\vec{r}_2) = \lambda\hat{P}_{12}\Phi(\vec{r}_1,\vec{r}_2) = \lambda^2\Phi(\vec{r}_1,\vec{r}_2) = \Phi(\vec{r}_1,\vec{r}_2). \tag{3.7}$$

The solution is now obvious:

$$\lambda^2 = 1 \Rightarrow \lambda = \pm 1 \Rightarrow \Phi(\vec{r}_2,\vec{r}_1) = \pm\Phi(\vec{r}_1,\vec{r}_2) \tag{3.8}$$

The states with positive sign are the symmetric (or para-) states and the states with minus sign are the anti-symmetric (or ortho-) states with respect to the spatial wave function. The spin dependence of the Hamiltonian is neglected. The spin-orbit interaction and the spin-spin interaction contributes very little to the energy of the helium bound states.

Now let's discuss the question of the spin. Up to the two electron system the total wave function can be separated into two independent parts, the spin part $\chi(1,2)$ and the spatial part $\Phi(\vec{r}_1, \vec{r}_2)$:

$$\Psi(1,2) = \Phi(\vec{r}_1, \vec{r}_2) \cdot \chi(1,2) \tag{3.9}$$

The complete wave function has to be anti-symmetric due to the Pauli principle. This conditions can be satisfied in two ways:

- The spatial part is symmetric, and the spin-dependent part is anti-symmetric. This can be realized with a single spin function. Therefore it is called 'spin-singlet' state.
- The spatial part is anti-symmetric, and the spin-dependent part is symmetric. This can be achieved with three different spin functions that is why it is called 'spin-triplet' state.

A detailed description can be found e.g. in [Bra83] in Chapter 6.

When the helium Hamiltonian does not contain any spin-dependent operators, no transition between the singlet and triplet states can happen. We calculate both the singlet and the triplet spectrum but in the following only the singlet spectrum will be used and examined. We neglect the singlet-triplet transitions in our collision calculations. These transitions contribute only a little to the cross sections in light systems.

3.2 The wave function

We expand the helium eigenstates $\Phi_j(\vec{r}_1, \vec{r}_2)$ in terms of linear independent two-particle basis functions f_μ

$$\Phi_j(\vec{r}_1, \vec{r}_2) = \sum_\mu b_\mu^{[j]} f_\mu(\vec{r}_1, \vec{r}_2) \tag{3.10}$$

This is the configuration interaction (CI) approximation. Here

$$f(\vec{r}_1, \vec{r}_2) = N(\phi_1(\vec{r}_1)\phi_2(\vec{r}_2) \pm \phi_2(\vec{r}_1)\phi_1(\vec{r}_2)) \tag{3.11}$$

is a normalized, symmetrized or anti-symmetrized product of two single-particle wave functions. The positive sign stands for singlet states and the negative for triplet states. To describe the bound part of the spectrum we use Slater-type functions and regular Coulomb wave packages for the continuum states

The one-particle functions are not orthogonal to each other. There is a finite overlap between different Slater-Slater and Slater-Coulomb wave packet functions. Due to this the normalization constant is not the well known $N = \frac{1}{\sqrt{2}}$ but

$$N = \frac{1}{\sqrt{2 \pm 2 \cdot \langle \phi_1(\vec{r}_1) | \phi_2(\vec{r}_2) \rangle^2}}. \tag{3.12}$$

In practical calculations the factor N can be neglected because the total CI wave function has to be normalized to one and our diagonalization procedure ensures it automatically.

3.2.1 Slater functions

The complete form of the Slater function is

$$S_{n,l,m,\kappa}(\vec{r}) = c(n,\kappa) r^{n-1} e^{-\kappa r} Y_{l,m}(\theta, \varphi), \tag{3.13}$$

where $c(n,\kappa)$ is the normalization constant:

$$c(n,\kappa) = \frac{(2\kappa)^{n+1/2}}{\sqrt{(2n)!}}. \tag{3.14}$$

The n, l, m are the principal, azimuthal, and magnetic quantum numbers respectively. The κ is the screening factor, (which is rather a parameter and not a real quantum number). Typical κ values lie between $0.14 - 3.25$. Large screening factors mean more localized orbitals than the smaller screening factors. To describe bound states, Gauss functions can be also used, as in quantum chemistry or in earlier works (in this field) of Busic [Bus96], Hildenbrand [Hil94], and Gramlich [Gra89]. Gauss functions have the advantage that the electron-electron interaction matrix elements can be analytically calculated. In electron transfer processes [Bus96], translation factors appear and in this case the Gauss functions have a further advantage, since the matrix elements can be done analytically.

3.2.2 Coulomb wave package

For the ionized states regular Coulomb wave packages* will be used:

*From now on the different expressions 'Coulomb wave functions', 'Coulomb package', or simply 'package' or 'packet' will be used to avoid continuous repetition; they all mean the same.

$$C_{k,l,m,\tilde{Z}}(\vec{r}) = q(k,\Delta k) \int_{k^2/2-\Delta_k^2/4}^{k^2/2+\Delta_k^2/4} F_{l,\tilde{Z}}(k,r) k dk Y_{l,m}(\theta,\varphi), \tag{3.15}$$

where $q(k,\Delta k)$ is the normalization constant

$$q(k,\Delta k) = \frac{2}{\sqrt{\Delta k \cdot \tilde{k}}} \tag{3.16}$$

Δk stands for the width of the package and $\tilde{k} = (k + (k + \Delta k))/2$ is the mean value of the package.

The regular Coulomb function is $F_{l,\tilde{Z}}(k,r)$ where $\tilde{Z}$ is the effective charge of the particle. The spherical harmonic $Y_{l,m}(\theta,\varphi)$ provides for proper angular dependence.

The integration over the Coulomb function $F_{l,\tilde{Z}}(k,r)$ is needed, to have discrete number of wave functions in the continuum, and in this way it can be incorporated into our finite basis. The regular Coulomb wave function is used (instead of the irregular ones) because it has no singularity at the origin and matrix elements can be calculated easily. It can be shown [Abr70] that the radial Coulomb wave function is real.

The properties of the Coulomb wave function can be found in different books e.g. [Abr70], [Lan68]. The well known 'Dirac delta normalization' of the Coulomb function is not suitable for a finite basis-set calculation, that is why the packets are constructed. A package wave function created in the energy interval $[E_k - \Delta E_k/2 : E_k + \Delta E_k/2]$ is orthogonal to all the other packages which lie outside this energy interval. When two different packages have an overlapping energy range, then the corresponding overlap matrix element is also not zero. With a clever selection of the energy ranges this is avoidable.

The radial Coulomb wave function reads

$$\begin{aligned} F_{l,\tilde{Z}}(k,r) = \; & \sqrt{\tfrac{2k}{\pi}} e^{\frac{\pi\tilde{Z}}{2k}} \tfrac{(2kr)^l}{(2l+1)!} e^{-ikr} \mid \Gamma(l+1-i\tilde{Z}/k) \mid \times \\ & {}_1F_1(1+l+i\tilde{Z}/k, 2l+2, 2ikr) \end{aligned} \tag{3.17}$$

Here, Γ is the Gamma function, and ${}_1F_1$ is the confluent hyper-geometric function with complex argument [Abr70]. The Coulomb wave function has an oscillating behavior. The above mentioned additional k integration produces an extra 'bumpy-like' character. To give a qualitative explanation for this behavior let us consider the following integral:

$$\int_{k'}^{k'+\Delta k'} \cos(kr) dk = \frac{\sin((k'+\Delta k')r) - \sin(k'r)}{r}. \tag{3.18}$$

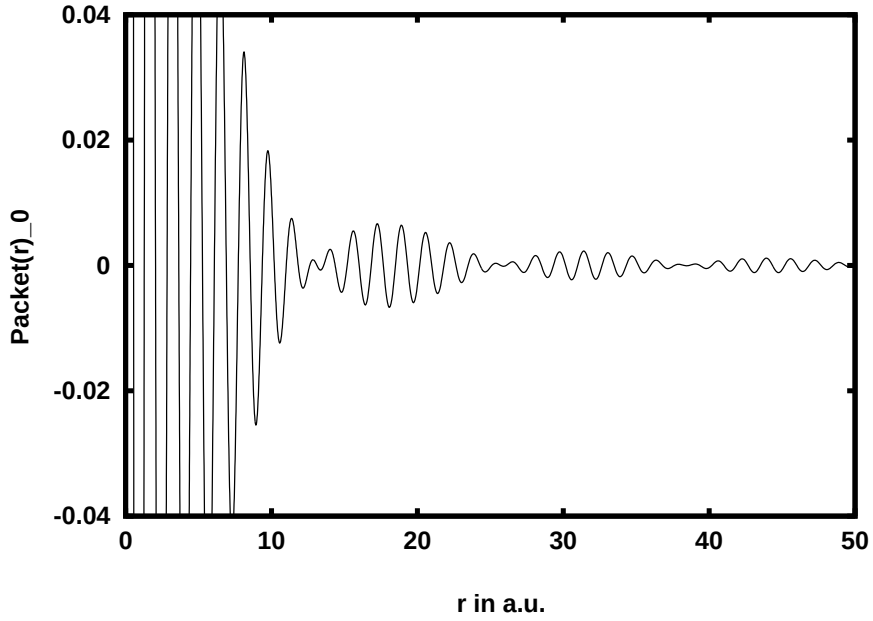

Figure 3.2: A Coulomb wave package with the parameter set:
$l = 0$, $\tilde{Z} = 2$, $k = 3.5\, a.u.$ and $\Delta k = 0.5$ a.u.

We may say that the oscillation of the Coulomb wave function comes from its sine or cosine dependence, if we integrate it on a small finite interval than we get two waves with slightly different frequencies. The 'bumpy-like' character is simply the interference between this two frequencies.

A nice packet is visualized in figure 3.2. The quick oscillations come from the energy of the package $\rho = kr$ and the 'bumpy-like' oscillations comes from the integration. The visualized package has a relative high energy $k = 3.5$ a.u. In our later basis we will use packages with lower energy, because the soft electrons give the predominant contributions to the ionization cross section.

In our code we calculate and tabulate the packages up to distances of 300 or 400 a.u. and save them in tables. Later spline or polynomial interpolation is used to get their value at any position. The packages are normalized to unity with an accuracy better than 99,3 percent.

The whole diagonalization process has three different kind of parameters; the Slater functions have the screening factors κ and the Coulomb packets the values of $\tilde{Z}$ which is the effective charge; the width of the Coulomb packet Δk is also a parameter. The screening factors have to be optimized, to have accurate bound states. Two different kind of Coulomb wave packets are used; the first is with $\tilde{Z} = 1$ for the single-ionized

states, and $\tilde{Z} = 2$ when both of the electrons are ionized. The packages with $\tilde{Z} = 2$ show quicker oscillations than the ones with $\tilde{Z} = 1$; due to this feature all the corresponding matrix elements are smaller. $\tilde{Z}$, the effective charge can be different from one or two, but it does not make much difference. We would rather operate with the width and the number of packages in our basis to create favorable states. This two kind of wave packets ($\tilde{Z} = 1, 2$) are not orthogonal, and give a contribution to the overlap matrix element which can not be neglected. The major difference between the s, p, d Coulomb wave functions (or packages) is at in the origin. All the three packages in Fig 3.3 have the same parameters $\tilde{Z} = 2, k = 0, \Delta k = 0.5$. The s packet starts linearly from a non-zero value, the p packet starts linearly from the origin and the d packet starts quadratically from the origin, as one can recognize from Fig 3.3.

This characteristics makes it possible to calculate the electron-electron interaction matrix element at the origin with the help of the multiple series.

To evaluate the energy integral (to get a package) we used a simple Romberg integration. To calculate the Coulomb wave function we used different approaches ($\rho = kr$,$\eta = \frac{\tilde{Z}}{k}$) :
-**Small arguments ($\rho \leq 2$):** We used the well-known series expansion from [Abr70], (formulas: [14.1.3-14.1.7])

$$F_l(\eta, \rho) = C_l(\eta)\rho^{l+1}\Phi_l(\eta, \rho), \tag{3.19}$$

where the normalization constant contains a complex gamma function:

$$C_l(\eta) = \frac{2^l e^{-\pi\eta/2}|\Gamma(l + 1 + i\eta)|}{\Gamma(2l + 2)}. \tag{3.20}$$

For $\Phi_l(\eta, \rho)$ exists a convergent sum:

$$\Phi_l(\eta, \rho) = \sum_{k=l+1}^{\infty} A_k^l(\eta)\rho^{k-l-1} \tag{3.21}$$

and for the coefficients the following recursion relation:

$$(k + l)(k - l + 1)A_k^l = 2\eta A_{k-1}^l - A_{k-2}^l \quad (k > l + 2), \tag{3.22}$$

where the first two values are

$$A_{l+1}^l = 1, \quad A_{l+2}^l = \frac{\eta}{l + 1}. \tag{3.23}$$

-**Larger arguments**($\rho > 2$) An expansion in terms of Bessel functions [Abr70][14.4.1] was used:

$$F_l(\eta, \rho) = C_l(\eta)\frac{(2l + 1)!}{(2\eta)^{2l+1}}\rho^{-l} \cdot \sum_{k=2l+1}^{\infty} b_k t^{k/2} I_k(2\sqrt{t}), \tag{3.24}$$

where $t = 2\eta\rho$ and $\eta > 0$. The recurrence relation for b_k is

$$4\eta^2(k-2l)b_{k+1} + kb_{k-1} + b_{k-2} = 0 \quad (k > 2l+2) \tag{3.25}$$

with $b_{2l+1} = 0, b_{2l+2} = 0$.

-**for the d functions** the recurrence relation [Abr70][14.2.3] was applied

$$l[(l+1)^2+\eta^2]^{-1/2}F_{l+1}(\eta,\rho) = (2l+1)\left[\eta + \frac{l(l+1)}{\rho}\right]F_l(\eta,\rho) - (l+1)[l^2+\eta^2]^{-1/2}F_{l-1}(\eta,\rho) \tag{3.26}$$

-**For large asymptotic r values** the asymptotic [Bet57][3.32] formula was taken

$$F_{l,r\to\infty} = \frac{c(k)}{\sqrt{2\tilde{Z}r}} I_{2l+1}(\sqrt{8\tilde{Z}r}) \tag{3.27}$$

where $c(k)$ is a constant. The matching points were optimized by hand.

The wave function is tabulated up to some hundred a.u. Later, interpolation formulas are used to get the approximate value between two tabulated points. For small r ($r <$ first tabulated value of the wave function), a 4-point interpolation polynomial is used, otherwise a linear combination of sine and cosine functions.

3.3 Matrix elements

To solve the eigenvalue problem of the helium, the matrix elements have to be calculated first. Different integrals arise, due to the different properties of the Slater functions and Coulomb wave packets. We use different effective charges $\tilde{Z} = 1$ and $\tilde{Z} = 2$ to make a better approximation for the single and double continuum states. This causes more matrix elements, because the wave packets with different charges are not orthogonal anymore. To distinguish between the Slater and the Coulomb packet functions, let us use the following notation: $S_{n,l,m,\kappa}$ for Slater functions and $C_{k,l,m,\tilde{Z}}$ for Coulomb packages. The quantities which have to be calculated are:

- the overlap integrals:

$$\begin{aligned} &\langle S_{n_1,l_1,m_1,\kappa_1}(\vec{r})|S_{n_2,l_2,m_2,\kappa_2}(\vec{r})\rangle \\ &\langle S_{n,l_1,m_1,\kappa}(\vec{r})|C_{k,l_2,m_2,\tilde{Z}}(\vec{r})\rangle \\ &\langle C_{k_1,l_1,m_1,\tilde{Z}_1}(\vec{r})|C_{k_2,l_2,m_2,\tilde{Z}_2}(\vec{r})\rangle \end{aligned} \tag{3.28}$$

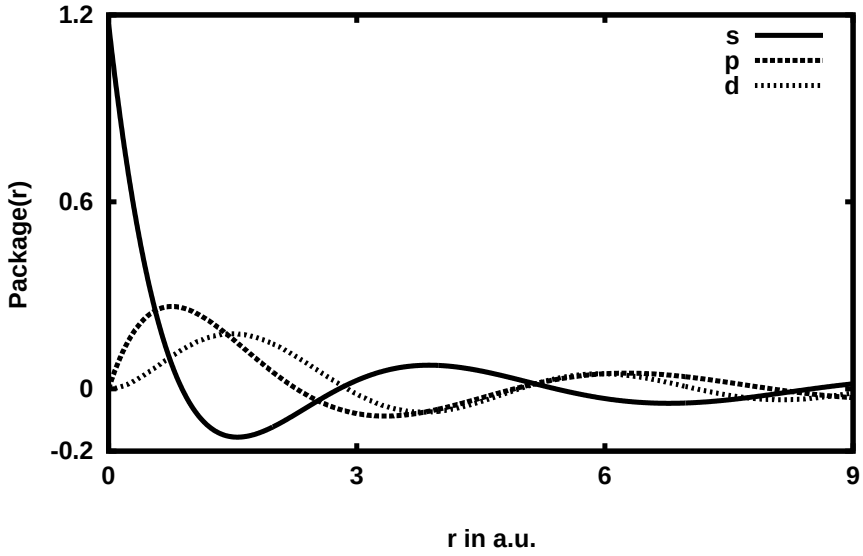

Figure 3.3: Radial wave functions in the origin

- the potential energy:

$$\begin{aligned}\langle S_{n_1,l_1,m_1,\kappa_1}(\vec{r})|-\frac{2}{r}|S_{n_2,l_2,m_2,\kappa_2}(\vec{r})\rangle\\ \langle S_{n,l_1,m_1,\kappa}(\vec{r})|-\frac{2}{r}|C_{k,l_2,m_2,\tilde{Z}}(\vec{r})\rangle\\ \langle C_{k_1,l_1,m_1,\tilde{Z}_1}(\vec{r})|-\frac{2}{r}|C_{k_2,l_2,m_2,\tilde{Z}_2}(\vec{r})\rangle\end{aligned} \tag{3.29}$$

- the kinetic energy:

$$\begin{aligned}\langle S_{n_1,l_1,m_1,\kappa_1}(\vec{r})|-\frac{1}{2}\Delta|S_{n_2,l_2,m_2,\kappa_2}(\vec{r})\rangle\\ \langle S_{n,l_1,m_1,\kappa}(\vec{r})|-\frac{1}{2}\Delta|C_{k,l_2,m_2,\tilde{Z}}(\vec{r})\rangle\\ \langle C_{k_1,l_1,m_1,\tilde{Z}_1}(\vec{r})|-\frac{1}{2}\Delta|C_{k_2,l_2,m_2,\tilde{Z}_2}(\vec{r})\rangle\end{aligned} \tag{3.30}$$

- the electron-electron interaction:

$$\langle S_{n_1,l_1,m_1,\kappa_1}(\vec{r}_1)S_{n_3,l_3,m_3,\kappa_3}(\vec{r}_2)|\frac{1}{r_{12}}|S_{n_2,l_2,m_2,\kappa_2}(\vec{r}_1)S_{n_4,l_4,m_4,\kappa_4}(\vec{r}_2)\rangle$$
$$\langle S_{n_1,l_1,m_1,\kappa_1}(\vec{r}_1)S_{n_3,l_3,m_3,\kappa_3}(\vec{r}_2)|\frac{1}{r_{12}}|S_{n_2,l_2,m_2,\kappa_2}(\vec{r}_1)C_{k_4,l_4,m_4,\tilde{Z}_4}(\vec{r}_2)\rangle$$
$$\langle S_{n_1,l_1,m_1,\kappa_1}(\vec{r}_1)C_{k_3,l_3,m_3,\tilde{Z}_3}(\vec{r}_2)|\frac{1}{r_{12}}|S_{n_2,l_2,m_2,\kappa_2}(\vec{r}_1)C_{k_4,l_4,m_4,\tilde{Z}_4}(\vec{r}_2)\rangle$$
$$\langle C_{k_1,l_1,m_1,\tilde{Z}_1}(\vec{r}_1)C_{k_3,l_3,m_3,\tilde{Z}_3}(\vec{r}_2)|\frac{1}{r_{12}}|S_{n_2,l_2,m_2,\kappa_2}(\vec{r}_1)S_{n_4,l_4,m_4,\kappa_4}(\vec{r}_2)\rangle$$
$$\langle C_{k_1,l_1,m_1,\tilde{Z}_1}(\vec{r}_1)C_{k_3,l_3,m_3,\tilde{Z}_3}(\vec{r}_2)|\frac{1}{r_{12}}|C_{k_2,l_2,m_2,\tilde{Z}_2}(\vec{r}_1)S_{n_4,l_4,m_4,\kappa_4}(\vec{r}_2)\rangle$$
$$\langle C_{k_1,l_1,m_1,\tilde{Z}_1}(\vec{r}_1)C_{k_3,l_3,m_3,\tilde{Z}_3}(\vec{r}_2)|\frac{1}{r_{12}}|C_{k_2,l_2,m_2,\tilde{Z}_2}(\vec{r}_1)C_{k_4,l_4,m_4,\tilde{Z}_4}(\vec{r}_2)\rangle \quad (3.31)$$

3.3.1 The overlap

We start with the simplest case, the Slater-Slater overlap:

$$\langle S_{n_1,l_1,m_1,\kappa_1}|S_{n_2,l_2,m_2,\kappa_2}\rangle = \int_{\vec{r}} S^*_{n_1,l_1,m_1,\kappa_1}(\vec{r})S_{n_2,l_2,m_2,\kappa_2}(\vec{r})d^3r =$$
$$c(n_1,\kappa_1)c(n_2,\kappa_2)\int_0^\infty r^{n_1+n_2-2}e^{-(\kappa_1+\kappa_2)r}r^2dr \times$$
$$\int_\theta\int_\varphi Y^*_{l_1,m_1}(\theta,\varphi)Y_{l_2,m_2}(\theta,\varphi)\sin(\theta)d\theta d\varphi. \quad (3.32)$$

The integration of the spherical harmonics $Y_{l,m}(\theta,\varphi)$ will not be written down in the following because it is analytic (and always the same):

$$\int_0^{2\pi}\int_0^{\pi} Y^*_{l_1,m_1}(\theta,\varphi)Y_{l_2,m_2}(\theta,\varphi)\sin(\theta)d\theta d\varphi = \delta_{l_1,l_2}\cdot\delta_{m_1,m_2}. \quad (3.33)$$

The radial part is the well-known Borel integral:

$$\int_0^\infty r^{n_1+n_2}e^{-(\kappa_1+\kappa_2)r}dr = \frac{(n_1+n_2)!}{(\kappa_1+\kappa_2)^{n_1+n_2+1}}. \quad (3.34)$$

The whole matrix element is at last:

$$\langle S_{n_1,l_1,m_1,\kappa_1}|S_{n_2,l_2,m_2,\kappa_2}\rangle = \delta_{l_1,l_2}\cdot\delta_{m_1,m_2}\cdot c(n_1,\kappa_1)\cdot c(n_2,\kappa_2)\cdot\frac{(n_1+n_2)!}{(\kappa_1+\kappa_2)^{n_1+n_2+1}} \quad (3.35)$$

When all the quantum numbers n_1, l_1, m_1, κ_1 are equal with n_2, l_2, m_2, κ_2, the overlap gives one.

The Slater-packet overlap:

$$\langle S_{n,l_1,m_1,\kappa}(\vec{r}_1)|C_{k,l_2,m_2,\tilde{Z}}(\vec{r}_2)\rangle = \int_{\vec{r}} S^*_{n,l_1,m_1,\kappa}(\vec{r})C_{k,l_2,m_2,\tilde{Z}}(\vec{r})d^3r =$$

$$c(n,\kappa)\cdot q(k,\Delta k)\cdot\delta_{l_1,l_2}\cdot\delta_{m_1,m_2}\cdot\int_0^\infty r^{n-1}e^{-\kappa r}\cdot\int_k^{k+\Delta k}F_{l_2}(\tilde{Z}/k,kr)dkr^2dr \quad (3.36)$$

Plugging the Coulomb function into the equation (without the normalization constants and deltas) we get for the radial integral:

$$\langle S_{n,l_1,m_1,\kappa}(r)|C_{k,l_2,m_2,\tilde{Z}}(r)\rangle = \int_0^\infty r^{n-1}e^{-\kappa r}\cdot\int_k^{k+\Delta k}\sqrt{\frac{2k}{\pi}}e^{\frac{\pi\tilde{Z}}{2k}-ikr}\times$$

$$\frac{(2kr)^{l_2}}{(2l_2+1)!}\mid\Gamma(l_2+1-i\tilde{Z}/k)\mid{}_1F_1(1+l_2+i\tilde{Z}/k,2l_2+2,2ikr)dkr^2dr \quad (3.37)$$

Let us consider now only the right hand side of the equation and exchange the order of the integration, writing first the k integration and then the radial one:

$$\langle S_{n,l_1,m_1,\kappa}(r)|C_{k,l_2,m_2,\tilde{Z}}(r)\rangle = \int_k^{k+\Delta k}\sqrt{\frac{2k}{\pi}}e^{\frac{\pi\tilde{Z}}{2k}}\mid\Gamma(l_2+1-i\tilde{Z}/k)\mid\frac{(2k)^{l_2}}{(2l_2+1)!}dk\times$$

$$\int_0^\infty{}_1F_1(1+l_2+i\tilde{Z}/k,2l_2+2,2ikr)r^{l_2+n-1}e^{-\kappa r}e^{-ikr}r^2dr \quad (3.38)$$

The r integral has a closed form [Gra81][Volume 2, 7.621-4]:

$$R_{2l_2+1}(\kappa,k,\tilde{Z}/k,l_2) = \int_0^\infty{}_1F_1(1+l_2+i\tilde{Z}/k,2l_2+2,2ikr)r^{l_2+n-1}e^{-\kappa r}e^{-ikr}r^2dr =$$

$${}_2F_1\left(n+l_2+2,1+l_2+i\tilde{Z}/k;2l_2+2;\frac{2ik}{\kappa+ik}\right)\frac{(n+l_2+1)!}{(\kappa+ik)^{n+l_2+2}} \quad (3.39)$$

The definition of the hyper-geometric function ${}_2F_1$ is [Abr70][15.1.1] :

$$ {}_2F_1(a,b;c;z) \;=\; \sum_{n=0}^{\infty} \frac{(a)_n (b)_n}{(c)_n} \frac{z^n}{n!} \;=\; \frac{\Gamma(c)}{\Gamma(a)\Gamma(b)} \sum_{n=0}^{\infty} \frac{\Gamma(a+n)\Gamma(b+n)}{\Gamma(c+n)} \frac{z^n}{n!} \tag{3.40} $$

It is clear that ${}_2F_1(a,b;c;z) = {}_2F_1(b,a;c;z)$ is symmetric in the first two variables. In our equation the variables a and c are integer numbers.

- If $a = c$, it means: $n = l_2$. Using [Abr70][15.1.8] we find:

$$ F(a,b;b;z) = (1-z)^{-a}. \tag{3.41} $$

  So the radial integral has the final form:

$$ R_{2l_2+1}(k) = \frac{(2l_2+1)!}{(\kappa+ik)^{2l_2+2}} \frac{1}{(1-2ik/(\kappa+ik))^{1+l_2+i\tilde{Z}/k}} \equiv \frac{(2l_2+1)!}{(\kappa+ik)^{l_2+1-i\tilde{Z}/k}} \frac{1}{(\kappa-ik)^{1+l_2+i\tilde{Z}/k}} \tag{3.42} $$

- if $n > l_2$, let us introduce $q = n - l_2$;

$$ R_{n+l_2-1}(k) = \int_0^{\infty} r^{\overbrace{n-l_2}^{=q}} \quad r \quad {}^{2l_2-1} e^{-\kappa r} e^{-ikr} \cdot {}_2F_1(...) r^2 dr = (-\quad 1 \quad)^q \frac{\partial}{\partial \kappa^q} R_{2l_2+1} \tag{3.43} $$

  To understand the formula above: when $n > l$, we may derive the I_{2l_2+1} integral with respect to κ to pull down an extra r monomial dependence. The expression is even true after the use of [Abr70][15.1.8]:

$$ R_{n+l_2-1}(k) \equiv (-1)^q (2l+1) \frac{\partial^q}{\partial \kappa^q} \left\{ \frac{1}{(\kappa+ik)^{(l_2+1-i\tilde{Z}/k)}} \frac{1}{(\kappa-ik)^{(l_2+1+i\tilde{Z}/k)}} \right\}. \tag{3.44} $$

  With complete induction the following formula can be proved:

$$ R_{n+l_2+1}(k) = \frac{(2l_2+1)!}{(\kappa^2+k^2)^{l_2+1}} \frac{1}{(\kappa-ik)^{n-l}} \sum_{s=0}^{n-l} \binom{n-l_2}{s} \left(\frac{\kappa-ik}{\kappa+ik} \right)^{s-i\tilde{Z}/k} \times P_s(l_2+1-i\tilde{Z}/k) \cdot P_{n-l_2-s}(l_2+1+i\tilde{Z}/k) \tag{3.45} $$

  where the Pochammer symbols are defined through the following relation:

$$ P_k(a) = \begin{cases} 1 & \text{for} \quad k=0 \\ a(a+1)\cdots(a+k-1) \quad = \dfrac{\Gamma(a+k)}{\Gamma(a)} & (\text{for } k \neq 0) \end{cases}. \tag{3.46} $$

- For the case $n < l_2$ no formula exists, because l_1 is always smaller than l_2 the angular integral is already zero.

At last the complete matrix element is:

$$\langle S_{n,l_1,m_1,\kappa}(\vec{r}_1)|C_{k,l_2,m_2,\tilde{Z}}(\vec{r}_2)\rangle = c(n,\kappa)\cdot q(k,\Delta k)\cdot \delta_{l_1,l_2}\times$$
$$\delta_{m_1,m_2}\cdot \int_k^{k+\Delta k} R_{2l_2+1}(k)\sqrt{\frac{2k}{\pi}}e^{\frac{\pi\tilde{Z}}{2k}}\mid \Gamma(l_2+1-i\tilde{Z}/k)\mid dk \tag{3.47}$$

To evaluate the remaining k integral we use the Romberg algorithm, as explained above.
The package-package overlap:

$$\langle C_{k_1,l_1,m_1,\tilde{Z}_1}(\vec{r})|C_{k_2,l_2,m_2,\tilde{Z}_2}(\vec{r})\rangle \tag{3.48}$$

If the $\tilde{Z}$ values are the same and the k intervals are different than there is no overlap. The wave packages are orthogonal to each other. (Numerically, there is an overlap $\approx 10^{-5}$; this is a further check for the accuracy of the calculation.) If the effective charges are different, there exists a small finite overlap. This was calculated straight numerically. A practical way to get satisfactory accuracy is the following: search for the first zero of the two package wave functions, choose the lower one, integrate from zero up to this value, then add this distance up as long as convergence is achieved.
A last remark on this matrix element:
Calculations neglecting the overlap between packages with a different effective nuclear charge $\tilde{Z}$ can push the ground state slightly lower than the experimental value. This contradicts the variational principle and is wrong.

3.3.2 The potential energy

The Slater-Slater case:

$$\langle S_{n_1,l_1,m_1,\kappa_1}|-\frac{Z_t}{r}|S_{n_2,l_2,m_2,\kappa_2}\rangle = -Z_t\int_{\vec{r}} S^*_{n_1,l_1,m_1,\kappa_!}(\vec{r})\frac{1}{r}S_{n_2,l_2,m_2,\kappa_2}(\vec{r})d^3r =$$
$$\delta_{l_1,l_2}\cdot\delta_{m_1,m_2}\cdot c(n_1,\kappa_1)\cdot c(n_2,\kappa_2)\cdot\frac{(n_1+n_2-1)!}{(\kappa_1+\kappa_2)^{n_1+n_2}} \tag{3.49}$$

The only difference between the overlap and the potential energy matrix elements is in the r dependence of the exponent. Instead of the former $r^{n_1+n_2-2}$ now we have an $r^{n_1+n_2-3}$ because there is an extra r in the denominator.

The Slater-packet case:
The method is the same as for the overlap: the only difference is: $q = n - l - 1$ because the $1/r$ potential lowers the exponent with the principle quantum number by one.

The packet-packet case:
The radial integral can be calculated only numerically with the method mentioned at the discussion of the overlap.

3.3.3 The kinetic energy

The Slater-Slater case:
To calculate this matrix element we need the Laplace operator in spherical coordinates:

$$\Delta = \frac{1}{r^2}\frac{\partial}{\partial r}\left(r^2\frac{\partial}{\partial r}\right) + \frac{1}{r^2\sin(\theta)}\frac{\partial}{\partial\theta}\left(\sin(\theta)\frac{\partial}{\partial\theta}\right) + \frac{1}{r^2\sin^2(\theta)}\frac{\partial^2}{\partial\varphi^2} = \frac{1}{r^2}\frac{\partial}{\partial r}\left(r^2\frac{\partial}{\partial r}\right) + \frac{1}{r^2}\hat{W} \tag{3.50}$$

where $\hat{W}$ is the angular part. The solution of its eigenvalue problem is well known:

$$\hat{W}Y_{l_2,m_2}(\theta,\varphi) = -l_2(l_2+1)Y_{l_2,m_2}(\theta,\varphi). \tag{3.51}$$

Let the radial part act on the Slater function:

$$\frac{1}{r^2}\frac{\partial}{\partial r}\left(r^2\frac{\partial}{\partial r}(r^{n2-1}e^{-\kappa_2 r})\right) = \left[n_2(n_2-1) - 2r\kappa_2 n_2 + r^2\kappa_2^2\right]\cdot r^{n_2-3}\cdot e^{-\kappa_2 r}. \tag{3.52}$$

Using all this formulas, the final form reads:

$$\langle S_{n_1,l_1,m_1,\kappa_1}| -\frac{1}{2}\Delta|S_{n_2,l_2,m_2,\kappa_2}\rangle = \delta_{l_1,l_2}\cdot\delta_{m_1,m_2}\cdot c(n_1,\kappa_1)\cdot c(n_2,\kappa_2)\times \left[\frac{1}{2}(l_2(l_2+1) - n_2(n_2-1))\frac{(n_1+n_2-2)!}{(\kappa_1+\kappa_2)^{n_1+n_2-1}} + \kappa_2 n_2\frac{(n_1+n_2-1)!}{(\kappa_1+\kappa_2)^{n_1+n_2}} - \frac{1}{2}\kappa_2^2\frac{(n_1+n_2)!}{(\kappa_1+\kappa_2)^{n_1+n_2+1}}\right] \tag{3.53}$$

The other two kinds of matrix elements are calculated with the help of the single-particle Schrödinger equation. Applying the kinetic energy operator plus the potential energy operator to the wave function gives the wave function multiplied with the corresponding energy. This is equivalent to saying that the sum of the

overlap and the potential matrix element is equal with the kinetic energy. With this trick no derivation of package wave function is needed.

We also tried a numerical derivation of the wave package but we showed that this method is unstable and may affect spurious sharp peaks. The detailed derivation will be shown for the package-package case only.

The Slater-package case
In this simple case we need to add the potential and the overlap matrix elements together The potential matrix element has to be multiplied by the charge of the corresponding wave package.

$$\begin{aligned} \langle S_{n,l_1,m_1,\kappa}(\vec{r})| -\frac{1}{2}\Delta|C_{k,l_2,m_2,\tilde{Z}}(\vec{r})\rangle &= \\ \delta_{l_1,l_2}\cdot\delta_{m_1,m_2}\cdot\left(\tilde{Z}\cdot\langle S_{n,l_1,m_1,\kappa}(\vec{r})|\frac{1}{r}|C_{k,l_2,m_2,\tilde{Z}}(\vec{r})\rangle\right. &+ \left.\frac{1}{4}\delta_{E_1,E_2}(E_1+E_2)\right) \end{aligned} \quad (3.54)$$

The package-package case
The single-particle radial Schrödinger equation with a wave package reads:

$$\left(-\frac{1}{2}\nabla^2-\frac{\tilde{Z}}{r}\right)q(k,\Delta k)\int F_l(\tilde{Z}/k,kr)kdk = Eq(k,\Delta k)\int F_l(\tilde{Z}/k,kr)kdk \quad (3.55)$$

We use ∇^2 instead of Δ from now on to avoid misunderstanding. $F_l(\tilde{Z}/k,kr)$ means now the radial Coulomb wave. The package has the average energy E. The angular part can be treated separately as usual and attracts no attention. Let us construct the mean value of the previous equation with another wave package with different parameters:

$$\begin{aligned} q(k_1,\Delta k_1)\cdot q(k_2,\Delta k_2)\int_0^\infty\left(\int_{k_1}^{k_1+\Delta k_1}F_{l_1}(\tilde{Z}_1/k_1,rk_1)k_1dk_1\left(-\frac{1}{2}\nabla^2-\frac{\tilde{Z}_2}{r}\right)\times\right. \\ \left.\int_{k_2}^{k_2+\Delta k_2}F_{l_2}(\tilde{Z}_2/k_2,rk_2)k_2dk_2\right)r^2dr = q(k_1,\Delta k_1)\cdot q(k_2,\Delta k_2)\times \\ \int_0^\infty\left(\int_{k_1}^{k_1+\Delta k_1}F_{l_1}(\tilde{Z}_1/k_1,rk_1)k_1dk_1\cdot\int_{k_2}^{k_2+\Delta k_2}E_2F_{l_2}(\tilde{Z}_2/k_2,rk_2)k_2dk_2\right)r^2dr \end{aligned} \quad (3.56)$$

Let us use the well known relation: $E_2 = k_2^2/2$ and put the potential energy term on the right hand side of the equation. To make the equation more transparent ignore the normalization constants for a while on both sides. The radial part of the kinetic

energy matrix element is:

$$\int_0^\infty \left(\int_{k_1}^{k_1+\Delta k_1} F_{l_1}(\tilde{Z}_1/k_1, rk_1) k_1 dk_1 \left(-\frac{1}{2}\nabla^2\right) \int_{k_2}^{k_2+\Delta k_2} F_{l_2}(\tilde{Z}_2/k_2, rk_2) k_2 dk_2 \right) r^2 dr =$$
$$\int_0^\infty \left(\int_{k_1}^{k_1+\Delta k_1} F_{l_1}(\tilde{Z}_1/k_1, rk_1) k_1 dk_1 \left(\frac{\tilde{Z}_2}{r}\right) \int_{k_2}^{k_2+\Delta k_2} F_{l_2}(\tilde{Z}_2/k_2, rk_2) \cdot k_2 dk_2 \right) r^2 dr +$$
$$\int_0^\infty \left(\int_{k_1}^{k_1+\Delta k_1} F_{l_1}(\tilde{Z}_1/k_1, rk_1) k_1 dk_1 \int_{k_2}^{k_2+\Delta k_2} F_{l_2}(\tilde{Z}_2/k_2, rk_2) \cdot \frac{k_2^2}{2} \cdot k_2 \cdot dk_2 \right) r^2 dr \qquad (3.57)$$

The first part is simply the potential energy matrix element mentioned above, multiplied with the effective charge of the corresponding package. We concentrate now on the second part: Insert $q(k, \Delta k) = 1/\sqrt{\Delta k \cdot \tilde{k}}$ into the last equation

$$\frac{1}{\sqrt{\Delta k_1 \cdot \tilde{k}_1}} \frac{1}{\sqrt{\Delta k_2 \cdot \tilde{k}_2}} \int k_1 dk_1 \int \frac{k_2^3}{2} dk_2 \underbrace{\int F_{l_1}(\tilde{Z}/k_1, rk_1) F_{l_2}(\tilde{Z}/k_2, rk_2) r^2 dr}_{=\delta(E_2 - E_1)} \qquad (3.58)$$

The Coulomb wave functions are orthogonal to each other and normalized to the delta function in energy. By using some identities the Dirac delta function has another equivalent form:

$$\delta(E_2 - E_1) \equiv \delta\left(\frac{k_2^2}{2} - \frac{k_1^2}{2}\right) = 2\delta((k_2 - k_1)(k_2 + k_1)) = \frac{\delta(k_2 - k_1)}{k_2} \qquad (3.59)$$

One of the two k integrations with the Dirac delta results $k_1 = k_2$. If we insert $\tilde{k} = (k + (k + \Delta k))/2$ then the normalization constant cancels two terms namely $\Delta k = k_b - k_a$ and $\tilde{k} = (k_a + k_b)/2$. After some algebraic manipulation we get:

$$\frac{1}{\Delta k \cdot \tilde{k}} \int_{k_a}^{k_b} \frac{k^3}{2} dk = \frac{1}{\Delta k \cdot \tilde{k}} \frac{(k_b^4 - k_a^4)}{8} = \frac{1}{2}\left(\frac{k_a^2 + k_b^2}{2}\right) \qquad (3.60)$$

The kinetic energy matrix element reads after all:

$$\langle C_{k_1,l_1,m_1,\tilde{Z}_1}(\vec{r})| -\frac{1}{2}\nabla^2 |C_{k_2,l_2,m_2,\tilde{Z}_2}(\vec{r})\rangle =$$
$$\delta_{l_1,l_2} \cdot \delta_{m_1,m_2} \left(\tilde{Z}_2 \cdot \langle C_{k_1,l_1,m_1,\tilde{Z}_1}(\vec{r})| \frac{1}{r} |C_{k_2,l_2,m_2,\tilde{Z}_2}(\vec{r}) + \frac{1}{4}\delta_{E_a,E_b}(E_a + E_b) \right) \qquad (3.61)$$

3.3.4 The electron-electron interaction

The electron-electron interaction is represented by a two particle matrix element which means double-fold integration over $\vec{r}_1$ and $\vec{r}_2$. Only six different combinations of the functions exist, all the other combination can be lead back to one of them using a cyclic permutation of the order of the wave functions. The six different kinds of integrals are given (3.31). Now we show how the matrix element can be calculated using a multipole expansion. In the following we outline the calculation, for the purely Slater case. The quantum numbers are n, l, m, κ and for the wave package case $k, l, m, \tilde{Z}$. The electron-electron interaction matrix element with our general wave functions reads:

$$I_{ee} \equiv \langle \phi_{\binom{n_1}{k_1},l_1,m_1,\binom{\kappa_1}{\tilde{Z}_1}}(\vec{r}_1)\phi_{\binom{n_3}{k_3},l_3,m_3,\binom{\kappa_3}{\tilde{Z}_1}}(\vec{r}_2)|\frac{1}{r_{12}}|\phi_{\binom{n_2}{k_2},l_2,m_2,\binom{\kappa_2}{\tilde{Z}_2}}(\vec{r}_1)\phi_{\binom{n_4}{k_4},l_4,m_4,\binom{\kappa_4}{\tilde{Z}_4}}(\vec{r}_2)\rangle \tag{3.62}$$

Let us use now the well-known multipole expansion for the electron-electron interaction:

$$\frac{1}{|\vec{r}_1 - \vec{r}_2|} = \sum_{l=0}^{\infty} \frac{1}{r_>}\left(\frac{r_<}{r_>}\right)^l P_l(cos\theta_{12}) = \sum_{l=0}^{\infty} \frac{4\pi}{2l+1}\frac{r_<^l}{r_>^{l+1}} \sum_{m=-l}^{l} Y^*_{l,m}(\theta_1,\varphi_1)Y_{l,m}(\theta_2,\varphi_2) \tag{3.63}$$

where

$$r_< = \begin{cases} r_1 & \text{for} \quad r_1 \le r_2 \\ r_2 & \text{for} \quad r_2 < r_1 \end{cases} \quad \text{and} \quad r_> = \begin{cases} r_1 & \text{for} \quad r_1 \ge r_2 \\ r_2 & \text{for} \quad r_2 > r_1 \end{cases} \tag{3.64}$$

Using this formula the matrix element reads:

$$\begin{aligned} I_{ee} = N_{1,2,3,4} \cdot \sum_{l=0}^{\infty} \frac{4\pi}{2l+1} \times \\ \sum_{m=-l}^{l} \int_{\Omega_1} Y^*_{l,m}(\theta_1,\varphi_1)Y^*_{l_1,m_1}(\theta_1,\varphi_1)Y_{l_2,m_2}(\theta_1,\varphi_1)d\Omega_1 \times \\ \int_{\Omega_2} Y_{l,m}(\theta_2,\varphi_2)Y^*_{l_3,m_3}(\theta_2,\varphi_2)Y_{l_4,m_4}(\theta_2,\varphi_2)d\Omega_2 \times \\ \int_{r_1}\int_{r_2} \frac{r_<^l}{r_>^{l+1}}\phi_1(r_1)\phi_3(r_2)\phi_2(r_1)\phi_4(r_2)r_1^2 r_2^2 dr_1 dr_2. \end{aligned} \tag{3.65}$$

To avoid confusions it is useful to introduce the shorthand notation $N_{1,2,3,4}$ which stands for the product of all the normalization constants. The angular momentum integrals, for example,

$$c_{l,l_3,l_4}^{m,m_3,m_4} \equiv \int\limits_{\Omega_2} Y_{l,m}(\theta_2,\phi_2) Y^*_{l_3,m_3}(\theta_2,\phi_2) Y_{l_4,m_4}(\theta_2,\phi_2) d\Omega_2 \tag{3.66}$$

can be evaluated with the help of the Wigner 3j symbols. The last row of (3.65) is the radial part of the integral giving most of the work:

$$W_l \equiv \int\limits_{r_1}\int\limits_{r_2} \frac{r_<^l}{r_>^{l+1}} \phi_1(r_1)\phi_3(r_2)\phi_2(r_1)\phi_4(r_2) r_1^2 r_2^2 dr_1 dr_2. \tag{3.67}$$

At first we analyze the angular integrals. The properties of the Wigner 3j symbols can be found in different books e.g. [Edm63] or [Cov81].

$$c_{l,l_3,l_4}^{m,m_3,m_4} = (-1)^{m_3}\sqrt{\frac{(2l+1)(2l_3+1)(2l_4+1)}{4\pi}} \underbrace{\begin{pmatrix} l & l_3 & l_4 \\ 0 & 0 & 0 \end{pmatrix}\begin{pmatrix} l & l_3 & l_4 \\ m & -m_3 & m_4 \end{pmatrix}}_{\text{Wigner 3j symbols}} \tag{3.68}$$

The Wigner 3j symbols are defined through the Clebsch-Gordan-coefficients. In our case:

$$\begin{pmatrix} l & l_3 & l_4 \\ 0 & 0 & 0 \end{pmatrix} = (-1)^{l-l_3}\cdot(2l_4+1)^{-\frac{1}{2}}\cdot \underbrace{(l,0,l_3,0|l_4,0)}_{\text{Clebsch- Gordan-coefficient}} \tag{3.69}$$

and for the second part:

$$\begin{pmatrix} l & l_3 & l_4 \\ m & -m_3 & m_4 \end{pmatrix} = (-1)^{l-l_3-m_4}\cdot(2l_4+1)^{-\frac{1}{2}}\cdot \underbrace{(l,m,l_3,-m_3|l_4,-m_4)}_{\text{Clebsch-Gordan-coefficient}} \tag{3.70}$$

Now the c coefficient reads:

$$c_{l,l_3,l_4}^{m,m_3,m_4} = (-1)^{m_3-m_4}\cdot\frac{1}{2l_4+1}\cdot\sqrt{\frac{(2l+1)(2l_3+1)(2l_4+1)}{4\pi}}\times (l,0,l_3,0|l_4,0)\cdot(l,m,l_3,-m_3|l_4,-m_4). \tag{3.71}$$

The Clebsch-Gordan coefficients are needed when we want to couple two single-particle wave functions with angular momentum $\vec{l_1}$ and $\vec{l_2}$ to a wave function with a total angular momentum $\vec{l} = \vec{l_1} + \vec{l_2}$.
Direct definitions for the 3-j symbols or for the Clebsch-Gordan coefficients are too

elaborate to mention here. These definitions can be found in the literature given above. The $c_{l,l_1,l_2}^{m,m_1,m_2} \cdot c_{l_3,l_4,l}^{m_3,m_4,m}$ coefficients have some important symmetry properties: it is always zero unless:

$$m = m_2 + m_1 \quad \text{and} \quad m = m_3 + m_4 \tag{3.72}$$

For the angular momentum, the triangular inequality is valid in any case:

$$|l_1 - l_2| \leq l \leq l_1 + l_2 \qquad |l_3 - l_4| \leq l \leq l_3 + l_4 \tag{3.73}$$

$|m| \leq l$ is trivially true for all angular momenta. For the parity it is true

$$\left.\begin{array}{ll} l + l_1 + l_2 & \text{even} \\ l + l_3 + l_4 & \text{even} \end{array}\right\} \Rightarrow l_1 + l_2 - l_3 - l_4 \quad \text{even} \tag{3.74}$$

In our work the maximal value of the total angular momentum of the helium wave function is $l = 2$, so the summation is not a long process.
At last let us analyze the remaining radial integral:

$$W_l \equiv \int_{r_1} \int_{r_2} \frac{r_<^l}{r_>^{l+1}} \phi_1(r_1)\phi_3(r_2)\phi_2(r_1)\phi_4(r_2) r_1^2 r_2^2 dr_1 dr_2 \tag{3.75}$$

If all four single-particle wave functions are Slater functions than the integral has a recursive solution. The detailed calculation can be found elsewhere [Pfe96]. In the following we present the starting formula of the calculation:

$$\begin{aligned} &W_l(n_1 + n_2, n_3 + n_4, \kappa_1 + \kappa_2, \kappa_3 + \kappa_4) = \\ &\int_0^\infty r_1^{n_1+n_2+l-2} e^{-(\kappa_1+\kappa_2)r_1} \int_{r_1}^\infty r_2^{n_3+n_4-l-3} e^{-(\kappa_3+\kappa_4)r_2} r_2^2 dr_2 r_1^2 dr_1 + \\ &\int_0^\infty r_1^{n_1+n_2-l-3} e^{-(\kappa_1+\kappa_2)r_1} \int_0^{r_1} r_2^{n_3+n_4+l-2} e^{-(\kappa_3+\kappa_4)r_2} r_2^2 dr_2 r_1^2 dr_1. \end{aligned} \tag{3.76}$$

For a more clear result some substitutions are needed:
$k_1 = n_1 + n_2$; $k_2 = n_3 + n_4$; $c_1 = \kappa_1 + \kappa_2$; $c_2 = \kappa_3 + \kappa_4$. Now briefly the result:

$$\begin{aligned} &W_l(k_1, k_2, c_1, c_2) = \\ &\frac{1}{c_2^{k_1+k_2+1}} \left(\frac{(k_2 - l - 1)! \cdot (k_1 + l)!}{\left(\frac{c_1}{c_2}\right)^{k_1+l+1}} - T_{k_1+k_2, k_2-l-1}\left(\frac{c_1}{c_2}\right) + T_{k_1+k_2, k_2+l}\left(\frac{c_1}{c_2}\right) \right) \end{aligned} \tag{3.77}$$

To evaluate the quantity T we need the starting expression:

$$T_{\mu,0}(c) = (\mu - 1)! \cdot \left(\frac{1}{c^\mu} - \frac{1}{(c+1)^\mu} \right) \tag{3.78}$$

where $\mu = k_1 + k_2 \quad c = c_1/c_2$ and the recurrence formula:

$$T_{\mu,s}(c) = s \cdot T_{\mu-1,s-1}(c) - \frac{(\mu-1)!}{(c+1)^\mu} \quad \text{for} \quad \mu > s \tag{3.79}$$

In all other cases when Coulomb wave packages enter, the double-fold radial integral can only be evaluated numerically. If the wave functions are Coulomb waves rather than wave packages further analytic manipulation would be possible as was shown before in the case of Slater-packet potential matrix element. In our code we have simply integrated the expressions numerically. The wave packages are tabulated and can be evaluated (with spline interpolation) at any r value. To evaluate this kind of integrals is not an easy task. We use the distance between $r_2 = 0$ and the r_2 value of the first zero of the package as a unit length for a 32-point Gauss integration routine. Then this length will be added to the r-value of the first zero and the integration will be repeated until the needed accuracy is achieved. When both wave functions are different packages with different oscillating behavior than the smaller first zero has to be taken. The product of the differently oscillating functions is an even more quickly oscillating function. We could not find faster way to solve this problem with high accuracy. Of course, the above mentioned algorithm has to be applied for both of the variables. This process is time consuming: calculation of a matrix element with 4 wave packages takes about 1-3 seconds even on a 300-600 MHz Pentium PC.

3.4 Diagonalization and densities

Having done the matrix element calculations, the complete Hamiltonian matrix has to be built up.

Only s, p and d single particle orbitals are included in the calculation. All the possible couplings of wave functions are done up to total angular momentum of $L = 2$ with the Clebsch-Gordon formalism. Here, the spin part of the wave function is separated, so the coupling was done only for the orbital momentum.

$$f_{l_1,l_2,L,M}(\vec{r}_1, \vec{r}_2) = \sum_{m_1=-l_1}^{l_1} \sum_{m_2=-l_2}^{l_2} C(l_1, l_2, m_1, m_2; L, M) f_{l_1,l_2,m_1,m_2}(\vec{r}_1, \vec{r}_2) \tag{3.80}$$

C are the Clebsch-Gordon (CG) vector coupling coefficients, and can be calculated with the help of the 3-j symbol [Cov81]. In atomic structure calculations the M must be equal with $m1 + m2$ which reduces the double sum to a single one.

$$f_{l_1,l_2,L,M}(\vec{r}_1,\vec{r}_2) = \sum_{m_1=-l_1}^{l_1} C(l_1,l_2,m_1,M-m_1;L,M) f_{l_1,l_2,m_1,M-m_1}(\vec{r}_1,\vec{r}_2) \quad (3.81)$$

The definition of the 3-j symbol is the following:

$$C(l_1,l_2,m_1,m_2;L,M) = (-1)^{l_1-l_2+M}[2L+1]^{1/2} \begin{pmatrix} l_1 & l_2 & L \\ m_1 & m_2 & -M \end{pmatrix} \quad (3.82)$$

With two d single-particle wave functions or with a p and a d wave function higher $L = 3, 4$ angular momentum states can be calculated. That would mean too many channels for the collision calculation. Therefore, we neglect them. The first table presents the possible couplings up to $L = 2$.

Total Spin	Parity	L=0	L=1	L=2
0	Even	ss+pp+dd	pp'+dd'	sd+pp+dd
0	Odd	—	sp+pd	pd
1	Even	ss+pp+dd	pp+dd	sd+pp+dd
1	Odd	—	sp+pd	pd

Table I. The possible couplings up to $L = 2$

The states with different spin, parity and total angular momenta are diagonalized separately, because no mixture is allowed among states with different symmetry properties. (No further interaction is considered in the Hamiltonian.) The notation pp' + dd' means that the corresponding p or d functions have to be different (non-equivalent electrons) otherwise the coupling gives zero.

The single particle wavefunctions are not orthogonal to each other, so the generalized eigenvalue problem has to be solved. Let us plug the wave function (3.11) into the time independent Schrödinger equation (3.1)

$$\sum_{\nu=1}^{N} b_\nu^{[j]} \hat{H} f_\nu(\vec{r}_1,\vec{r}_2) = E_j \sum_{\nu=1}^{N} b_\nu^{[j]} f_\nu(\vec{r}_1,\vec{r}_2). \quad (3.83)$$

Multiply it from left with another wave function and integrate over all the variables

we get

$$\sum_{\nu=1}^{N} b_\nu^{[j]} \int_{\vec{r}_1} \int_{\vec{r}_2} f_\mu^*(\vec{r}_1, \vec{r}_2) \hat{H} f_\nu(\vec{r}_1, \vec{r}_2) d^3r_1 d^3r_2 =$$

$$E_j \sum_{\nu=1}^{N} b_\nu^{[j]} \int_{\vec{r}_1} \int_{\vec{r}_2} f_\mu^*(\vec{r}_1, \vec{r}_2) f_\nu(\vec{r}_1, \vec{r}_2) d^3r_1 d^3r_2. \tag{3.84}$$

With the abbreviations

$$H_{\mu,\nu} = \int_{\vec{r}_1} \int_{\vec{r}_2} f_\mu^*(\vec{r}_1, \vec{r}_2) \hat{H} f_\nu(\vec{r}_1, \vec{r}_2) d^3r_1 d^3r_2 \tag{3.85}$$

and

$$F_{\mu,\nu} = \int_{\vec{r}_1} \int_{\vec{r}_2} f_\mu^*(\vec{r}_1, \vec{r}_2) f_\nu(\vec{r}_1, \vec{r}_2) d^3r_1 d^3r_2 \tag{3.86}$$

(3.84) is equivalent to writing:

$$\hat{H}\vec{b}^{[j]} = E_j \hat{F}\vec{b}^{[j]}. \tag{3.87}$$

$\hat{H}$ is the Hamiltonian matrix and the $\hat{F}$ is the overlap matrix. Both of the matrices have to be symmetric and real, because the operators are hermitian. For the numerical solution of (3.87) we use a routine from the GSI IMSL-Library. The routine has an extra condition for the overlap; it has to be positive definite, otherwise no numerical solution can be achieved [Wil65].

The diagonalization itself does not consume much time and computer capacity. Just to compare: to calculate the Hamiltonian matrix and the overlap matrix with a realistic basis (25-30 single-particle wave functions) with Coulomb wave packages takes some hours and the diagonalization is about half a minute on a normal Pentium PC.

The routine has a double precision accuracy which is more than enough. For the ground state of the helium atom $E = -2.904$ a.u. three digits after the comma is sufficient.

The number of the eigenvalues is proportional to the square of the number of the single-particle wave functions. This will be shown in the next section.

The diagonalization procedure gives different eigenvalues (and eigenvectors) which have to be characterized first. An energy eigenvalue lying over 0 a.u. can be a single- or a double-ionized state as well, it is hard to say the right answer in fact. To

calculate the single and double total ionization cross sections we must unequivocally qualify all the states lying in the continuum.

There are different methods to solve this problem, we mention now three of them:

1, Analyzing the electron densities

One way is to calculate the electron densities for the corresponding energy state and then investigate it. The electron density allows us to distinguish between the different states. The following formula gives the expectation value of the density:

$$\rho_j(\vec{r}) = \left\langle \Phi_j(\vec{r_1},\vec{r_2}) \left| \sum_{i=1}^{2} \delta(\vec{r}-\vec{r_i}) \right| \Phi_j(\vec{r_1},\vec{r_2}) \right\rangle = \int_{\vec{r}_1} |\Phi_j(\vec{r}_1,\vec{r})|^2 \, d^3r_1 + \int_{\vec{r}_2} |\Phi_j(\vec{r},\vec{r}_2)|^2 \, d^3r_2. \tag{3.88}$$

The Dirac delta functions are the density operator. The integrals on the right side are symmetric in the case of symmetric and antisymmetric wave functions. According to this, the density reads:

$$\rho_j(r) = 2 \cdot \int_{\vec{r}_1} |\Phi_j(\vec{r}_1,\vec{r})|^2 \, d^3r_1 \tag{3.89}$$

We calculated the radial electron density $r^2\rho(r)$ multiplied by r^2.

Let us discuss the results:
The densities for the ground state or for single-excited states are well localized with some well-defined peaks. The 1^1S ground state has only one peak at $r \approx 2$a.u. which is approximately the atomic radius of the helium atom. All other single excited states have more than one peak. This densities show an exponential decay as function of the distance. Figure 3.4 shows the radial electron densities of the three lowest states.
The next figure 3.5 shows two low-lying auto-ionizing states which are quasi-bound states.
The auto-ionizing states can be quite simply recognized. There are different large CI calculations which give us their exact energy value([Bac91], [She77] or [Lip77]).
The single ionized states have a sharp peak close to the origin due to the bound electron and then some oscillations even up to large distances. The essential difference between a single-ionized state approximated purely with bound functions and with Coulomb packets can be seen in figure 3.6.
The pure Slater case has very few and very broad oscillations and has still an exponential decay for large distances. The package case looks more realistic with its long-range oscillating behavior. The oscillations can be seen even at 300 a.u. distance in our calculations.

For double-ionized states the effect is the same. Without packets the density is still of bound state-types there are several peaks at small distances and the 'far away' ($r > 20$ a.u.) oscillations can practically not be seen. In contrast to this the mixed case has very nice equidistant oscillations up to large distances. Densities of two double-ionized states are presented on figure 3.7.
The total density is normalized to two because we have two electrons. Check of the norm via the density is another way to test the accuracy. In our calculations it is always satisfied with an accuracy better than 99.8 percent.
The densities presented above are all for the total angular momentum $L = 0$ case without any angular correlated parts. In the $L = 1$ and 2 (angular momentum) cases the densities depend on the angles θ and φ. To visualize the radial dependence, the angles must be fixed to a certain value. The properties of the angular dependent densities are the same as in the case of spherical densities.

At last we should mention the handicap of this method.
In realistic calculations with two or three hundred states there are several problematic densities. An example: with the help of the packages the low lying single continuum, slightly above -2 a.u. can be nicely covered with states but when we look at the densities of the corresponding states we can not see any oscillations at all. These states are high-lying bound states e.g. 5^1S or 6^1S or even higher, badly approximated and lying in the continuum. Of course they have some single-ionized parts, but only with the help of the densities we can not go any further in their characterization. Several calculations show that if we consider these important low-lying states as completely ionized states than our cross sections will be enormous.
Conclusion: The investigation of the densities is not satisfactory. The diagonalization produces wave functions which are a complete mixture of all the configurations, and hinds their interpretation.

2, Projection method

A better method is the projection operator formalism of Feshbach. It is commonly used in atomic or nuclear physics. The idea is simple: one splits the Hilbert space into different sub-spaces, which are sub-spaces with bound, ionized and mixed states. Operators are constructed and projected on the wave functions to filter out the states of interest.

In our context the formalism is quite simple. We get our wave function after the diagonalization in the form of (3.10)

$$|\Phi_j(\vec{r}_1, \vec{r}_2)\rangle = \sum_\mu b_\mu^{[j]} f_\mu(\vec{r}_1, \vec{r}_2) \tag{3.90}$$

The sum contains all the symmetrized product combination of the single-particle wave functions, from the lowest ss Slater-Slater combination up to the energetically highest packet-packet combination.

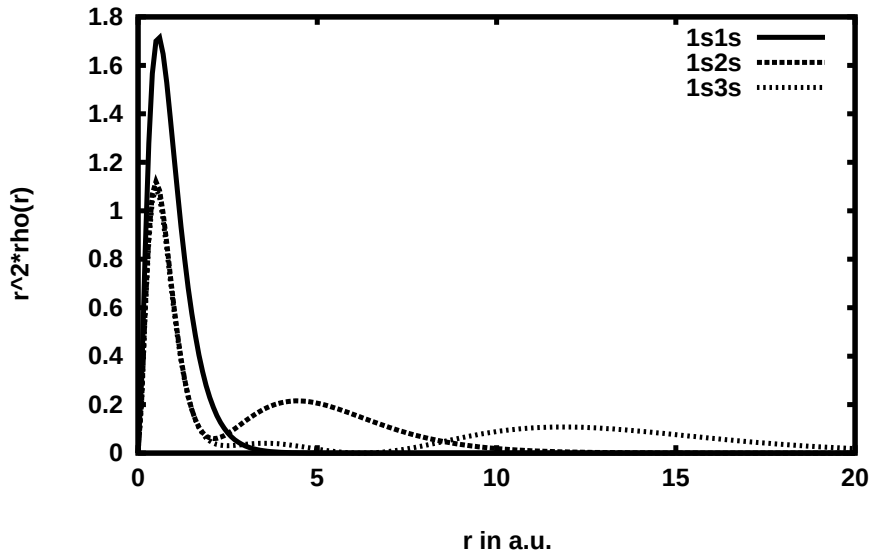

Figure 3.4: Electron density of the ground state and the following two single-excited states.

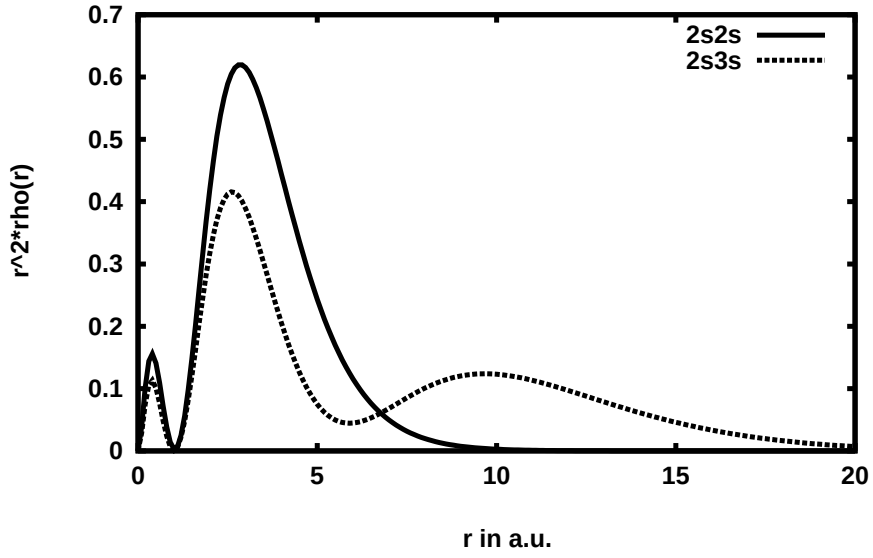

Figure 3.5: Electron densities of double-excited states.

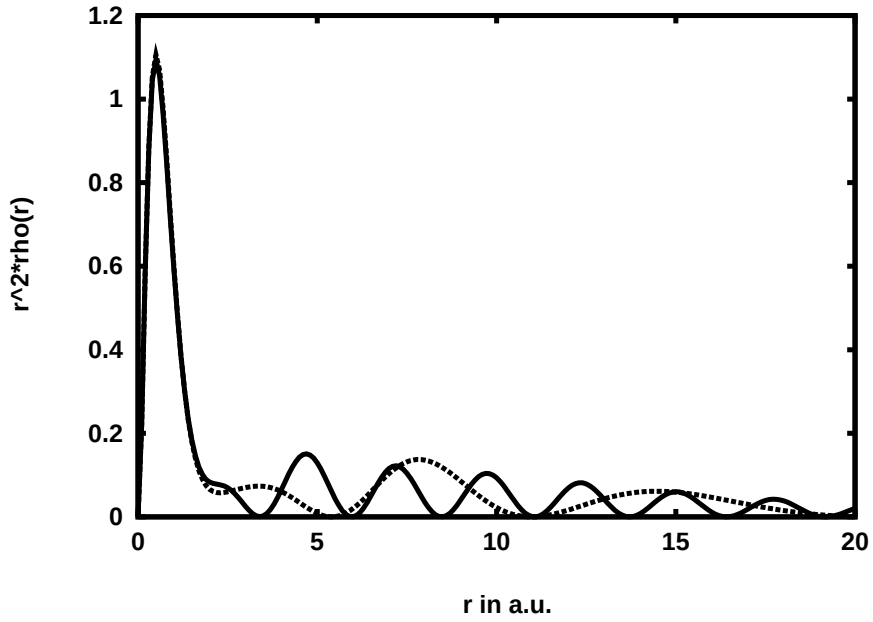

Figure 3.6: Electron densities of single-ionized states, solid line: with packages and dashed line: without packages.

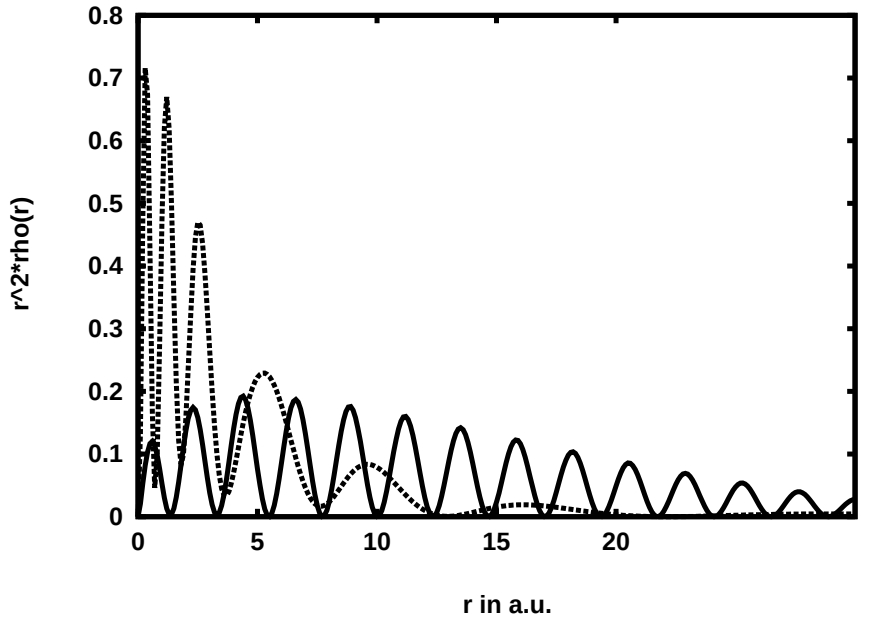

Figure 3.7: Electron densities of double-ionized states, solid line: with packages and dashed line: without packages.

Now we need another Hilbert space which is split into three orthogonal sub-spaces containing **bound-bound**, *bound-ionized*, and IONIZED-IONIZED states.

There are different ways to construct these Hilbert spaces. For the **bound-bound** sub-space bound-bound wave functions can be used e.g. from different CI or from Hartree-Fock calculations. For the IONIZED-IONIZED sub-space the 2C or even the fully correlated 3C symmetrized Coulomb wave function can be used [Spi99].

In former times even ionized states were approximated only by the sum of Slater-like orbitals where the exponents $\kappa_i = \alpha_0\beta, \alpha_0\beta^2, \alpha_0\beta^3, ..., \alpha_0\beta^N$ are a geometrical sequence with given α_0 and β. One can find more about this and about the pseudo-potential-Feshbach method in [Bac91].

Our idea is to use almost the same single-particle wave function set as for the diagonalization, but we orthogonalize it first.
To do this we take the same single-particle wave function set as before use it as a basis for the He^+ (or even for the hydrogen) problem and diagonalize it. The solution is an orthogonal single-particle wave function basis set. After that we may say that all the positive energies and the corresponding wave functions represent ionized electron states. The negative energy states are considered as bound states. With this assumption the three sub-spaces are constructed automatically. This statement is still not rigorously true, but gives a practical way to classify the states.

When using two orthogonalized single-particle wave functions with the proper normalizations and couplings between them, the helium wave functions can be constructed. Why are these wave functions approximately equal to the original helium wave functions (3.90) ? Because in the helium basis we use two different effective charges to distinct the single- and the double-ionized electrons.

This is the crucial point: If the effective charge of the He^+ wave function is changed the result will be slightly different.

The formula for this projection reads:

$$\begin{aligned}\Phi_{He}(\vec{r}_1,\vec{r}_2) = &\underbrace{\left\langle \Phi_{\text{ort}}^{\mathbf{bo-bo}}(\vec{r}_1,\vec{r}_2) \mid \Phi_{He}(\vec{r}_1,\vec{r}_2)\right\rangle}_{a^{[\mathbf{bo-bo}]}} \Phi_{\text{ort}}^{\mathbf{bo-bo}}(\vec{r}_1,\vec{r}_2) + \\ &\underbrace{\left\langle \Phi_{ort}^{bo-ion}(\vec{r}_1,\vec{r}_2) \mid \Phi_{He}(\vec{r}_1,\vec{r}_2)\right\rangle}_{a^{[bo-ion]}} \Phi_{\text{ort}}^{bo-ion}(\vec{r}_1,\vec{r}_2) \; + \\ &\underbrace{\left\langle \Phi_{ort}^{\text{ION-ION}}(\vec{r}_1,\vec{r}_2) \mid \Phi_{He}(\vec{r}_1,\vec{r}_2)\right\rangle}_{a^{[\text{ION-ION}]}} \Phi_{\text{ort}}^{\text{ION-ION}}(\vec{r}_1,\vec{r}_2) \end{aligned} \tag{3.91}$$

Φ_{He} stands for the diagonalized helium wave function and the different Φ_{ort} stands for the helium wave function built up from orthogonalized single-particle orbitals. The first therm on the right hand side stands for **bound-bound** states, the second

for *bound-ionized*, and the last for DOUBLE-IONIZED sates. The three sub spaces are orthogonal to each other. The normalization is giving us

$$1 = \sum_i \left(|a_i^{[\mathbf{bo-bo}]}|^2 + |a_i^{[bo-ion]}|^2 + |a_i^{[\mathrm{ION-ION}]}|^2 \right). \tag{3.92}$$

The coefficients $|a_i|^2$ are the probabilities of the states being single- or double-ionized or not. Extensive analysis of the diagonalized spectrum will be given using this method in the following section.

At last we show a scheme which helps to understand how to calculate the projection explained above:

$$\left\langle \mathcal{S} \left(\sum_{i=1}^{n} a_i \phi_i(\vec{r}_1) \right) \cdot \left(\sum_{j=1}^{n} a_j \phi_j(\vec{r}_2) \right) \middle| \sum_{l=1}^{N} b_l \mathcal{S} \left\{ \phi_1(\vec{r}_1) \cdot \phi_2(\vec{r}_2) \right\}_l \right\rangle \tag{3.93}$$

$\mathcal{S}$ stands for symmetrization. The 'ket' state is clear, this is the helium wave function that comes from the diagonalization, and the 'bra' state is the symmetrized product of the orthogonalized single-particle orbitals.

The CI wave functions always have all the three components, this is why they are called Configuration Interaction wave functions. Having done the projection we do not have any problem with the classification any more. After the time-evolution or even after the impact parameter integration, before the last summation all the channels have to be multiplied with the probabilities they contribute to single- and double-ionization or excitation. The only problem remaining is to have a preferably complete spectrum.

3, Method of complex coordinates

There is a mathematically correct method to filter out the resonances in the continuum. In this method all the r-coordinate in the Hamiltonian are multiplied with a complex phase factor: $r \to r \cdot e^{i\varphi}$. Then the Hamiltonian matrix is built up and diagonalized. The real part of the eigenvalues remain unchanged but the eigenvalues have an imaginary part. With the variation of the complex factor $e^{i\varphi}$ the imaginary part of the eigenvalue defines a curve in the complex plane. The imaginary parts of a single-ionized states are on a straight line as well as those of double-excited states. The gradient of the straight lines are characteristically different. This method is often used to filter out resonance states in the continuum. The benefit of this method to select single- and double-ionized states in the continuum is not much. The complex eigenvalues of the double-ionized states have much more difficult properties. The essential handicap of this method is (in our point of view) the complicated implementation and that no standard routines exist to solve the complex general eigenvalue problem. More about the complex-coordinate rotation method in [Ho79], [Ho87].

3.5 The helium spectrum

The qualitative spectrum of the helium atom is presented in figure 3.8.
It contains three basically different ranges:

- $[-2.904... - 2]$ a.u. Here lie the ground state and the single-excited states. Bound wave functions are obviously needed to describe these states.
- $[-2.0...0]$ a.u. Low-lying single-ionized continua with embedded double-excited states. These double-excited states are the so-called auto-ionizing states, metastable states emitting one electron after decay. A typical example is the 2s2s state. As mentioned before these states are easy to recognize. They are tabulated and the spatial densities are characteristical. To describe the soft single electron spectrum some states are needed between -2 a.u. and the first auto-ionizing state (for the L=0 spectrum it is -0.72 a.u.). This is of course true for the L=1 and L=2 spectra as well.
- $[0...\infty]$ a.u. This energy range is the most complex one and essential for us. This is the double-ionized spectrum overlapped with the highly energetic single-continuum. For our purposes the upper limit is about 20 a.u. which is more than enough as it will be shown later on.

The main goal of the diagonalization is not only to have a highly accurate bound helium spectrum, but the low lying states have to be approximated as accurate as possible. In this calculation no spin-orbit, spin-spin interaction, mass polarization or any other relativistic interactions are considered. The only effect which was taken into account is the correlation by the electron-electron interaction. If we use only s functions to approximate the ground state than the best energy value which can be reached is -2.879 a.u. This can not be lowered. Using p, d one-particle functions with the proper couplings the ground state value can be lowered. With 3s, 2p, 1d Slater function the calculated value is: -2.903 a.u. There is a well-detailed study on this topic [Ack95] where the non-relativistic helium Schrödinger equation is solved with the finite-element method on a lattice. The lowest ground-state energy for He which can be achieved is: -2.903 724 377 021 a.u. and for H^- the value is: -0.527 751 016 532 a.u. Precise calculations for the low-lying states of helium (or for helium-like ions) including relativistic, QED, and recoil corrections were given by Drake [Dra88], who combined variational methods and the relativistic $1/Z$ expansion in his unified method. For higher nuclear charge $4 \leq Z \leq 92$ relativistic configuration-interaction calculations for the ground state can be found in [Che94].

Table II. presents the nine lowest levels of the helium spectrum, the energies are experimental data, including relativistic corrections accordingly.

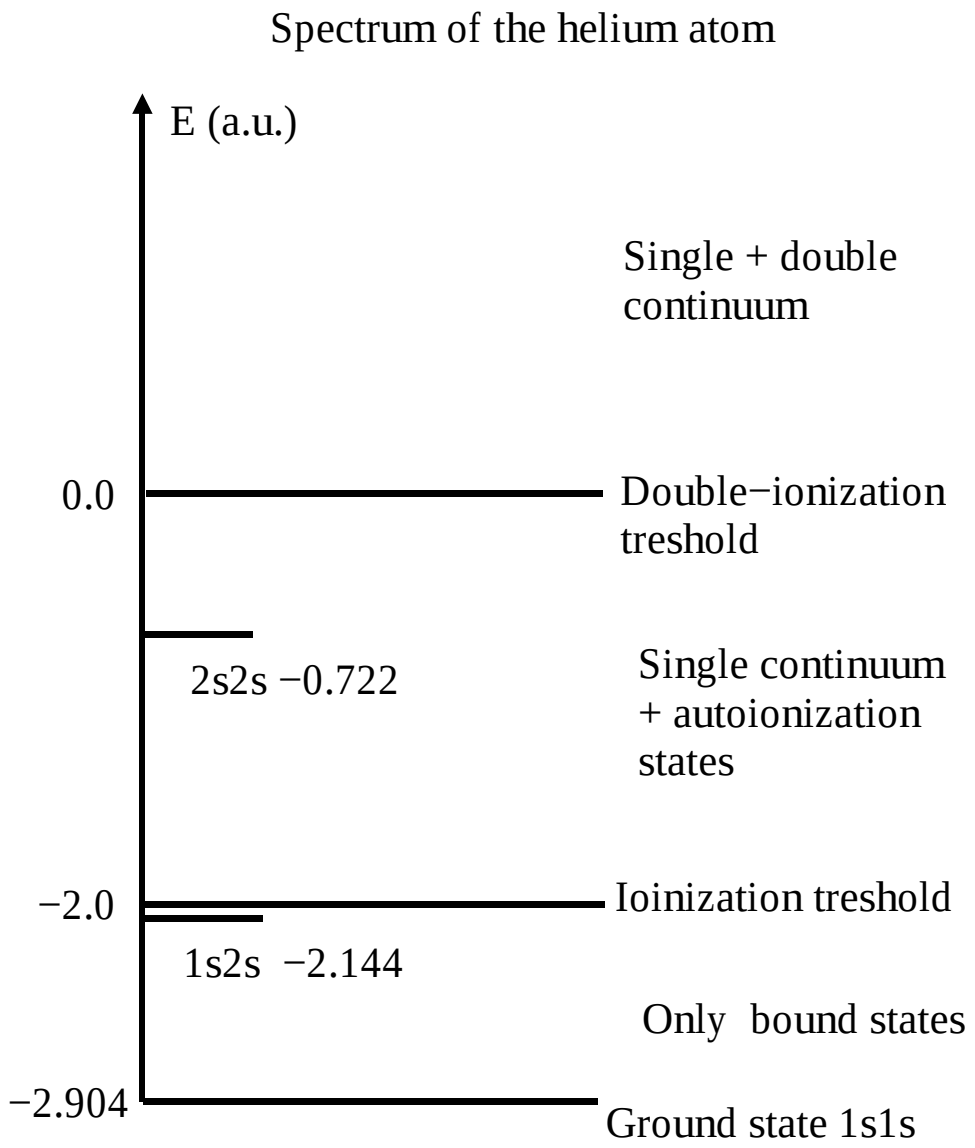

Figure 3.8: The L=0 spectrum of the helium atom, the ionization thresholds and two bound states.

$L=0$	$L=1$	$L=2$
4^1S	4^1P	4^1D
-2.0336	-2.0308	-2.0312
3^1S	3^1P	3^1D
-2.0612	-2.0551	-2.0556
2^1S	2^1P	–
-2.1459	-2.1238	–
1^1S	–	–
-2.9043	–	–

Table II. The nine lowest energy levels of the helium spectrum, experimental data from [Moo71].

These nine bound states are important to include in the coupled-channel calculations.

Now we present our basis functions and the corresponding spectra.
This is a non-angular-correlated calculation. This means that the $L = 0$ states are approximated only by **s** wave functions. The affect of the angular correlation presents itself by lowering the ground state. In the collision calculations the affect of the angular-correlated ground-state wave function can not be seen. All other low lying states such as $1s2s, 1s2p$ an so on can be slightly lowered by any further correlation, but in our case it is irrelevant. The angular correlation make the wave functions much more complicated and the spectrum will be much more complex. The interpretation and the classification of this spectrum is much harder and many states contribute only very little to the cross sections. At last some fully correlated calculation will also be discussed, but these are much more complex and will not be discussed always in detail here.

For fully angular correlated calculations the former screening factors κ have to be slightly modified. The number of the eigenvalues can be easily calculated from the number of the single-particle wave functions. A simple example for better understanding is the following:
Let us suppose that only two **s** single-particle wave functions are given, No. 1. and No. 2. In the singlet states, the spin part is antisymmetric and the space-dependent part must be symmetric. This means three possible combinations:

- both electrons are in the same state 1 (same wave function No. 1.)
- the two electrons are in different states (No. 1. and No. 2.)
- both electrons are in the same state 2 (same wave function No. 2.)

When the two electrons are in a spin triplet state, then the space part has to be anti-symmetric, and that can be realized only with different wave functions.

In table III. we present the number of the available energy levels. Let us abbreviate the number of the s single-particle wave functions with N_s the number of the p single-particle wave functions with N_p and number of the d single-particle wave functions with N_d respectively. For a more transparent description let us introduce following abbreviations:
(the index s stands for singlet and t is for triplet states)
$N\mathbf{s}_s = N_s * (N_s + 1)/2 \quad N\mathbf{s}_t = N_s * (N_s - 1)/2$
$N\mathbf{p}_s = N_p * (N_p + 1)/2 \quad N\mathbf{p}_t = N_p * (N_p - 1)/2$
$N\mathbf{d}_s = N_d * (N_d + 1)/2 \quad N\mathbf{d}_t = N_d * (N_d - 1)/2$
Where $N\mathbf{s_s}$ means the number of different helium singlet states which can be approximated with N_s single-particle s wave functions. With two different functions three different configurations can be realized as was shown above.

Total Spin	Parity	L=0	L=1	L=2
0	Even	$N\mathbf{s}_s + N\mathbf{p}_s + N\mathbf{d}_s$	*	$N_s \cdot N_d + N\mathbf{p}_s + N\mathbf{d}_s$
0	Odd	—	$N_s \cdot N_p + N_p \cdot N_d$	$N_p \cdot N_d$
1	Even	$N\mathbf{s}_t + N\mathbf{p}_t + N\mathbf{d}_t$	$N\mathbf{p}_t + N\mathbf{d}_t$	$N_s \cdot N_d + N\mathbf{p}_t + N\mathbf{d}_t$
1	Odd	—	$N_s \cdot N_p + N_p \cdot N_d$	$N_p \cdot N_d$

Table III. The number of the available energy levels. The * means a more complicated formula.

It is obvious from the table that the angular correlation enhances the number of the eigenvalues enormously. As was mentioned above, only the ground state will be lowered by the angular correlation, the additional energies due to the angular correlation belong to highly lying single- or double-ionized states. In the following tables we list the parameters of the wave function and the calculated energies. The star for $L = 1$ stands for a more complicated formula which is now irrelevant.

The number of Slater functions and their screening constants κ are well known from earlier calculations [Pfe96]. The number of packages is nearly as big as the number of bound state functions, this is needed but even more is better. Now we show why this kind of packages were taken. As we mentioned the ($-2.0 : -0.72$ a.u.) -'hole' has to be filled up with single-ionized states to cover the soft electron spectrum. As a rule-of-thumb we can say that every new package gives a new state in this energy range if the parameters are chosen adequately. If we need the first state at -1.8 a.u then we need roughly a following packet:
$E_1 = 0.2 a.u = k_{mid}^2/2 \quad \longrightarrow \quad k_{mid} = 0.63 \quad \longrightarrow \quad k_{mid} - \Delta k < k < k_{mid} + \Delta k$
The width of the desired packet is $[k_{mid} - \Delta k : k_{mid} + \Delta k]$. The desired energy

dictates only the middle value of the package. To choose the Δk we have some freedom. If we need a second state in the continuum with $E_2 = 0.4$ a.u. then we take
$(k_{mid_1} + \Delta k_1) \quad \leq \quad (k_{mid_2} - \Delta k_2)$,
otherwise we have a needless overlap between the packages. In this way the continuum can be covered equidistantly in energy, which means that the packages become always narrower as the k value increases.

Of course, we have electron-electron interaction and the Slater functions also produce states in this low lying region. Therefore the obtained energy will be slightly different from the given value. This concept works also for the double continuum, but $\tilde{Z}$ must be equal to two. As a last consequence this is valid for the L=1 and L=2 spectrum as well. In the last two cases the s packets also interact with the p and d packages, which shifts the energy values slightly a bit higher.

It is important to mention that the high-lying single- or double-ionized states produced purely by Slater functions remain or even go to higher values of the energy. Regardless of the parameters of the used packages, some highly-lying non-physical states remain due to the bound functions enclosed. These states give a relative big contribution to the single-ionized cross section if they are included in coupled-channel calculations. The following basis and the corresponding spectrum successfully covers the double continuum up to 6 a.u. The higher region between [6...12] a.u. is not or very barely presented. The highest energy range [12...17] is not so relevant for our calculations.

Some further remarks:
The distributions of packages with effective charge $\tilde{Z} = 1$ and 2 are different. This helps us to approximate the two different kind of continua a bit better.

In tables IV, V and VI we present the parameters of the basis functions. After that a long table (Table VII.) follows, where all the spectrum states are enumerated. The table contains the energy of the states, the classification of the state and weather it is used in the collision calculation or not. To understand this table some explanation is needed for the shorthand notations used:
$1\times \quad n$: A single-ionized state which is not used in the coupled-channel calculations.
$2\times \quad y$: A double-ionized state which is used in the coupled-channel calculations.
$b > 1\times \quad y$: A state which must be a single-ionized state (because of its energy) but its bound part is larger than the single-ionized part.
$b \approx 1\times \quad y$: A state which is a half-to-half mixture of the bound and the single-ionized configurations.
$1\times \approx 2\times \quad y$: A state with a half-to-half combination of single- and double-ionized configurations. After a careful analysis of the spectrum it turns out that pure double-ionized states are rare. This is an intrinsic property of our model.

Table IV. the **s** wave functions $(l = 0)$:

Function Type	Quantum numbers and parameters
Slater	n=1, κ=2.35
Slater	n=1, κ=1.27
Slater	n=2, κ= 1.48
Slater	n=2, κ=0.52
Slater	n=3, κ=1.30
Slater	n=3, κ=0.30
Slater	n=4, κ= 1.00
Slater	n=4, κ=0.25
Slater	n=5, κ=1.50
Coulomb	$k = 1.022,\ \Delta k = 0.185, \quad \tilde{Z} = 1.0,\ 2.0$
Coulomb	$k = 1.207,\ \Delta k = 0.157, \quad \tilde{Z} = 1.0,\ 2.0$
Coulomb	$k = 1.362,\ \Delta k = 0.145, \quad \tilde{Z} = 1.0,\ 2.0$
Coulomb	$k = 1.507,\ \Delta k = 0.131, \quad \tilde{Z} = 1.0,\ 2.0$

Table V. the **p** wave functions $(l = 1)$:

Function Type	Quantum numbers and parameters
Slater	n=2,κ=0.48
Slater	n=3,κ=1.00
Slater	n=3,κ= 0.29
Slater	n=4,κ=1.00
Slater	n=4,κ=0.22
Slater	n=5,κ=1.00
Coulomb	$\tilde{Z} = 1.0,\ k = 0.530,\ \Delta k = 0.260; \quad \tilde{Z} = 2.0,\ k = 1.860,\ \Delta k = 0.250$
Coulomb	$\tilde{Z} = 1.0,\ k = 0.790,\ \Delta k = 0.230; \quad \tilde{Z} = 2.0,\ k = 2.110,\ \Delta k = 0.224$
Coulomb	$\tilde{Z} = 1.0,\ k = 1.022,\ \Delta k = 0.185; \quad \tilde{Z} = 2.0,\ k = 2.330,\ \Delta k = 0.204$
Coulomb	$\tilde{Z} = 1.0,\ k = 1.207,\ \Delta k = 0.157; \quad \tilde{Z} = 2.0,\ k = 2.530,\ \Delta k = 0.189$
Coulomb	$\tilde{Z} = 1.0,\ k = 1.362,\ \Delta k = 0.145; \quad \tilde{Z} = 2.0,\ k = 2.710,\ \Delta k = 0.180$
Coulomb	$\tilde{Z} = 1.0,\ k = 1.507,\ \Delta k = 0.131; \quad \tilde{Z} = 2.0,\ k = 2.890,\ \Delta k = 0.172$

Table VI. the **d** wave functions $(l = 2)$:

Function Type	Quantum numbers and parameters
Slater	n=3, κ=1.00
Slater	n=3, κ=0.33
Slater	n=4, κ= 1.00
Slater	n=4, κ=0.23
Coulomb	$\tilde{Z} = 1.0,\ k = 0.530,\ \Delta k = 0.260; \quad \tilde{Z} = 2.0,\ k = 1.860,\ \Delta k = 0.250$
Coulomb	$\tilde{Z} = 1.0,\ k = 0.790,\ \Delta k = 0.230; \quad \tilde{Z} = 2.0,\ k = 2.110,\ \Delta k = 0.224$
Coulomb	$\tilde{Z} = 1.0,\ k = 1.022,\ \Delta k = 0.185; \quad \tilde{Z} = 2.0,\ k = 2.330,\ \Delta k = 0.204$
Coulomb	$\tilde{Z} = 1.0,\ k = 1.207,\ \Delta k = 0.157; \quad \tilde{Z} = 2.0,\ k = 2.530,\ \Delta k = 0.189$

No.	Energy in a.u.	Config./ Used (y) or not (n)
L=0 Spectrum		
1	-2.877	1^1S y
2	-2.144	2^1S y
3	-2.060	3^1S y
4	-2.033	4^1S y
5	-1.985	5^1S n
6	-1.792	$b > 1 \times$ y
7	-1.369	$b > 1 \times$ y
8	-1.186	$b \approx 1 \times$ n
9	-1.155	$1 \times$ y
10	-0.963	$1 \times$ n
11	-0.880	$1 \times$ n
12	-0.729	$2s2s$ n
13	-0.717	$1 \times$ n
14	-0.571	$2s3s$ y
15	-0.537	$2s4s$ y
16	-0.507	$2s5s$ y
17	-0.360	$1 \times$ y
18	-0.318	$1 \times$ y
19	-0.264	$1 \times$ y
20	-0.241	$1 \times$ y
21	-0.181	$1 \times$ y
22	-0.153	$1 \times$ n
23	-0.133	$1 \times$ y
24	-0.114	$1 \times$ n
25	-0.077	$1 \times$ y
26	-0.052	$1 \times$ y
27	0.021	$1 \times$ y
28	0.045	$1 \times$ n
29	0.213	$1 \times$ y
30	0.257	$1 \times$ n
31	0.274	$1 \times$ n
32	0.293	$1 \times$ n
33	0.411	$1 \times$ n
34	0.468	$1 \times$ y
35	0.530	$1 \times$ y
36	0.603	$1 \times$ n
37	0.606	$1 \times$ n
38	0.632	$1 \times$ y
39	0.701	1s $1 \times$ y
40	0.716	$1 \times$ n
41	0.760	$1 \times$ n

No.	Energy in a.u.	Config./ Used (y) or not (n)
42	0.782	$1 \times$ n
43	0.795	$1 \times$ n
44	0.818	$1 \times$ n
45	0.869	$1 \times$ y
46	0.903	$1 \times$ y
47	0.944	$1 \times$ n
48	0.971	$1 \times$ n
49	0.985	$1 \times$ n
50	1.032	$1 \times$ y
51	1.051	$1 \times$ y
52	1.058	$1 \times$ n
53	1.119	$1 \times$ n
54	1.151	$1 \times$ n
55	1.204	$1 \times$ n
56	1.230	$1 \times$ n
57	1.411	$1 \times$ n
58	1.428	$1 \times$ n
59	1.594	$1 \times$ n
60	1.706	$1 \times$ y
61	1.770	$1 \times$ n
62	1.839	$1 \times$ n
63	1.856	$1 \times$ n
64	1.961	$1 \times$ y
65	1.971	$1 \times$ n
66	1.996	$1 \times$ n
67	2.019	$1 \times$ y
68	2.029	$1 \times$ n
69	2.085	$1 \times$ n
70	2.197	$1 \times$ n
71	2.248	$1 \times$ y
72	2.428	$1 \times$ n
73	2.610	$1 \times$ y
74	2.845	$1 \times$ n
75	2.941	$1 \times$ n
76	3.200	$2 \times$ n
77	3.715	$2 \times$ y
78	4.897	$2 \times$ y
79	11.938	$2 \times$ y
80	12.462	$2 \times$ n
81	12.548	$2 \times$ y
82	12.576	$1 \times$ n
83	12.593	$1 \times$ y

No.	Energy in a.u.	Config./ Used (y) or not (n)
84	12.636	$2\times$ y
85	12.923	$2\times$ n
86	13.078	$2\times$ n
87	13.325	$2\times$ n
88	13.516	$2\times$ n
89	13.855	$2\times$ n
90	16.500	$2\times$ n
91	27.385	$2\times$ n
L=1 Spectrum		
1	-2.123	2^1P y
2	-2.055	3^1P y
3	-2.030	4^1P y
4	-1.922	5^1P n
5	-1.735	$1\times$ y
6	-1.313	$1\times$ y
7	-0.648	$2s2p$ y
8	-0.581	$2s3p$ y
9	-0.545	$2s4p$ y
10	-0.535	$2s5p$ y
11	-0.517	$2s6p$ y
12	-0.501	$2s7p$ y
13	-0.454	$1\times$ y
14	-0.353	$1\times$ y
15	-0.321	$1\times$ n
16	-0.287	$1\times$ y
17	-0.273	$1\times$ n
18	-0.251	$1\times$ n
19	-0.244	$1\times$ n
20	-0.211	$1\times$ n
21	-0.165	$1\times$ y
22	-0.162	$1\times$ n
23	-0.142	$1\times$ n
24	-0.134	$1\times$ n
25	-0.105	$1\times$ n
26	-0.102	$1\times$ n
27	-0.075	$1\times$ y
28	-0.058	$1\times$ n
29	-0.042	$1\times$ n
30	-0.021	$1\times$ n
31	0.020	$1\times$ y
32	0.064	$1\times$ y

No.	Energy in a.u.	Config./ Used (y) or not (n)
33	0.103	$1\times$ n
34	0.121	$1\times$ y
35	0.216	$1\times$ y
36	0.261	$1\times$ n
37	0.283	$1\times$ n
38	0.292	$1\times$ y
39	0.321	$1\times$ y
40	0.346	$1\times$ n
41	0.369	$1\times$ y
42	0.414	$1\times$ y
43	0.476	$1\times$ y
44	0.499	$1\times$ y
45	0.545	$1\times$ y
46	0.611	$1\times$ y
47	0.627	$1\times$ n
48	0.628	$1\times$ n
49	0.636	$1\times$ n
50	0.728	$1\times$ n
51	0.732	$1\times$ y
52	0.748	$1\times$ n
53	0.796	$1\times$ n
54	0.821	$1\times$ y
55	0.869	$1\times$ n
56	0.882	$1\times$ n
57	0.922	$1\times$ n
58	0.950	$1\times$ n
59	0.975	$1\times$ n
60	1.044	$1\times$ y
61	1.070	$1\times$ n
62	1.121	$1\times$ n
63	1.122	$1\times$ n
64	1.133	$1\times$ n
65	1.153	$1\times$ n
66	1.243	$1\times$ n
67	1.300	$1\times$ n
68	1.450	$1\times$ n
69	1.566	$1\times$ n
70	1.598	$1\times$ n
71	1.632	$1\times$ n
72	1.861	$1\times$ y
73	1.869	$1\times$ n
74	1.942	$1\times$ n

No.	Energy in a.u.	Config./ Used (y) or not (n)
75	1.968	$1 \times \quad n$
76	1.972	$1 \times \quad n$
77	1.999	$1 \times \quad n$
78	2.003	$1 \times \quad n$
79	2.048	$1 \times \quad y$
80	2.076	$1 \times \quad n$
81	2.122	$1 \times \quad n$
82	2.214	$1 \times \quad n$
83	2.385	$1 \times \quad n$
84	2.437	$1 \times \quad n$
85	2.464	$1 \times \quad n$
86	2.489	$1 \times \quad n$
87	2.493	$1 \times \quad n$
88	2.571	$1 \times \quad n$
89	2.603	$1 \times \quad n$
90	2.644	$1 \times \quad n$
91	2.686	$1 \times \quad n$
92	2.861	$1 \times \quad n$
93	2.879	$1 \times \quad n$
94	2.940	$1 \times \quad n$
95	2.963	$1 \times \quad n$
96	2.971	$1 \times \quad n$
97	3.027	$1 \times \quad y$
98	3.048	$1 \times \quad n$
99	3.087	$1 \times \quad n$
100	3.177	$1 \times \quad n$
101	3.277	$1 \times \quad n$
102	3.293	$1 \times \quad n$
103	3.351	$1 \times \quad y$
104	3.367	$1 \times \quad n$
105	3.280	$1 \times \quad n$
106	3.453	$1 \times \quad n$
107	3.457	$1 \times \quad n$
108	3.476	$1 \times \quad n$
109	3.578	$1 \times \quad n$
110	3.665	$1 \times \quad n$
111	3.709	$1 \times \quad n$
112	3.775	$1 \times \quad y$
113	3.784	$1 \times \quad n$
114	3.812	$1 \times \quad n$
115	3.843	$1 \times \quad n$

No.	Energy in a.u.	Config./ Used (y) or not (n)
116	3.880	$1 \times \quad n$
117	3.900	$1 \times \quad n$
118	3.953	$1 \times \quad n$
119	3.991	$1 \times \quad n$
120	4.084	$1 \times \quad y$
121	4.149	$1 \times \quad n$
122	4.208	$1 \times \quad n$
123	4.270	$1 \times \quad n$
124	4.287	$1 \times \quad n$
125	4.294	$1 \times \quad n$
126	4.319	$1 \times \quad n$
127	4.352	$1 \times \quad n.$
128	4.395	$1 \times \quad n$
129	4.512	$1 \times \quad n$
130	4.573	$1 \times \quad n$
131	4.621	$1 \times \quad n$
132	4.757	$2 \times \quad y$
133	4.784	$1 \times \quad n$
134	4.837	$2 \times \quad n$
135	5.014	$2 \times \quad y$
136	5.035	$2 \times \quad n$
137	5.141	$2 \times \quad n$
138	5.228	$2 \times \quad n$
139	5.337	$2 \times \quad n$
140	5.445	$2 \times \quad n$
141	5.537	$2 \times \quad n$
142	5.729	$2 \times \quad n$
143	5.892	$2 \times \quad n$
144	6.376	$2 \times \quad y$
145	12.467	$1 \times \quad n$
146	12.549	$1 \times \quad n$
147	12.576	$1 \times \quad n$
148	12.668	$1 \times \quad n$
149	12.837	$1 \times \quad n$
150	13.269	$1 \times \quad y$
151	14.294	$1 \times \quad y$
152	14.820	$1 \times \quad n$
153	15.312	$1 \times \quad y$
154	15.747	$1 \times \quad n$
155	16.178	$1 \times \quad y$
156	16.667	$1 \times \quad n$

No.	Energy in a.u.	Config./ Used (y) or not (n)
L=2 Spectrum		
1	-2.055	3^1D y
2	-2.031	4^1D y
3	-1.938	5^1D n
4	-1.325	$b > 1\times$ y
5	-0.554	$2s3p$ y
6	-0.530	$2s34$ n
7	-0.437	$1\times$ n
8	-0.303	$1\times$ y
9	-0.266	$1\times$ y
10	-0.258	$1\times$ y
11	-0.241	$1\times$ n
12	-0.223	$1\times$ n
13	-0.172	$1\times$ y
14	-0.156	$1\times$ n
15	-0.146	$1\times$ n
16	-0.122	$1\times$ n
17	-0.108	$1\times$ n
18	-0.072	$1\times$ n
19	-0.046	$1\times$ n
20	-0.011	$1\times$ n
21	0.029	$1\times$ y
22	0.167	$1\times$ y
23	0.205	$1\times$ n
24	0.228	$1\times$ n
25	0.237	$1\times$ n
26	0.266	$1\times$ n
27	0.310	$1\times$ n
28	0.376	$1\times$ n
29	0.494	$1\times$ y
30	0.536	$1\times$ n
31	0.610	$1\times$ n
32	0.636	$1\times$ n
33	0.724	$1\times$ y
34	0.767	$1\times$ n
35	0.799	$1\times$ n
36	0.823	$1\times$ n
37	0.878	$1\times$ n
38	0.951	$1\times$ n
39	0.976	$1\times$ n
40	0.989	$1\times$ n

No.	Energy in a.u.	Config./ Used (y) or not (n)
41	1.020	$1\times$ y
42	1.038	$1\times$ n
43	1.123	$1\times$ n
44	1.154	$1\times$ y
45	1.206	$1\times$ n
46	1.344	$1\times$ n
47	1.487	$1\times$ n
48	1.504	$1\times$ n
49	1.727	$1\times$ n
50	1.795	$1\times$ n
51	1.821	$1\times$ n
52	1.908	$1\times$ n
53	1.970	$1\times$ n
54	1.988	$1\times$ n
55	2.000	$1\times$ n
56	2.073	$1\times$ n
57	2.230	$1\times$ n
58	2.298	$1\times$ n
59	2.312	$1\times$ n
60	2.325	$1\times$ n
61	2.412	$1\times$ y
62	2.481	$1\times$ n.
63	2.608	$1\times$ n
64	2.685	$1\times$ n
65	2.731	$1\times$ n
66	2.805	$1\times$ n
67	2.812	$1\times$ n
68	2.833	$1\times$ n
69	2.886	$1\times$ n
70	2.916	$1\times$ n
71	2.936	bound n
72	3.085	$2\times$ n
73	3.178	$1\times$ n
74	3.293	$2\times$ n
75	3.310	$1\times \approx 2\times$ n
76	3.385	$1\times$ n
77	3.578	$2\times$ n
y 78	3.671	$1\times$ n
79	3.780	$2\times$ n
80	3.864	$2\times$ n
81	3.872	$1\times$ n

No.	Energy in a.u.	Config./ Used (y) or not (n)
82	4.061	$2\times \quad n$
83	4.253	$2\times \quad n$
84	4.400	$2\times \quad n$
85	4.411	$2\times \quad n$
86	4.648	$1\times \approx 2\times$
87	4.723	$1\times \approx 2\times$
88	4.752	$1\times \approx 2\times$
89	4.836	$1\times \quad n$
90	4.875	$1\times \quad n$
91	5.237	$1\times \quad n$
92	5.581	$1\times \quad n$
93	5.783	$1\times \quad n$
94	5.984	$2\times \quad n$
95	6.191	$2\times \quad y$
96	6.790	$2\times \quad n$
97	12.550	$1\times \quad n$
98	12.577	$1\times \quad n$
99	12.659	$1\times \quad n$
100	13.23	$1\times \quad n$
101	14.173	$1\times \quad n$
102	14.681	$1\times \quad n$
103	15.175	$1\times \quad n$
104	17.113	$1\times \quad n$

After these tables we present two diagrams to visualize the distribution of the of states figure. (3.9) and the distribution of the channels used in the collision calculations figure (3.10).

In the interval between 6 and 11 a.u. we found no states. It is worth to mention that an $L = 1$ state splits into three different channels and the $L = 2$ state into five due to their magnetic quantum number dependence. The second figure (3.10) presents set of used channels, but also other sets were used in the calculations. This will be discussed in Chapter 5 in detail.

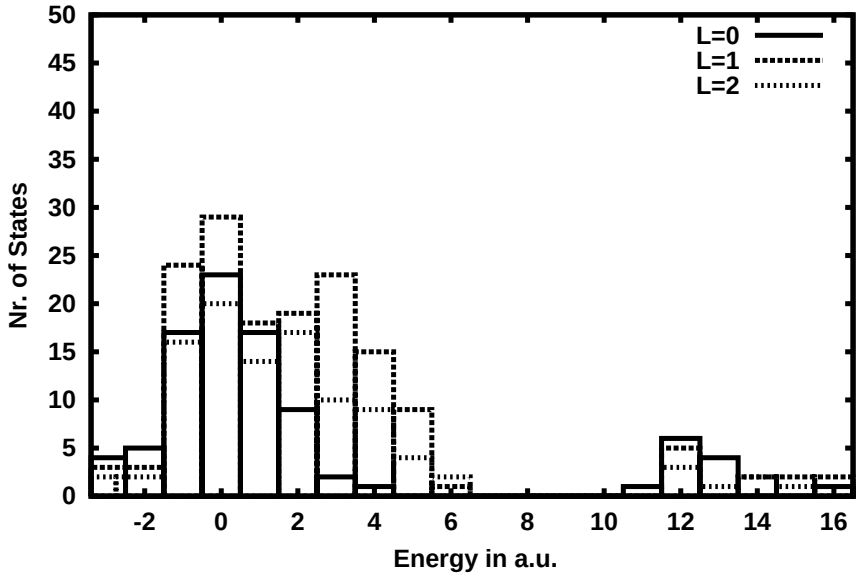

Figure 3.9: The energy distribution of the energy levels produced by the basis given above. All 91 $L = 0$ 156 $L = 1$ and 104 $L = 2$ states are presented. The first bar means the energy range between (-3...-2 a.u.) the second between (-2...-1 a.u.) and so on.

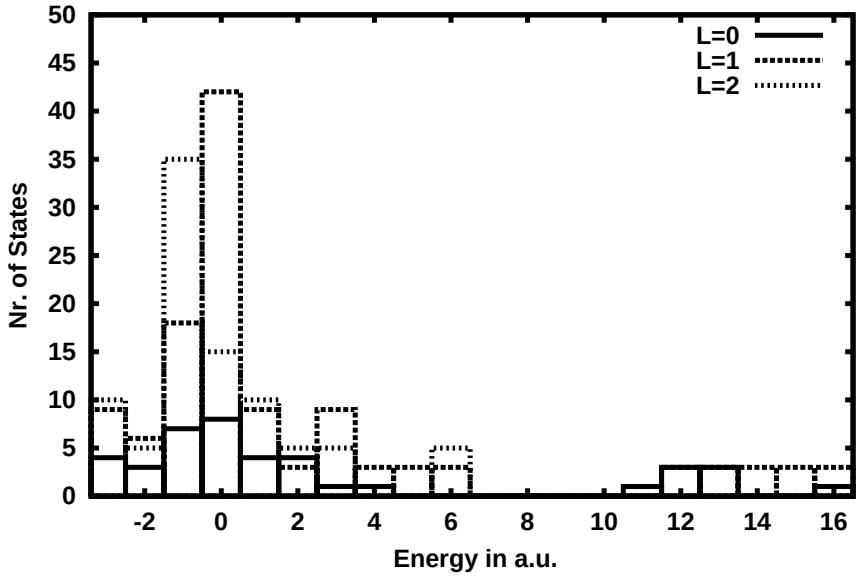

Figure 3.10: The energy distribution of the used channels (all together 277). The notation is the same as before.

Chapter 4

The collision process

4.1 Coordinate system

We have chosen a coordinate system with the z-axis parallel with the projectile beam. Figure 4.1 shows the situation of the collision process. The target nucleus (now the helium nucleus) is in the origin. The projectile flies in the xy plane parallel with the z-axis on a straight-line from left to right. The minimal distance between the target and the projectile is at the time $t = 0$, when the projectile crosses the x-axis. The minimal distance between the two nuclei is the so-called impact parameter.

In this study the projectile is described as a classically moving point charge. For 'naked' fully ionized projectiles this is a good approximation for any impact parameter. For not fully ionized projectiles this approximation can be questionable at the small impact parameter region. We carried out calculations for U^{90+} which is not fully ionized but is a strongly bound system compared with the helium atom, and has a relatively small ion radius.

4.2 The time-dependent Hamiltonian

In the following section the time-dependent interaction between the projectile and the electrons of the helium atom will be discussed and analyzed. The total Hamiltonian can be separated into two parts as was already shown in (2.1). Let's now start with the full Hamiltonian using the minimal coupling for the vector potential:

$$\hat{H}(\vec{r}_1, \vec{r}_2, t) = \frac{(\vec{p}_1 + \vec{A}(\vec{r}_1, t))^2}{2} + \frac{(\vec{p}_2 + \vec{A}(\vec{r}_2, t))^2}{2} - \frac{2}{r_1} - \frac{2}{r_2} + \frac{1}{r_{12}} - \Phi(\vec{r}_1, t) - \Phi(\vec{r}_2, t). \tag{4.1}$$

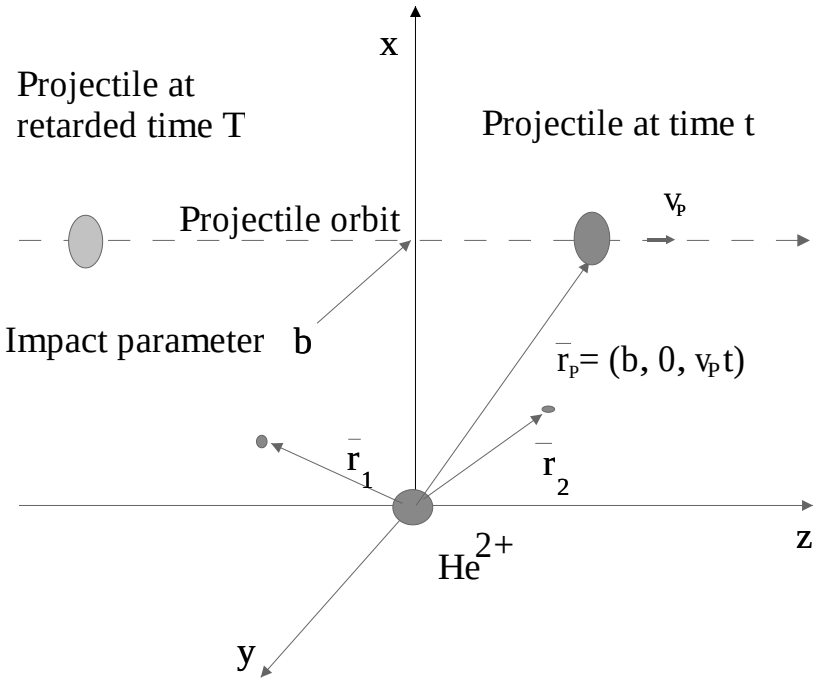

Figure 4.1: The coordinate system

The electromagnetic field induced by the projectile contains the scalar potential $\Phi(\vec{r},t)$ and the vector potential $\vec{A}(\vec{r},t)$. The velocity of light is already included in the operator $\vec{A}(\vec{r},t)$. The explicite form of the operators will be shown below.

To separate the electromagnetic potentials from the kinetic energy we need to square the canonical impulse:

$$\hat{H}(\vec{r}_1,\vec{r}_2,t) = -\frac{1}{2}\Delta_1 - \frac{1}{2}\Delta_2 - \frac{Z_T}{r_1} - \frac{Z_T}{r_2} + \frac{1}{r_{12}} + \frac{1}{2i}\mathrm{div}_1\vec{A}(\vec{r}_1,t) + \frac{1}{2i}\mathrm{div}_2\vec{A}(\vec{r}_2,t) + \frac{1}{2i}\vec{A}(\vec{r}_1,t)\mathrm{grad}_1 + \frac{1}{2i}\vec{A}(\vec{r}_2,t)\mathrm{grad}_2 + \frac{1}{2}\vec{A}^2(r_1,t) + \frac{1}{2}\vec{A}^2(r_1,t) - \Phi(\vec{r}_1,t) - \Phi(\vec{r}_2,t) \quad (4.2)$$

The first five terms are well known from the former chapter; the remaining eight terms need further investigation. The divergence terms can be reformulated:

$$\mathrm{div}\left(\vec{A}(\vec{r},t)\phi(\vec{r})\right) = \phi(\vec{r})\left(\mathrm{div}\,\vec{A}(\vec{r},t)\right) + A(\vec{r},t)\,(\mathrm{grad}\,\phi(\vec{r})) \quad (4.3)$$

where $\phi(\vec{r})$ is the wave function. The velocity of the projectile is comparable to the velocity of light that is why the retardation effects have to be taken into account. The projectile is considered as a point particle. The Compton wavelength of the projectile is negligible short compared to the wavelength of the electrons that is why the semiclassical approximation is valid. A further simplification is that the projectile moves on a straight-line trajectory. This is a good approximation which is justified for heavy ions. The variation of the kinetic energy of the projectile after the collision is only a couple of meV [Knu84]. The classical fields are the well known Liénard-Wiechert potentials [Jac81]

$$\Phi(\vec{r},t) = \frac{\gamma_p Z_p}{R(t)} \qquad \vec{A}(\vec{r},t) = \frac{1}{c^2}\frac{\gamma_p v_p Z_p}{R(t)}\vec{e}_z. \quad (4.4)$$

with

$$R(t) = \sqrt{(x-b)^2 + y^2 + \gamma_p^2(z-v_p t)^2} \qquad \gamma_p = \sqrt{\frac{1}{1-(v_p/c)^2}} \quad (4.5)$$

We take the derivative of the vector potential with respect to z in such a way that only the z coordinate is not zero. Then it reads as following:

$$\mathrm{div}\vec{A}(\vec{r},t) = \frac{\partial}{\partial z}A_z(\vec{r},t) = -\frac{1}{c^2}\cdot v_p \cdot \gamma_p^3 \cdot Z_p \cdot \frac{(z-v_p t)}{[R(t)]^3} \quad (4.6)$$

Inserting the Liénard-Wiechert potentials into the Schrödinger equation the projectile-electron interaction operator $\hat{V}(t)$ has the final form:

$$\hat{V}(t) = \overbrace{-\gamma_p Z_p \left[\frac{1}{R_1(t)} + \frac{1}{R_2(t)}\right]}^{\hat{V}_1=\phi(\vec{r}_1,t)+\phi(\vec{r}_2,t)} - \overbrace{iv_p\gamma_p Z_p \frac{1}{c^2}\left[\frac{1}{R_1(t)}\frac{\partial}{\partial z_1} + \frac{1}{R_2(t)}\frac{\partial}{\partial z_2}\right]}^{\hat{V}_2=\frac{1}{2}(\vec{A}(\vec{r}_1,t)\vec{p}_1+\vec{A}(\vec{r}_2,t)\vec{p}_2)} +$$
$$\overbrace{\frac{v_p^2\gamma_p^2 Z_p^2}{2c^4}\left[\frac{1}{[R_1(t)]^2} + \frac{1}{[R_1(t)]^2}\right]}^{\hat{V}_3=\vec{A}^2(\vec{r_1},t)/2+\vec{A}^2(\vec{r_2},t)/2} + \overbrace{i\frac{v_p\gamma_p^3 Z_p}{2c^2}\left[\frac{z_1 - v_p t}{[R_1(t)]^3} + \frac{z_2 - v_p t}{[R_2(t)]^3}\right]}^{\hat{V}_4=\frac{1}{2i}(div(\vec{A}(\vec{r_1},t))+div(\vec{A}(\vec{r_2},t)))} \quad (4.7)$$

The single operators $\hat{V}_j$ are apiece not hermitian but the sum of all four is hermitian. In this study the spin-magnetic field interaction is neglected. In the case of helium or light helium-like targets this interaction is three orders of magnitude smaller than the scalar interaction. Just to mention, the spin-magnetic field interaction has the following form:

$$\hat{H}_{Spin} = -\vec{\mu}_1\vec{B}(r_1) - \vec{\mu}_2\vec{B}(r_2) \quad \text{with} \quad \vec{B} = \text{curl}\vec{A} \equiv \text{rot}\vec{A} \quad (4.8)$$

This interaction mixes the triplet and the singlet states. This means that the number of the channels automatically would increase with a factor of two.

4.2.1 The calculation of the coupling matrix

The first step to solve the coupled-channel-equations is to build up the coupling matrix.

For singlet states the wave function is a linear combination of symmetrized single-particle wave functions as was shown in the chapter before. The interaction operator is a sum of two one-electron matrix elements because the target has two electrons:

$$\hat{V}(\vec{r}_1, \vec{r}_2, t) = \hat{V}(\vec{r}_1, t) + \hat{V}(\vec{r}_2, t). \quad (4.9)$$

To calculate the coupling matrix we need to evaluate the following expression:

$$\tilde{H}_{ij} = \left\langle \sum_{\mu=1}^{M} b_\mu^{[i]}[\phi_1(\vec{r}_1)\phi_2(\vec{r}_2) + \phi_2(\vec{r}_1)\phi_1(\vec{r}_2)] \middle| \hat{V}(\vec{r}_1, t) + \right.$$
$$\left. \hat{V}(\vec{r}_2, t) \middle| \sum_{\nu=1}^{M} b_\nu^{[j]}[\phi_3(\vec{r}_1)\phi_4(\vec{r}_2) + \phi_4(\vec{r}_1)\phi_3(\vec{r}_2)] \right\rangle \quad (4.10)$$

The indeces 1,2,3,4 stand for the four (different) quantum number sets with respect to the corresponding wave functions. Let us go one formal step further:

$$\tilde{H}_{ij} = 2 \cdot \sum_{\mu=1}^{M} \sum_{\nu=1}^{M} b_{\nu}^{[i]} b_{\mu}^{[j]} \cdot \Big[\langle \phi_1(\vec{r}_1) | \hat{V}(\vec{r}_1, t) | \phi_3(\vec{r}_1) \rangle \cdot \langle \phi_2(\vec{r}_2) | \phi_4(\vec{r}_2) \rangle +$$
$$\langle \phi_1(\vec{r}_2) | \phi_4(\vec{r}_2) \rangle \cdot \langle \phi_2(\vec{r}_1) | \hat{V}(\vec{r}_1, t) | \phi_3(\vec{r}_1) \rangle + \langle \phi_1(\vec{r}_2) | \phi_3(\vec{r}_2) \rangle \cdot \langle \phi_2(\vec{r}_1) | \hat{V}(\vec{r}_1, t) | \phi_4(\vec{r}_1) \rangle +$$
$$\langle \phi_2(\vec{r}_2) | \phi_3(\vec{r}_2) \rangle \cdot \langle \phi_1(\vec{r}_1) | \hat{V}(\vec{r}_1, t) | \phi_4(\vec{r}_1) \rangle \Big] . \tag{4.11}$$

The two electrons are indistinguishable that is why the factor two arises. It is enough to calculate the matrix element only once:

$$\langle \phi_1(\vec{r}_1) | \hat{V}(\vec{r}_1, t) | \phi_3(\vec{r}_1) \rangle \equiv \langle \phi_1(\vec{r}_2) | \hat{V}(\vec{r}_2, t) | \phi_3(\vec{r}_2) \rangle . \tag{4.12}$$

As in the structure calculation, we here need three different kinds of matrix elements to calculate:

$$\begin{gathered} \langle S_{n_1,l_1,m_1,\kappa_1}(\vec{r}) | \hat{V}(\vec{r}, t) | S_{n_2,l_2,m_2,\kappa_2}(\vec{r}) \rangle \\ \langle S_{n,l_1,m_1,\kappa}(\vec{r}) | \hat{V}(\vec{r}, t) | C_{k,l_2,m_2,\tilde{Z}}(\vec{r}) \rangle \quad \text{or} \quad \langle C_{k,l_1,m_1,\tilde{Z}}(\vec{r}) | \hat{V}(\vec{r}, t) | S_{n,l_2,m_2,\kappa}(\vec{r}) \rangle \\ \langle C_{k_1,l_1,m_1,\tilde{Z}_1}(\vec{r}) | \hat{V}(\vec{r}, t) | C_{k_2,l_2,m_2,\tilde{Z}_2}(\vec{r}) \rangle \end{gathered} \tag{4.13}$$

The pure Slater case is the easiest work and the package-package is the most complicated and time consuming case.

4.2.2 The matrix elements for operator V_2

As it was shown before the $\hat{V}_2$ contains a differential operator $\frac{\partial}{\partial z}$ which acts on the wave function standing behind. The operator can be expressed with spherical coordinates in the following way:

$$\frac{\partial}{\partial z} = \cos(\theta) \frac{\partial}{\partial r} - \frac{\sin(\theta)}{r} \frac{\partial}{\partial \theta} \tag{4.14}$$

The radial derivation can be done analytically only for the Slater wave function case. In the packet wave function case we use an analytic derivative of the interpolating polynomial or sinus function. The angular derivation means no problem for any wave function. The general formula reads:

$$\frac{\partial}{\partial z} \left[\phi(r) Y_{l,m}(\theta, \varphi) \right] = \cos(\theta) \cdot Y_{l,m}(\theta, \varphi) \frac{\partial}{\partial r} \phi(r) - \frac{\phi(r)}{r} \cdot \sin(\theta) \frac{\partial}{\partial \theta} Y_{l,m}(\theta, \varphi) \tag{4.15}$$

In [Edm63] there are two useful formulas for the angular part:

$$\cos(\theta)Y_{l,m} = \sqrt{\frac{(l+1)^2 - m^2}{(2l+1)\cdot(2l+3)}} \cdot Y_{l+1,m} + \sqrt{\frac{(l)^2 - m^2}{(2l-1)\cdot(2l+1)}} \cdot Y_{l-1,m} \tag{4.16}$$

and

$$-\sin(\theta)\frac{\partial}{\partial\theta}Y_{l,m} = (l+1)\sqrt{\frac{(l)^2 - m^2}{(2l-1)\cdot(2l+1)}} \cdot Y_{l-1,m} - l \cdot \sqrt{\frac{(l+1)^2 - m^2}{(2l+1)\cdot(2l+3)}} \cdot Y_{l+1,m} \tag{4.17}$$

With the help of these relations and with the first derivative of the Slater function a long and complicated formula can be achieved for the cases where the ket function is a Slater one. From the last two formulas it is clear that this interaction gives contribution only between different angular momentum states.

4.2.3 Symmetries

The calculation of the matrix elements is time consuming that is why it is essential to take advantage of all the symmetry properties. The matrix elements with Liènard-Wiechert potentials have three different symmetry properties:

- time reversal symmetry
- azimuthal symmetry
- symmetry in the magnetic quantum numbers

With the proper usage of all these symmetries the calculation time can be reduced drastically, already the time-reversal symmetry helps us to save up 50 percent of the calculations. The exploitation of the symmetry in the magnetic quantum numbers for the $l = 1$ angular momentum matrix elements gives us a further 30 percent shrinkage of the calculation. In the case of $l = 2$ this setback is even more.

Time reversal symmetry

Here we show that the matrix elements for positive and negative times are the same up to a sign. We show the prove for the scalar potential term only:

$$\langle\phi_1(\vec{r})|\Phi(\vec{r},t)|\phi_2(\vec{r})\rangle = \gamma Z_p \int_{\vec{r}} \frac{\phi_1^*(\vec{r})\phi_2(\vec{r})}{\sqrt{(x-b)^2 + y^2 + \gamma^2(z - v_p t)^2}} d^3\vec{r}_1 \tag{4.18}$$

Time reversal means: the sign of $v_p t$ will change from minus to plus in the denominator. To see what happens after this operation we have to transform the matrix element back to the initial form. Let us use Cartesian coordinates and introduce the following substitution:
$z \to -z, \quad dz \to -dz, \quad$ and $\quad t \to -t$

$$\int_{-\infty}^{\infty} F(x,y,z,-t)dt = -\int_{\infty}^{-\infty} F(x,y,-z,-t)dz \tag{4.19}$$

After this transformation the sign of the z coordinate of the wave function also changes to $\phi(x,y,-z)$. In the language of spherical coordinates this simply means the following:

$$(r,\theta,\varphi) \xrightarrow{z\longrightarrow -z} (r,\pi-\theta,\varphi) \tag{4.20}$$

If we mirror a vector on the xy plane, then only the θ coordinate changes. With the help of the well known parity transformation: [Bra83]

$$Y_{l,m}(\pi-\theta,\varphi+\pi) = (-1)^l \cdot Y_{l,m}(\theta,\varphi) \tag{4.21}$$

and with the former transition $z \to -z$ we get:

$$Y_{l,m}(\pi-\theta,\varphi) = (-1)^l \cdot Y_{l,m}(\theta,\varphi) \cdot \underbrace{e^{-im\pi}}_{=(-1)^m} = (-1)^{l+m} \cdot Y_{l,m}(\theta,\varphi). \tag{4.22}$$

The full matrix element for $V(\vec{r},t) = \hat{V}_1 + \hat{V}_3$ after all:

$$\langle\phi_1(\vec{r})|V(\vec{r},-t)|\phi_2(\vec{r})\rangle = (-1)^{l_1+l_2+m_1+m_2}\langle\phi_1(\vec{r})|V(\vec{r},t)|\phi_1(\vec{r})\rangle \tag{4.23}$$

This relation is valid for the real operators: $\hat{V}_1,\ \hat{V}_3$. For the **complex** operators as: $\hat{V}_2,\ \hat{V}_4$ an extra -1 enters in the exponent.

$$\langle\phi_1(\vec{r})|\hat{V}_2(\vec{r},-t)|\phi_2(\vec{r})\rangle = (-1)^{l_1+l_2+m_1+m_2+1}\langle\phi_1(\vec{r})|\vec{V}_2(\vec{r},t)|\phi_2(\vec{r})\rangle \tag{4.24}$$

The cause of this is the existence of the first derivative in $\hat{V}_1(\vec{r},t)$. In $\hat{V}_3(\vec{r},t)$ the numerator contains an extra $(z-v_p t)$ term which needs another identity transformation:

$$(-z+v_p t) = -(z-v_p t) \tag{4.25}$$

With the help of this symmetry relation the matrix elements are easily calculated for negative time.

Azimuthal-symmetry of the matrix elements

To show the azimuthal-symmetry of the matrix elements let us use now spherical coordinates for the distance $R(t)$ given in the interaction:

$$R(t) = \sqrt{(x-b)^2 + y^2 + \gamma_p^2 (z - v_p t)^2} = \sqrt{(r\sin\theta\cos\varphi - b)^2 + (r\sin\theta\sin\varphi)^2 + \gamma_p^2 \cdot (r\cos\theta - v_p t)^2} \tag{4.26}$$

The sinus and cosines functions are periodic to 2π:
$\cos(2\pi - \varphi) = \cos(\varphi)$ and $\sin^2(2\pi - \varphi) = \sin^2(\varphi)$ therefore $R(t)$ is symmetric to $\varphi = \pi$.
The φ dependence of the wave function part of the matrix element reads:

$$f(\varphi) = e^{i(m_1 - m_2)\varphi} \tag{4.27}$$

which has a symmetric real and and antisymmetric imaginary part. The matrix elements with the operators: $\hat{V}_1, \hat{V}_3, \hat{V}_4$ are symmetric to $\varphi = \pi$ and the complex part is antisymmetric. The imaginary part gives zero after all, and needs no integration. The $\hat{V}_2$ contains four parts like $\hat{V}_1$ and has the same property as the other three. (This symmetry enhances the accuracy e.g. integration routines in general produce better results when the used interval is smaller.)

Symmetry of the magnetic quantum numbers

Choosing the coordinate system mentioned above gives us a further symmetry. A symmetry between matrix elements with positive and negative magnetic quantum numbers. There is a formula which connects the spherical harmonics with positive and negative magnetic quantum number:

$$Y^*_{l,m} = (-1)^m \cdot Y_{l,-m}. \tag{4.28}$$

It we apply this to our matrix elements then we get the following:

$$\langle \phi_{m_1} \left| \hat{V} \right| \phi_{m_2} \rangle = (-1)^{m_1 + m_2} \langle \phi_{-m_2} \left| \hat{V} \right| \phi_{-m_1} \rangle. \tag{4.29}$$

For **p** single-particle wave functions 30 percent of the integrals can be saved, for **d** functions it is 40 percent.

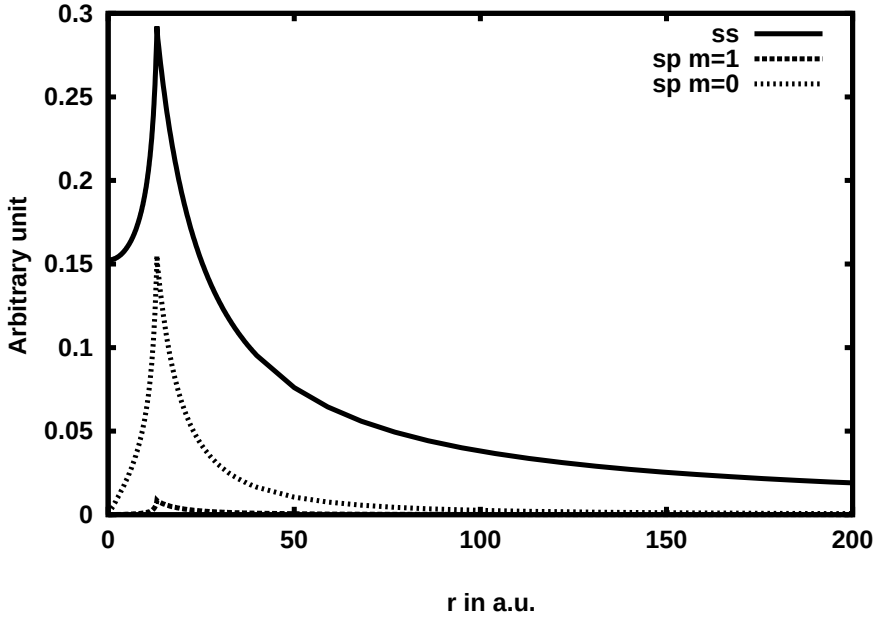

Figure 4.2: Different multipoles for b= 1.6 a.u, t= 0.8 a.u and $\gamma = 3.1$. The solid line is for l=0 transitions, the dotted line is for s-p transition with m=0 and the dashed line is for s-p transition with magnetic quantum number difference m = 1.

4.2.4 The angular integration

The Liénard-Wiechert potential matrix elements have an angular dependence and that means a threefold integrations for every time point and for every impact parameter. Without any tricks even a Slater-Slater matrix element took some seconds on a modern workstation in the year of 2001. The general package-package matrix element is rather not to mention (10-25 seconds!). In a realistic calculation when the number of the matrix elements is in the magnitude of ten thousands (or even more) this method breaks down.

In the following I will show, that the angular integration can be 'pulled out' from every matrix element at every different time point and impact parameter.

Different methods can be applied to solve this problem, one of them is used in [Bal91]. This is a multipole decomposition, the method is too complex to implement in our calculation. This method was successfully applied for pair-productions. [Gai01]. Another multipole expansion method can be found in [Meh89].

In most of the cases the φ integration can be done analytically which is also a great help. Now I show how it can be done. Let us look at the term:

$$\hat{V}_1(\vec{r},t) = -\gamma_p Z_p \left[\frac{1}{R_1(\vec{r},t)}\right]. \tag{4.30}$$

The corresponding matrix element has the form:

$$\langle\phi_1(\vec{r})|\hat{\Phi}(\vec{r},t)|\phi_2(\vec{r})\rangle =$$

$$-\int_0^\infty\int_0^{2\pi}\int_0^{\pi} \frac{\gamma_p Z_p \phi_1(r)\phi_2(r) Y^*_{l_1,m_1}(\theta,\varphi) Y_{l_2,m_2}(\theta,\varphi)\sin(\theta)}{\sqrt{(r\sin(\theta)\cos(\varphi)-b)^2+(r\sin(\theta)\sin(\varphi))^2+\gamma^2(r\cos(\theta)-v_p t)^2}} d\varphi d\theta r^2 dr. \tag{4.32}$$

Let us concentrate only on the φ dependence. After some algebraic manipulation the φ integral has the following form:

$$\int_0^{2\pi} \frac{h(r,\theta)\cos((m_2-m_1)\varphi)}{\sqrt{f(b,r,\theta)-g(b,r,\theta)cos(\varphi)}} d\varphi. \tag{4.33}$$

The $h(r,\theta)$, $f(r,\theta,b)$ and $g(b,\theta)$ are functions but behave like constants in the φ integration. The numerator has a simple cosines dependence remaining from the spherical harmonics due to the symmetry. The given integral is the Elliptic Integral of the First Kind [Abr70]. For the simplest case where both wave functions are **s** functions, the result is the following:

$$4\frac{\text{Elliptic}K(-\frac{2g(b,r,\theta)}{f(b,r,\theta)-g(b,r,\theta)})}{\sqrt{f(b,r,\theta)-g(b,r,\theta)}} h(r,\theta) \tag{4.34}$$

The properties of the EllipticK function can be found in [Abr70]. This result looks nice, but there are several problems with it:

- the θ integrand becomes complicated hence it can not be done analytically,(two further numerical integrations remain),
- to get a good routine to calculate the EllipticK function up to $\pi/2$ is hard, convergence problems emerge at the upper border,
- for different spherical harmonics $Y(\theta,\varphi)_{l,m}$ the integral has a different form, containing more and more terms,
- not only $\hat{V}_1(\vec{r},t)$ but also the $\hat{A}^2$ term is needed. This gives much more complicated formulas.

Due to these problems, we don't use this method. We simply follow the easiest way and integrate the two variables numerically.

$$\text{Multipole}(r,\gamma,b,t) = \int_{\Omega} \frac{Y_{l_1,m_1}(\theta,\varphi)^* \cdot Y_{l_2,m_2}(\theta,\varphi)}{R(r,\theta,\varphi,\gamma,b,t)} d\Omega \tag{4.35}$$

We use s, p, d single-particle wave functions as already mentioned. Considering all the different angular and magnetic quantum numbers for both wave functions (keeping out the symmetries), 45 different cases emerge. Some of them contributes quite small, e.g.:
$\langle\phi(\vec{r})_{l=2,m=-2}|\hat{\Phi}(\vec{r},t)|\phi(\vec{r})_{l=0,m=0}\rangle$. The two spherical harmonics in the matrix elements are orthogonal to each other but the Coulomb term between makes a small modification at 'not so small' distances; due to this, a small contribution remains. When both spherical harmonics are the same the corresponding integral will be the largest. Figure 4.2 shows three different multipole moments equ. 4.35 for physically relevant parameters. The solid line is for s-s transitions the dotted line corresponds to s-p transitions with magnetic quantum number m=0 and the dashed line corresponds to s-p transition with m=1. The maxima lies at $r_{\max} = \sqrt{b^2 + \gamma^2 \cdot (v_p \cdot t)}$ and becomes 'peaky' as γ gets larger. The presented moments are for collision with $\gamma = 3.14$. The figure shows multipole momentums only for the $\frac{1}{R(\vec{r},t)}$ dependent operators such as $\hat{V}_1$ and for $\hat{V}_2$; the remaining two have a different dependence and give negligible contributions. The most accurate calculations are needed for small t and b when $r_{\max} \approx r_{\text{Atomic Radius}}$

4.2.5 The radial integration

As we mentioned before three different kind of matrix elements exist, namely:
1, Slater-Slater type,
2, Slater-Coulomb package or Coulomb package-Slater like and
3. the pure package-package like.
The interaction matrix elements scale with Z_{proj} only, and those with $\hat{V}_3$ scale with Z^2_{proj}. Due to this only one projectile charge is needed to calculate at a given collision energy. This is usually the proton.

Let us now discuss the integrals and start with the first case:
The Slater functions are positive at any distance so the matrix elements conserve their sign. The Slater functions have an exponential decay, which gives no contributions for larger distances. The range of the integrals can be limited to $r_{max} = 50$ a.u. since for usual screening constant κ we have $e^{-(\kappa 1+\kappa 2)r} < 10^{-6}$ otherwise. The multipole momentum function which was discussed above is a peaky function with

changing properties. For huge time it is flat and the maximum lies out of the r_{max} range. This means no interactions. The time-dependent matrix elements for some fixed impact parameters have a nice decaying property. Thirty different time points are enough for every impact parameter.

The second matrix elements are the mixed type. The range is enhanced compared with the former case, but not much. The package wave function has a long oscillating tale which can be seen when the screening factor is small (the damping is also small). The $\tilde{Z} = 2$ matrix elements are always smaller than the $\tilde{Z} = 1$ ones due their larger oscillatory behavior.

The third type is when both radial wave functions are the Coulomb packages. These are of the hardest type to calculate properly. When the energy difference is large, then the knots are not far from each other and many oscillations come into play. Due to their slow decay even the far distance Coulomb interaction gives relevant contributions. The highly energetic wave functions oscillate rapidly and for small distances small time steps have to be taken. The figure 4.3 shows the radial dependence of two different package-package matrix elements for a given impact parameter. The solid line shows a matrix element where both packages have the same parameters. The result looks like the density of an ionized electron multiplied with a peaky multipole momentum showed above. This gives a global minimum of the integrand. The whole integrand has a minus sign. The dashed line presents an even interesting interaction. The two packages are different in energy and width. According to this a further envelope oscillation comes up and the integrand becomes even positive at some distances.
The matrix elements give non-vanishing contributions even for large projectile-target distances due to the long Coulomb tail. The matrix elements containing only Coulomb wave packages have different signs. The channels which contain this kind of matrix elements have a much larger amplitude diversity than the channel containing only Slater-Slater matrix elements.

For a not-so-modest basis calculation, which means more then two hundred channels, many ten thousands of three dimensional integrals have to be calculated.

4.2.6 The symmetry of the channels

With the help of the matrix elements the whole coupling matrix is built up. Due to the different symmetries of the matrix elements the channels have different symmetries in time also. The figure 4.4 shows two basically different channels. The solid line is the third channel which is the 3^1S state; it is a bound state without oscillations, and has an even parity. Contrary to this the dashed line shows the channel 119. with $E = 0.414$. This is an $L = 1$ single-ionized state with magnetic

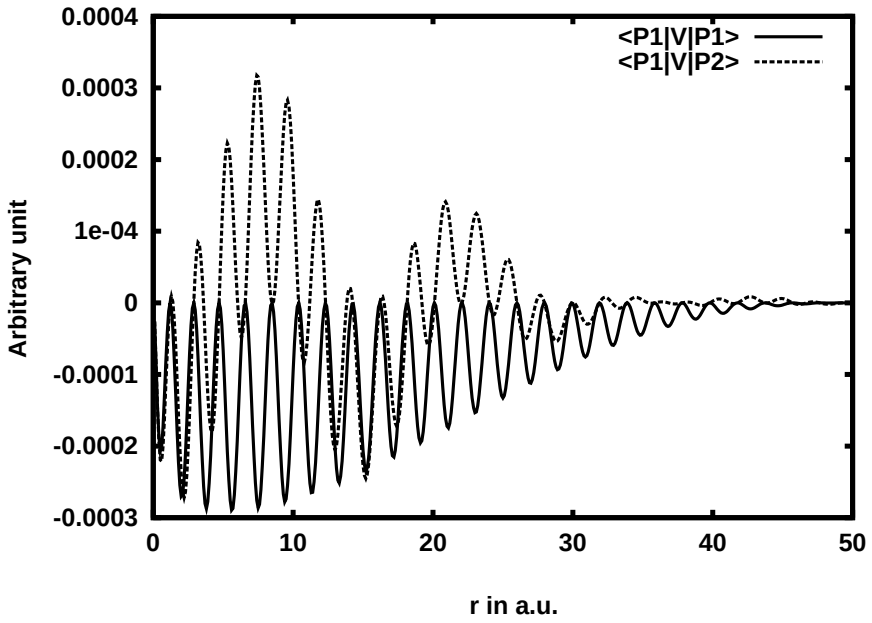

Figure 4.3: Typical radial integrands of the package-package matrix elements, the two packages P1 and P2 have different energies.

quantum number m=+1, hence has odd parity. This is a favorable low energetic single-ionized channel with oscillating behavior.

4.2.7 The question of different interaction operators

The rigorous usage of the minimal coupling gives us four interaction terms as: $\hat{\Phi}$, $\hat{A}^2$, div$\hat{A}$, $\hat{A}\hat{p}$. The $\hat{A}\hat{p}$ gives further four terms as was shown before. Inclusion of all these terms without any approximation makes the whole calculations enormous even on many powerful workstations. Let us calculate now the number of the matrix elements for the basis given above:
We have 13 s, 12 p and 8 d single-particle wave functions. Due to the magnetic quantum number dependence the **sp** transitions give three channels and the **sd** transitions five. Note that this number becomes larger for further **pd** and **dd** transitions. Define now: $N = (13s + 12p*3 + 8d*5)$. The number of the matrix elements (using the hermiticity or antihermiticity) for a given time and impact parameter is: $7 * N * (N + 1)/2 = 7 * 4005 = 28035$ The factor seven stands for the different interactions shown above. To obtain sufficient accuracy the whole calculation has to be repeated for different time points and impact parameters. An example for eight different impact parameters with 25 time points each $25 * 8 * 28035 = 5.607.000$ numerical integrations are needed.

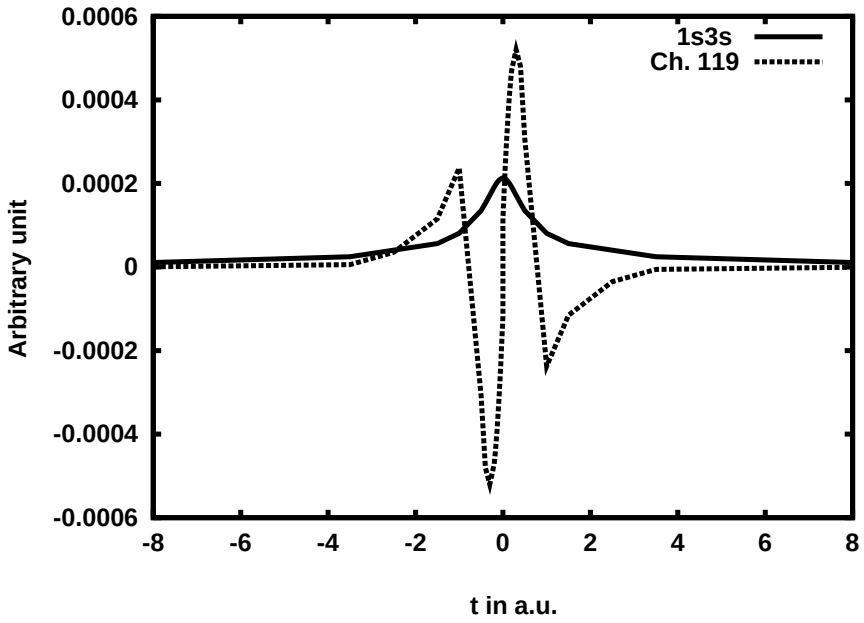

Figure 4.4: The time-dependence of different channels with different symmetries. The solid line shows the time-dependence of the 3^1S channel, the dashed line is a single-ionized $L = 1$ channel (E =0.414 a.u.).

A former study [Pfe99] obviously says that the scalar therm $\hat{\Phi}(\vec{r}, t)$ is the only contributing term in the range of small gamma values $\gamma \leq 3.1$ All the other three interaction term can be neglected in this situation. In our case the highest energy is 1 Gev/nucleus which corresponds to $\gamma = 2.07$. We used only the scalar term in our calculations. Only in the highly charged uranium case was the $\hat{A}^2$ term taken into account; this term scales with Z^2_{Proj} and we wanted to test this contribution. Even in this case this interaction can be neglected.

4.3 Time-evolution

After having built up the coupling matrix the resulting differential equation system has to be solved. The first order perturbation theory is a special case of the coupled-channel equation, namely by considering only the first row. This row contains the transition matrix elements from the ground state to the final state.

The following pictures 4.5 and 4.6 show how the absolute square of the probabilities is changing in time. We consider the collision of helium with 500 MeV/amu Kr^{36+} projectile at an impact parameter b=5 a.u. The first figure 4.5 shows the probability of the ground state, which starts from unity and reaches a finite value after the

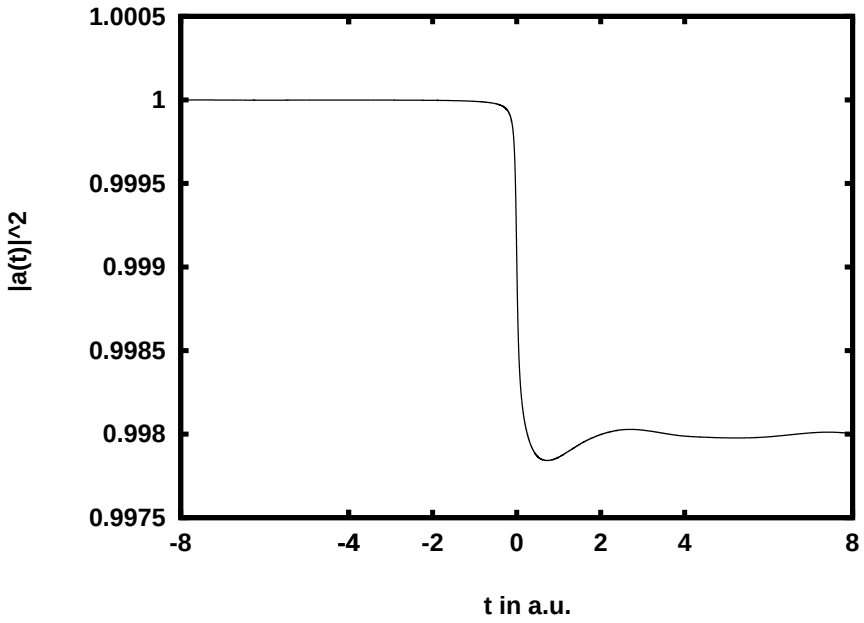

Figure 4.5: A time evolution of the ground state along the collision process. The projectile is 500 Mev/amu Kr^{36+}, the impact parameter is $b = 5$ a.u.

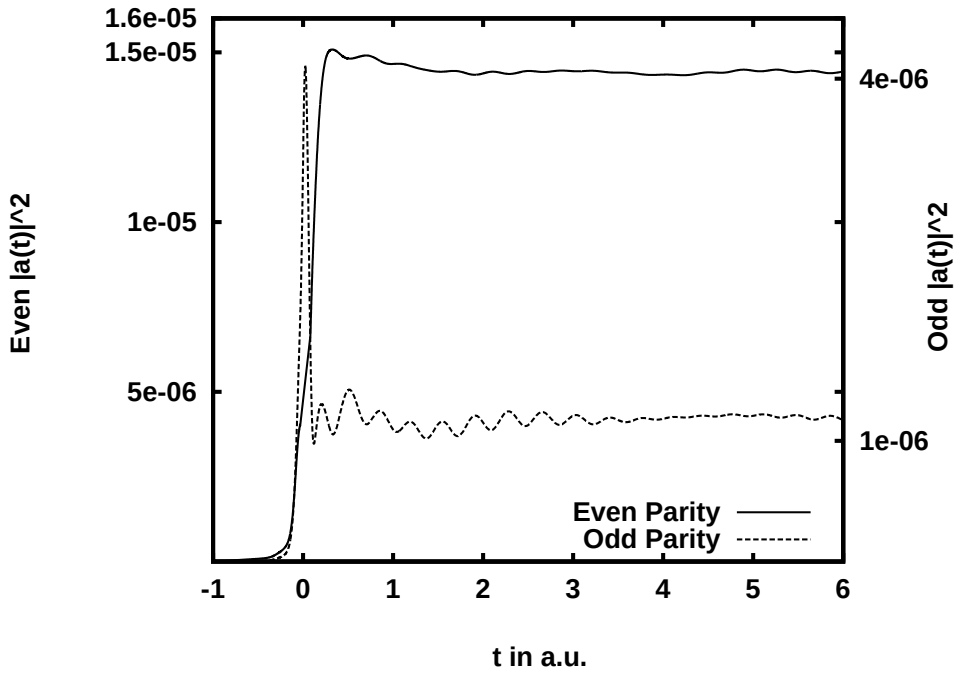

Figure 4.6: A typical time evolutions of two single-ionized channels along the collision process with different symmetries. The solid line shows a channel with even and the dashed line with odd parity. The energy of the channels is $E = -0.454$ a.u. the total angular momentum is $L = 1$, collisions system is the same as above.

collision. The second figure 4.6 shows how the population of different channels (Channel 82 and Channel 83) with different symmetries changes in time. These channels have the same energy $E = -0.454$ and total angular momenta $L = 1$. The solid line shows a channel with even parity and the dashed line shows a channel with odd parity.

To solve the differential equations we used a fifth order Runge-Kutta-Fehlberg formula which automatically adjusts the smallest time step [Sch86]. The coupling matrix was interpolated with a quadratic spline to enhance the accuracy [Pre86]. The only handicap of this method is the enormous memory claim. The whole coupling matrix is needed at all calculated time points at a given impact parameter. This condition limits the number of channels to 300-500.

The conservation of the norm is always fulfilled, and differs only 10^{-8} from unity after about 50000 time steps.

The whole time integration is a quick numerical process compared with the matrix element calculation.

It is worth to mention, that for different impact parameters different time intervals are needed to get the asymptotic ($t \longrightarrow \infty$) coupling matrices. At small impact parameters the amplitudes are very sharp and have a quick decay (short range), contrary for large impact parameters the amplitudes are very small but decay slowly. This means that for large impact parameters less time points are enough to get satisfying accuracy but for small impact parameters the number of time steps must be much higher. When we include packages in our basis, then for small impact parameters $b \approx r_{atom}$ the t=0 region becomes very sensitive and needs more time points than the pure Slater basis set.

In ionization we only need to represent the soft electron continuum sufficiently, contrary to pair production calculations where the high energetic electrons and positrons are also important [Gai01]. The high energetic packages oscillate very rapidly and the coupling matrix must be calculated very densely in time. In our case when k_{max} is lower than 4-5 a.u. then no extra time step is needed for the packages.

4.4 The impact-parameter integration

After having done the time-evolution, we have the probabilities for the different channels. To get the total cross sections we finally have to integrate over the impact parameter:

$$\sigma_k = 2\pi \int_0^\infty b P_k(b, t \to \infty) db \tag{4.36}$$

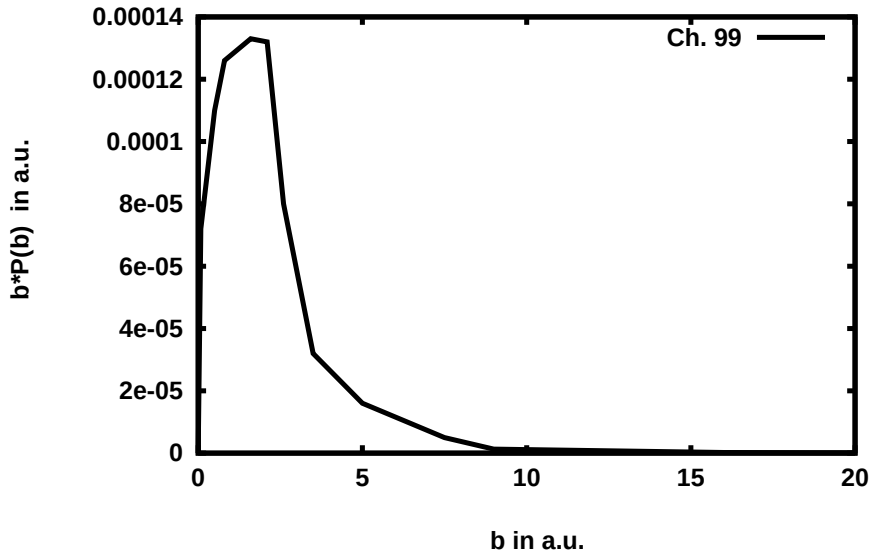

Figure 4.7: A typical $bP(b)$ dependence.

To reach a satisfactory accuracy, 8-11 different impact parameter are needed. A typical set of impact parameters(in a.u.) is:
$b\{0.003,\ 0.008,\ 0.5,\ 1.6,\ 2.6,\ 5,\ 9,\ 16,\ 30,\ 90\}$
For the uranium case we used an extra b= 200 a.u. impact parameter. The maximum of the integrand lies between $2-10$ a.u. for helium, depending on the channel. When the impact parameter is as large as the atomic radius then the distance between the electrons and the projectile is minimal, hence the weighted ionization probability is the greatest. The maximum impact parameter needed depends on the energy.
For $\gamma \approx 1 \quad b_{\max} = 30$, for higher values of γ-s $b_{max} = 200$ is needed. A typical $bP(b)$ function is shown in figure 4.7.
For the single-ionized channel (Ch. No. 99) E=0.064 a.u. for a 2.31 MeV/amu alpha projectile. The function has one maximum and then an exponential decay. The single- or double-ionized states have a longer tail than the bound states. As it was mentioned before, after the impact parameter integration all the channel cross sections are multiplied with the probabilities for the separation in excitation, single- and double-ionization (which are the results of the projection) and then summed up.

Chapter 5

Results

In this chapter, we present our results and discuss them.

At first the numerical routines had to be tested. The test of the diagonalization was already mentioned.

The test of the scattering calculations is much more difficult, because all the three calculations (coupling matrix, time evolution and impact parameter integration) must be correct and only the final results, the cross sections, are what one can compare with other theories or experimental data.

To make the test calculations easier we calculated only some well known excitation cross sections. The following table VIII shows some state-selective excitation cross sections for proton helium collision at a given energy.

Experimental data ([Hip74])		Results of coupled-channel calculations
$E_p = 1.0$	MeV	
$\sigma(2^1P)$	4.91	4.72
$\sigma(3^1P)$	1.26	1.31
$\sigma(4^1P)$	0.53	0.54

Table VIII. State-selective cross sections (in 10^{-18} cm^2) for proton helium collision.

It is worth to mention, that the results above are independent of the usage of any packets. We made two calculations at first with Slater basis functions without packages and after this with the packets. The deviation between the two calculations are only one or two percent.

After this we went further to a system which was calculated before but only with Slater basis functions.

The low energy proton-helium collision is a benchmark to test and compare different theories. We choose a projectile velocity of $v_p = 12\ a.u.$ corresponding to E = 3.6 MeV. The Massey-Parameter is $Z_p/v_p = 0.08$ which lies in the perturbative region. The table IX. shows different results for this system. The presented experimental value was interpolated between two measured data from [Sha85]. The first row gives the kind of the calculation. The first calculation is a coupled channel calculations, which was done without packages. The second is a bit modified including some wave packages. The third one is our calculation with the basis discussed. The last three results come from FIM perturbation calculations. The 9s9p means the applied basis. The FIM method was briefly discussed in the first Chapter.

Art of result:	Single-Ion.	Double-ion.	Ratio
	$\sigma^+(10^{-19})cm^2$	$\sigma^{++}(10^{-21})cm^2$	(10^{-3})
Exp. value [Sha85]	70.7	19.2	2.71
CC Calc.[Pfe99]	58.58	6.59	1.12
[Pfe99]+ 6s4p Packet	*65.20*	*16.03*	*2.46*
Our basis	**66.52**	**18.66**	**2.80**
FIM [For94] 9s9p	62.45	12.24	1.96
FIM [For94] 9s9p5d	68.2	23.69	3.03
FIM [For94] 9s9p9d	70.0	18.9	2.70

Table IX. Different calculations for the 3.6 MeV/amu proton helium collision system.

We chose this energy to study the effect of the packages. We can see the very nice convergence behavior of the different calculations. Without any Coulomb wave packages [Pfe99] the double continuum is badly approximated. As we apply some packages even without **d** functions the double ionization cross sections become reasonably higher. With the help of **d** functions our calculations become more realistic and come closer to the experimental value.

The Forced Impulse Method calculations from Ford and Reading are more accurate including more than a thousand states. The FIM calculations were done at 3 MeV which we interpolate to get comparable data at E=3.6 MeV. In this perturbative region the cross sections can be interpolated with a straight line.

After this calculation we made a calculation for the antiproton helium system. The results are in Table X. The basis and the projectile energy remains the same, only the sign of the matrix elements were changed. The understanding the difference between the proton and antiproton collision is an open problem since long time. There are many calculations (and also measurements) available for the proton-helium and antiproton-helium collision system. More on this see [Knu92].

Our results are as good as for the proton case.

Art of result:	Single-Ion.	Double-ion.	Ratio
	$\sigma^{+}(10^{-19})cm^2$	$\sigma^{++}(10^{-21})cm^2$	(10^{-3})
Exp. value [Hve94]	70.08	27.9	3.98
Our Basis	**66.11**	**25.12**	**3.7**
FIM [For94] 9s9p	62.01	15.5	2.50
FIM [For94] 9s9b5d	68.2	28.6	4.2
FIM [For94] 9s9b9d	70.04	27.7	3.96

Table X. Different calculations for the 3.6 MeV/amu antiproton helium collision system. The notation is the same as before.

After exhaustive tests we choose some systems which were also investigated in experiments.

1. U^{92+} with 1GeV/amu [Mos97]
2. U^{90+} with 60,120,420 MeV/amu [Ber92b]
3. Kr^{36+} with 1GeV/amu and 500 MeV/amu [Ber92a]
4. C^{6+} with 100MeV/amu [Bap98]
5. He^{2+}, Li^{3+}, B^{5+} and C^{6+} with 2.31 MeV/amu [Knu84]

These collisions cover the whole range from light to very heavy projectiles.

For systems where the projectile fields are not so strong, even the first Born approximation gives good results. There is a scaling rule of the first Born cross sections for the single-ionization:

$$\sigma \propto bP(b) \propto |a|^2 \propto |\langle\phi|\frac{Z_{Proj}}{R(b)}|\phi\rangle^2 \cdot \propto Z^2_{Proj}. \tag{5.1}$$

The last four projectiles have the same energy which means that it is sufficient to make the first order calculations only for one projectile. It is worth to mention that the coupled-channel method does not have this scaling property.

The following three tables XI., XII. and XIII. show the single- and double-ionization total cross sections and the ratio for the above mentioned systems. The tables contain the energy of the projectile, the corresponding γ value and the Massey-parameter Z_p/v_p which is the ratio of the charge to the velocity of the projectile. This quantity was already analyzed in the first chapter. The table additionally contains the experimental values of the total cross section and the results of the coupled-channel calculations (C. C.) and the first order Born approximation. For the first three systems (1.,2.,3.) the perturbation can not be applied since the Z_p/v_p ratio is too high.

Table XI. Single-ionization total cross sections (σ^{+}):

Proj.	Energy MeV/amu	γ	v amu	Z/v amu	Exp. value $[10^{-16}cm^2]$	C. C. $[10^{-16}cm^2]$	I. Born $[10^{-16}cm^2]$
U^{92+}	1000	2.07	120.01	0.76	7.4 ± 30 %	4.8	12.1
U^{90+}	60	1.06	46.58	1.92	$13\ -77\% + 150\%$	9.25	35.3
U^{90+}	120	1.12	63.43	1.41	$38\ -50\% + 190\%$	18.6	28.2
U^{90+}	420	1.45	98.64	0.91	$9.8\ -70\% + 200\%$	12.1	21
Kr^{36+}	500	1.53	98.71	0.36	$0.9\ -50\% + 50\%$	1.09	6.5
Kr^{36+}	1000	2.07	120.01	0.30	$0.72\ -50\% + 50\%$	0.9	5.9
C^{6+}	100	1.1	58.76	0.1	0.1 ±30%	0.097	0.11
He^{2+}	2.31	1.002	9.65	0.20	0.44 ± < 5 %	0.40	0.46
Li^{3+}	"	"	"	0.31	0.98 ± < 5 %	0.90	1.038
B^{5+}	"	"	"	0.51	2.44 ± <8 %	2.11	2.88
C^{6+}	"	"	"	0.62	3.3 ± < 8 %	3.05	4.15

Table XII. Double-ionization total cross sections (σ^{++}):

Proj.	Energy MeV/amu	γ	v amu	Z/v amu	Exp. value $[10^{-16}cm^2]$	C. C. $[10^{-16}cm^2]$	I. Born $[10^{-16}cm^2]$
U^{92+}	1000	2.07	120.01	0.76	0.15 ± 30 %	0.14	0.52
U^{90+}	60	1.06	46.58	1.92	$0.9\ -70\% + 200\%$	0.56	2.4
U^{90+}	120	1.12	63.43	1.41	$1.8\ -50\% + 100\%$	0.7	2.8
U^{90+}	420	1.45	98.64	0.91	$0.3\ -70\% + 200\%$	0.57	1.46
Kr^{36+}	500	1.53	98.71	0.36	0.016 ±50%	0.010	0.07
Kr^{36+}	1000	2.07	120.01	0.30	0.011 ±50%	0.012	0.016
C^{6+}	100	1.1	58.76	0.1	0.00026 ±30%	0.00022	0.0003
He^{2+}	2.31	1.002	9.65	0.20	0.0022 ± < 10 %	0.0026	0.003
Li^{3+}	"	"	"	0.31	0.0085 ± < 10 %	0.0059	0.007
B^{5+}	"	"	"	0.51	0.059 ± < 11 %	0.032	0.015
C^{6+}	"	"	"	0.62	0.092 ± < 11 %	0.15	0.025

Table XIII. The Ratio: $R = \frac{\sigma^{++}}{\sigma^{+}}$

Proj.	Energy MeV/amu	γ	v amu	Z/v amu	Exp. value $[10^{-3}]$	C. C. $[10^{-3}]$	I. Born $[10^{-3}]$
U^{92+}	1000	2.07	120.01	0.76	20.27 $\pm$30 %	29.1	42.9
U^{90+}	60	1.06	46.58	1.92	63 $-40\% + 33\%$	60	67.9
U^{90+}	120	1.12	63.43	1.41	50 $-35\% + 25\%$	37	99.2
U^{90+}	420	1.45	98.64	0.91	30 $-40\% + 33\%$	47.1	69.5
Kr^{36+}	500	1.53	98.71	0.36	17.2	9.1	10.7
Kr^{36+}	1000	2.07	120.01	0.30	14.3	13	2.7
C^{6+}	100	1.1	58.76	0.1	2.6	2.6	2.72
He^{2+}	2.31	1.002	9.65	0.20	5.0 $\pm$ <9 %	6.5	6.5
Li^{3+}	"	"	"	0.31	8.6 $\pm$ < 9 %	6.5	6.7
B^{5+}	"	"	"	0.51	24.3 $\pm$ <9 %	15.1	5.2
C^{6+}	"	"	"	0.62	28.0 $\pm$ <9 %	49.1	6.32

To visualize the agreement and the discrepancy between the different theories and the experiment it is useful to present the scaled cross sections on logarithmic scale shown in Figs. 5.2, and 5.3. The open symbols are theoretical results the full symbols are experimental values. For all our single-ionization results we fitted a regression line. Let us begin to discuss our results now:
Of course we changed the number of used channels a bit to describe different collision systems, the 'one-fits-all' attitude of mind comes to little results. The systems we chose are basically different, fast and heavy charged projectiles produce quicker ionized electrons than the light and slow projectiles. This means that we used extra twenty channels over the $E = 5$ a.u. energy range. For slow and light projectiles the electron spectrum is completely low energetic which means that many channels were taken from the $[0 - 2]$ a.u. double continuum and channels with energy more than 7 a.u. were completely neglected.

In the first four systems the projectiles are fast uranium nuclei which represent a strong perturbation. It is clear that the perturbation theory breakes down. In the second system, the perturbation Z_p/v_p is approximately 2 the discrepancy between the coupled-channel result and the first Born value for the single-ionization is a factor of 8.5. In all the other cases the discrepancy is a bit lower. It is interesting that even for the double-ionization the perturbation theory gives larger results than the coupled-channel calculations. In an earlier work [Pfe99] the double ionization cross sections for strongly interacting systems are always smaller than coupled-channel results due to the poor representation of the double continuum. In the following tables the ratios of partial cross sections are showed. In this strongly interacting case the $L = 1, 2$ contributions are dominant. Only about 10 % come from the

$L = 0$ momenta states. The tables present results only with the scalar term. We did some other calculation with all the other terms, but the results are not much different. It is true that the $\hat{A}^2$ term scales with Z^2_{proj} but γ is still small. For the first projectile system the single-ionization cross section is enhanced by a factor of 5 percent from the tabulated value:
$\sigma_{TabXI.} = 4.8 \cdot 10^{-16} cm^2 \quad \sigma_{\hat{A}^2} = 5.04 \cdot 10^{-16} cm^2$
The first value is from the table and the second one contains the contribution from the $\hat{A}^2$ term. For the double-ionization cross section it is about the same:
$\sigma_{TabXII.} = 0.14 \cdot 10^{-16} cm^2 \quad \sigma_{\hat{A}^2} = 0.16 \cdot 10^{-16} cm^2$
At last some words about the channels were used here.

Figure (5.1) shows the distribution of the channel cross sections in the energy for the 1 GeV/amu Kr^{36+} system. We can see very clearly that the most contributing states are the soft electrons. The energy range from 0-6 a.u. contributes most to the cross section. The contributions decay exponentially in this region. In the higher energy range $[12 - 17]$ a.u. the contributions enhance enormously. This can be explained by the properties of the Slater type functions. They produce highly energetic states which show less oscillating behavior than the states produced with Coulomb wave packages. This states gives us a large contribution to the cross sections but can not be interpreted as physical as the states built from packages. These states remain in the basis in any case. When we look further for higher energy range $E > 20$ a.u. we can see that the contribution of this unphysical kind of states also decay. We present only one channel for $E = 27.38$ a.u. but all the other channels have the same property.

The first four systems are our well-studied candidates. We tried to make calculation with completely angular-correlated wave functions also. This means that we used pp and dd configurations to describe the L=0 states. The essence is that helium ground-state is lowered as was mentioned before. The low energetic continuum becomes much more complicated and the states are a complete mixture of all possible configurations. The unphysical high energetic states due to the disliked behavior of the Slater packets remain. Our result is negative, we could not find a reasonable channel set for our system. The calculated cross sections are much lower than they should be. This remark is only to inform about the complexity of this problem.

Now we carry on with the discussion for the Kr^{36+} projectile. For this system the coupled-channel calculations gives a good result for both cross sections. The used channels are practically the same, the basis is only a bit shifted to the low energetic range which means 4 or 6 extra channels. We used only the scalar term as usual. The first Born approximation works not too well still a factor five exists between the two different results.

For 100 MeV/amu C^{6+} system the coupled channel calculations and the first Born give us the same results. The channels with energy higher than 6 a.u. were com-

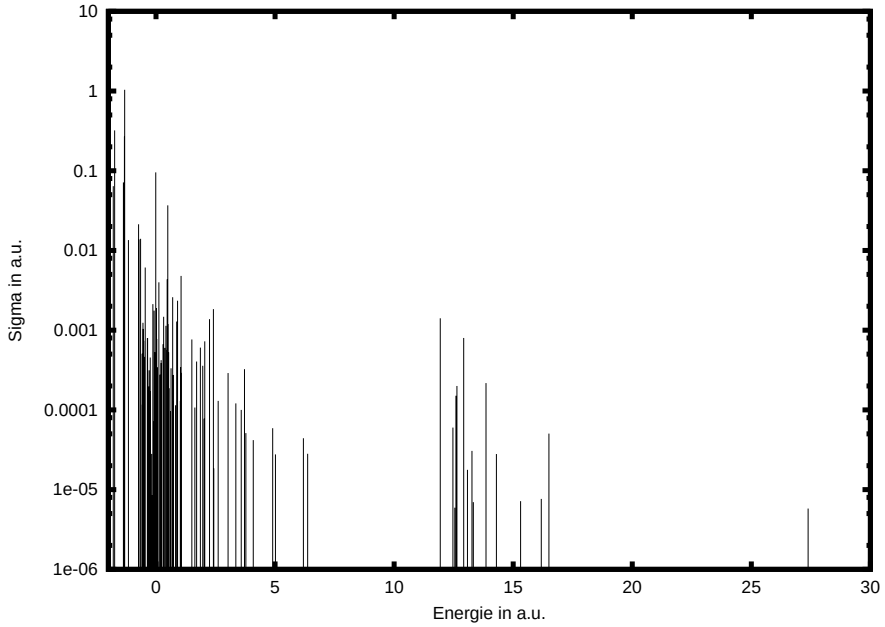

Figure 5.1: The distribution of all the 277 channel cross sections in energy for the 1 GeV/amu Kr^{36+} helium collision system.

pletely neglected.

The last four collision systems have the same energy. The perturbation enhances as the projectile charge increases. The projectile velocity is small, so all the channels with energy larger than 6 a.u. were neglected. The first Born single-ionization cross sections scale as was mentioned above. The coupled-channel results do not.

In figures 5.2 and 5.3 we present our couple-channel results, that give us a better review. The first Born results are not presented. The cross sections are scaled with the charge of the projectile. This helps us to show all our results on the same plot. For the single-ionization we calculated regression line to show the approximate scaling behavior. The equation of the regression is:

$$\lg\left(\frac{\sigma^+}{Z_p}\right) = 3.86 - 0.87\lg\left(\frac{v_p^2}{Z_p}\right) \tag{5.2}$$

Just to compare we cite now the regression line from [Pfe99].

$$\lg\left(\frac{\sigma^+}{Z_p}\right) = 3.63 - 0.78\lg\left(\frac{v_p^2}{Z_p}\right) \tag{5.3}$$

In the equations *lg* means base ten logarithm. We do not present a regression line for the double-ionization cross sections because no linear scaling is verified.

At last the ratios of partial cross sections are presented. The discussion will follow the tables.

Table XIV. Ratios of partial single-ionization cross sections

Proj.	Energy MeV/amu	Z/v	$\frac{\sigma^{+}(L=0)}{\sigma^{+}}$ in %	$\frac{\sigma^{+}(L=1)}{\sigma^{+}}$ in %	$\frac{\sigma^{+}(L=2)}{\sigma^{+}}$ in %
U^{92+}	1000	0.76	8.45	91.42	0.13
U^{90+}	60	1.92	4.37	95.23	0.21
U^{90+}	120	1.41	6.6	93.22	0.18
U^{90+}	420	0.91	9.19	90.66	0.15
Kr^{36+}	500	0.36	10.28	89.62	0.10
Kr^{36+}	1000	0.30	10.39	89.50	0.11
C^{6+}	100	0.1	11.03	88.92	0.05
He^{2+}	2.31	0.20	10.51	89.4	0.09
Li^{3+}	"	0.31	10.39	89.50	0.11
B^{5+}	"	0.51	10.04	89.84	0.12
C^{6+}	"	0.62	9.84	90.02	0.14

Table XV. Ratios of partial double-ionization cross sections

Proj.	Energy MeV/amu	Z/v	$\frac{\sigma^{++}(L=0)}{\sigma^{++}}$ in %	$\frac{\sigma^{++}(L=1)}{\sigma^{++}}$ in %	$\frac{\sigma^{++}(L=2)}{\sigma^{++}}$ in %
U^{92+}	1000	0.76	7.66	91.49	0.85
U^{90+}	60	1.92	4.05	89.39	6.56
U^{90+}	120	1.41	1.53	95.97	2.50
U^{90+}	420	0.91	0.82	98.65	0.53
Kr^{36+}	500	0.36	6.79	92.42	0.79
Kr^{36+}	1000	0.30	1.18	98.75	0.07
C^{6+}	100	0.1	7.21	90.80	1.99
He^{2+}	2.31	0.20	7.78	90.65	1.57
Li^{3+}	"	0.31	6.99	90.19	2.82
B^{5+}	"	0.51	7.75	88.85	3.40
C^{6+}	"	0.62	7.76	87.66	4.58

As we can see the dipole transition is dominant in both ionization processes.
For the single-ionization the trend is clearer: the stronger the interaction the higher the dipole dominance. In the single-ionization case the $L = 2$ contribution is always two magnitudes smaller than the contribution from the $L = 0$ transitions, because that the number of the L=2 transitions channels is not high enough.
The distributions for double-ionization cross sections are not as clear. In some cases the L=0 and 2 partial cross sections are of similar magnitude. We can explain it only when we remember that all the states are classified with a projection onto another Hilbert space. All the states have single and double-ionization and a bound part. The question is the choice of the Hilbert space for projection. If we change this slightly than the cross sections and the angular distributions also change. This uncertainty is about 10-20 percent which is important to mention.

At last a remark on the double-to-single- ionization ratio. It is well known that for proton helium collisions a high energy shake-off limit exists. This value is: $R = 2.5 \times 10^{-3}$ which was already experimentally verified. For heavier systems this limit is still not reached.

We also tried to calculate differential cross sections with respect to the projectile. In the small-angle region the eikonal-approximation is valid for the projectile. This approximation gives us the following formulas for the differential cross section [Bra92][3.232]

$$\frac{d\sigma}{d\Omega} = |f(\theta, \phi)|^2 \tag{5.4}$$

where the amplitude is the Bessel transformed of the solution of the coupled-channel calculations:

$$f(\theta, \phi) = i\mu v_{proj} exp[-i\Delta m\phi](i)^{\Delta m} \int_0^\infty bJ_{\Delta m}(\mu v_{proj}\theta)pdb. \tag{5.5}$$

Here, μ is the reduced mass of the system, v_{proj} is the velocity of the projectile, and Δm is the difference between the magnetic quantum numbers of the bra and the ket state. In our model we use *a priori* the Straight-Line Approximation. Since the projectiles are very heavy, these calculations give nothing new. The differential cross sections contribute only for the forward direction $\theta \approx 0$.

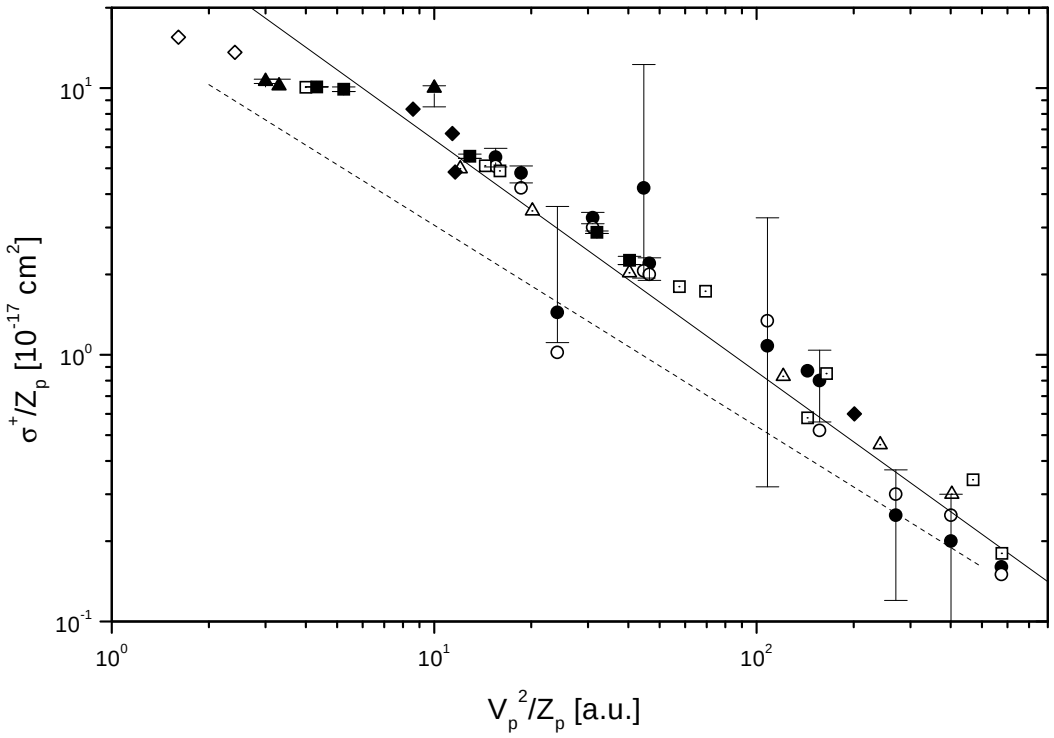

Figure 5.2: Scaled single-ionization cross sections. All the full symbols are experimental data and the open ones are theoretical results. The open circles are our calculations and full circles are the experimental data respectively. The full line is a regression line through our data points (Equ. (5.3)). The dashed line represents the CTMC results by McKenzie and Olson [McK87]. The open triangles and open diamonds are results of FIM calculations of [For94] and of IEV calculations of [For97] respectively for low energy protons. The open squares are close coupling calculations by [Pfe99]. The full diamonds are experimental data from [Knu84] for $2 \leq Z_p \leq 8, \quad 0.13 \leq E \leq 15$MeV/amu. The full triangles are further experimental data from [Ber92a] for the systems: $24 \leq Z_p \leq 92$ up to 1 GeV/amu. The full squares are further experimental results for p^+, He, Li in the energy range: $50 < E < 2380$keV/amu [Sha85]

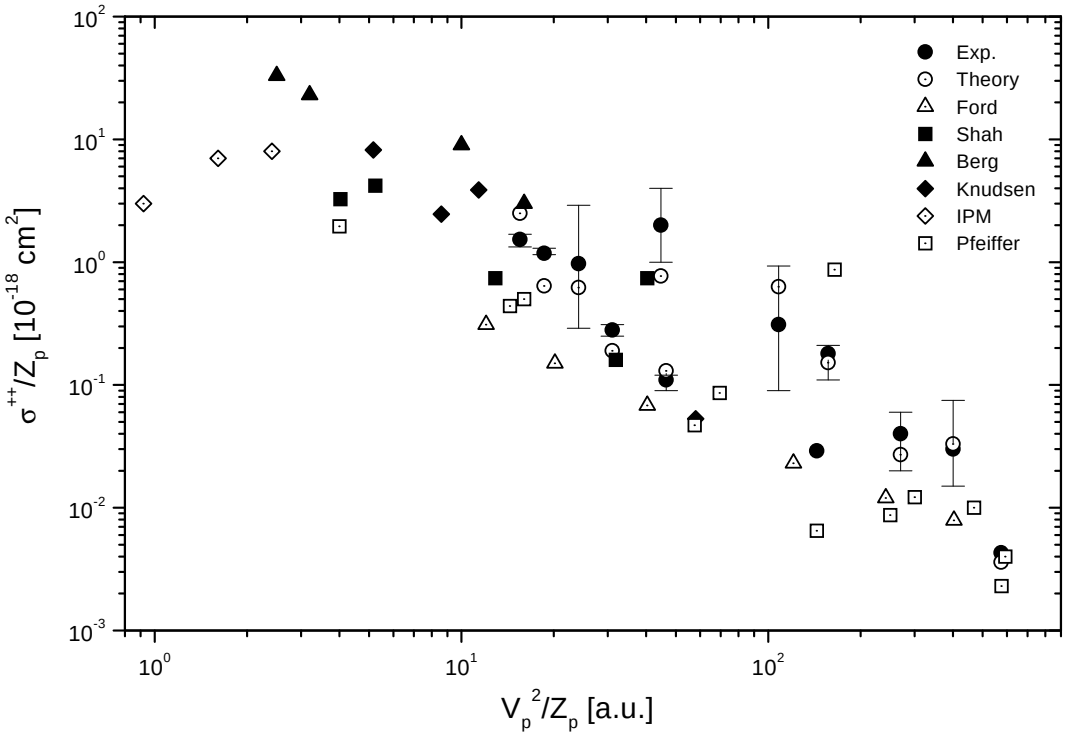

Figure 5.3: Scaled double-ionization cross sections. Notations are as in Fig. 5.2.

Chapter 6

Summary and Outlook

In our work an implementation of the coupled-channel method was presented and was applied to different collision systems. The first chapter gives an introduction and the motivation of this work.
The second chapter shows different theories which can be used to solve different ionization problems.
Chapter 3 shows the spectrum of a two-electron atom (or ion) and how it can be calculated. Physical and technical details were mentioned as well.
The fourth chapter gives a detailed description how the ion-atom collision process can be solved with the help of the coupled-channel or perturbation methods. All the problems which come into play were discussed.
In chapter 5 our results are presented and discussed. We may say that our calculations give a new verification that the one-centre coupled-channel model is a reliable non-perturbative method which gives us quantitatively good results.

The goal of this chapter is to outline the advantages and the disadvantages of the used method and to give further ideas for developments and applications. This will be done in four items:

- **Advantages:**
  The coupled-channel method is a powerful tool to describe ionization and excitation in the strongly coupled interaction region. As some results show the deviation between the experimental and the calculated values can be better than 5 percent. With the help of the straight-line approximation and the minimal-coupling of the Liénard-Wiechert fields the theory is well defined and 'exact' compared to other methods. It does not contain free parameters. The only 'degree of freedom' is the size and the quality of the basis. Of course there are 'technical parameters' emerging in the implementation e.g. the realization of the Coulomb wave packages. Different effective charges or widths are possible.

- **Disadvantages:**
  Even in our times (2001) to calculate numerically some hundred thousands of three dimensional integrals 'is a problem'. The accuracy and the complexity of the coupled-channel calculation is the great handicap of the method. The clear classification of the states without any contradiction and 'hand waving' is also an unsolved problem. This kind of coupled-channel method gives us only the total cross sections. Differential cross sections with respect to the ionized electrons are not so easy to calculate in this model.

- **Further development:**
  The real challenge is to make the coupled-channel calculation more quicker. Maybe it is possible with using the multipole approximation for the Liénard-Wiechert potentials shown in [Bal91]. Sophisticated algorithms can be developed to optimize the number of time points for each impact parameter to reduce computation time. To include spin-orbit interaction would be also interesting but not essential for light systems. To include additional angular-correlations for the wave function is a straightforward development way. The dark side of this development is that the wave functions become more complicated and the classification of the states would be even harder.

  The Lienard-Wiechert potentials can be easily exchanged by other interactions e.g. neglecting retardation, or simply using the dipole approximation. This is a simplification rather than a positive development but would be interesting to test.

  The Coulomb wave packages can be also calculated in another way. Here we simply used non-overlapping neighboring energy intervals. Is is possible to use an envelope function on this interval e.g. a Gauss function. With this trick the corresponding package will show less oscillations which makes the calculation of the integrals easier. Of course the normalization and the overlaps have to be revised. In our case this function is one, all the k values contribute the same in the integral, we have 'average value packages'.

  To calculate angular or energy differential cross sections in respect to the outgoing electron or electrons can be done also.

- **Further application:**
  When the charge of the target is changed (e.q. $Z = 1, 3, 4...$), then ionization of helium-like ions can be easily calculated. H^- as the strongest correlated system would be the first interesting candidate. In this case the basis has to be revised, the screening-factors have to be re-optimized. In the cases with $Z = 3, 4, ...$ the electron-electron interaction is essential. For heavier systems it can be neglected. A detailed study for proton and antiproton helium collision would be essential up to 3 MeV/amu. We did only one test calculation for this

systems as was shown. The most interesting system would be the antiproton H^- collision.

Chapter 7

Zusammenfassung (Summary in German)

Die Ionisation von Helium in Schwerionen- Kollisionen ist ein fundamentales atomphysikalisches Problem. Die gebundenen Elektronen in He-Atom sind stark korreliert. Insbesondere auf den Doppeltionisationsquerschnitt hat diese Korrelation entscheidenden Einfluß.

Im Rahmen dieser Arbeit wurde das Einzentren-Gekoppelte-Kanäle-Modell realisiert und für unterschiedliche Stoßsysteme Rechnungen durchgeführt.

Unter den vielfältigen Modellen zur Beschreibung des Ionisationsprozesses zeichnet sich die Methode der Gekoppelten Kanäle dadurch aus, dass sie die Korrelation vollständig berücksichtigt. Für hochgeladene Projektile und langsame Kollisionen,bei denen das Verhältnis Z_{Proj}/v_{Proj} in der Gröessenordnung 1 ist, liefert die Born'sche Störungstheorie falsche Ergebnisse.

Im ersten Schritt muss man eine Basis wählen und den Helium-Hamiltonoperator diagonalisieren. Unsere Idee war, dass wir nicht nur gebundene Slater-Funktionen, sondern auch reguläre Coulomb-Wellenpakete nehmen, womit wir das Einfach- und Doppel-Kontinuum besser beschreiben können. Wir approximieren die Helium-Wellenfunktion durch eine Summe symmetrisierter Einteilchen-Wellenfunktionen.

Mit ausschließlich Slater-Funktionen kann man praktisch nur die gebundenen Zustände (Grundzustand, einfach und doppelt angeregte Zustände) gut beschreiben. Der Diagonalisationsprozess liefert Pseudo-Zustände, welche als einfach bzw. doppelt ionisiert interpretiert werden können. Diese Zustände haben nicht-lokalisierte Wellenfunktionen mit unendlich vielen Knotenpunkten. Solche Wellenfunktionen sind mit nur gebundenen Funktionen gar nicht oder höchstens sehr schlecht realisierbar.

Wenn man reguläre Coulomb-Wellenpakete in die Basis mit einbezieht, dann liefert die Diagonalisation Zustände, deren wesentlicher Anteil durch diese Pakete gegeben ist. Allerdings müssen diese Zustände noch klassifiziert werden. Nur die Energieeigenwerte und die zugehörigen Elektrondichten anzusehen, ist dazu nicht ausreichend. Testrechnungen zeigen, dass die tiefliegenden einfach ionisierten Zustände einen großen Anteil von angeregten Zuständen haben. Wenn man diese Zustände als rein einfach ionisiert betrachtet, hebt das die Wirkungsquerschnitte unphysikalisch hoch.

Das Klassifikationsproblem haben wir teilweise gelöst. Wir orthogonalisieren unsere Einteilchen-Wellenfunktionen dadurch, dass wir aus Wasserstoff-ähnlichen Einteilchen-Wellenfunktionen die Zweiteilchen-Wellenfunktion aufbauen. Das Wasserstoffatom hat orthogonale gebundene und kontinuierliche Zustände. Wenn ein Zustand energetisch über Null liegt, definieren wir ihn als ionisiert; liegt er unter Null, definieren wir ihn als gebunden. Beim Helium haben wir drei orthogonale Hilbert-Unterräume:
beide Elektronen sind gebunden,
ein Elektron ist gebunden und eines ist ionisiert,
beide Elektronen sind ionisiert.
Diese Klassifikation ist mathematisch nicht streng korrekt, aber sie stellt eine brauchbare Methode dar. Wenn allerdings die Zahl der Coulomb-Wellenpakete wesentlich größer als die Zahl der Slater-Funktionen ist, dann ist diese Närung fast exakt.

Wir projizieren unsere ursprüngliche Helium-Wellenfunktion auf diese neue aus orthogonalisierten Einteilchen-Wellenfunktion aufgebaute Helium-Wellenfunktion. Die quadrierten Koeffizienten liefern die Warscheinlichkeiten für den doppelt gebundenen, einfach ionisierten oder doppelt ionisierten Anteil. Diese drei Anteile müssen zusammen 1 ergeben.

Mit dieser Methode können wir den Vorteil der Konfigurations Wechselwirkung Wellenfunktion ausnutzen. Alle Zustände sind eine Mischung aus allen möglichen Konfigurationen.

Für praktische Rechnungen brauchen wir eine möglichst vollständige Basis.

In dieser Arbeit wurde eine Basis mit s-, p- und d-Funktionen benutzt. Ihre Zusammensetzung aus Einteilchenfunktionen lautet wie folgt:
9 gebundene s-Funktionen, 4 s-Coulombpakete,
4 gebundene p-Funktionen, 6 p-Coulombpakete, und
4 gebundene d-Funktionen, 4 d-Coulombpakete.

Ohne weitere Winkelkorrelationen liefert der Diagonalisationprozess 91 Zustände mit Gesamtdrehimpuls L=0, 156 Zustände mit L=1 und 104 Zustände mit L=2. Mit dieser Basis ist das niederenergetische Kontinuum bis E = 5 a.u. äquidistant bedeckt. Dieses Energieintervall liefert den überwiegenden Beitrag zur Ionisation.

Die Projektil-Potentiale sind die Liénard-Wiechert- Potentiale, die mit dem Elektronen-Impuls minimal gekoppelt werden.

Wir betrachen die Projektile als Punktladungen, die auf klassischen geraden Bahnen laufen ('Straight-Line-Approximation' in der 'Semiklassischen Näherung').

Frühere Arbeiten zeigen [Pfe99], dass für nicht sehr große Geschwindigkeiten ($\gamma \leq 3$) der Potential-Term den dominanten Beitrag liefert. Alle andere Terme sind eine oder mehrere Größenordnungen kleiner und damit vernachlässigbar. Dies gilt sogar für sehr hochgeladene U^{92+}-Projektile in diesem Energiebereich.

Das Liénard-Wiechert-Potential hat eine Winkelabhängigkeit. Deswegen müssen die zugehörigen Matrixelemente dreifach integriert werden.

Die Abhängigkeit von der magnetischen Quantenzahl spaltet die L=1-Zustände in drei und die L=2-Zustände in fünf Kanäle auf.

Aus der oben beschriebenen Basis haben wir die wichtigsten Zustände ausgewählt; sie liefern 277 Kanäle.

Die Wechselwirkungsmatrixelemente sind nur numerisch berechenbar. Die Rechnung muss für jeden Stoßparameter und für jeden Zeitpunkt ausgeführt werden. In unserem Fall bedeutet dies mehrere zehntausend numerische Integrale. Die gesamte Berechnung kann durch Ausnutzung von Symmetrien beschleunigt werden. Die Matrixelemente haben drei verschiedene Symmetrien: Zeitumkehr-Symmetrie, Azimutal-Symmetrie und Symmetrie bezüglich der magnetischen Quantenzahlen. Zusätzliche Zeit kann man durch die Beobachtung einsparen, dass die Winkelintegrale für alle Einteilchen-Wellenfunktionen identisch sind mit $l = 0, 1, 2$. Daher genügt es, die Integrale nur einmal auszurechnen. Diese Idee zahlt sich besonders bei größeren Basen aus.

Nach der Berechnung der Wechselwirkungs-Matrixelemente muss die Kopplungs-Matrix aufgebaut und die Gekoppelten-Kanäle-Gleichungen gelöst werden. Die quadrierten Absolutwerte der Koeffizienten sind die Wahrscheinlichkeiten für die verschiedene Kanäle.

Multipliziert man die Wahrscheinlichkeiten mit dem Stoßparameter und integriert über diesen, so erhält man den totalen Wirkungsquerschnitt.

Wir haben für zwölf verschiedene Stoßysteme, für die Messdaten verfügbar sind, Rechungen durchgeführt.

Neben dem Verfahren der gekoppelte-Kanäle haben wir zum Vergleich außerdem die erste Ordnung der Born'schen Störungstheorie benutzt. Unsere Ergebnisse sind auf den Seiten 77-88 tabelliert. Die Resulate aus den Gekoppelten-Kanäle-Rechnungen stimmen mit den experimentellen Werten gut überein. Die Born'sche Rechnungen liefern hingegen für große Werte von Z_{Proj}/v_{Proj} zu hohe Querschnitte.

Chapter 8

Appendix

To get the cross-sections, various numerical steps are needed. In the next we summarise the codes which were needed for the computation. Major parts of the codes were developed personally. The usage of external codes will be mentioned.

- **Packet.for**
  Calculates and tabulates the Coulomb wave packets with different energy, packet size, and effective charge. A library routine is used for the complex gamma function. Different formulas are used for the Coulomb wave function. The packet integration is done with the Romberg algorithm. The code was partially developed by Prof. Grün.

- **Diag.for**
  Solves the diagonalisation problem, with the help of a International Mathematical & Statistical Library (IMSL) Routine. The results are the eigenvalues and the eigenvectors. The code was developed here. For the Clebsch-Gordon coefficients we used a ready Routine from R. Shyam.

- **Channel.for**
  Calculates the time-dependent matrix elements and builds up the coupling matrix, different projectile-electron operators can be used: complete coupled channel, only potential term, with-or without retardation. The above mentioned Clebsch-Gordon algorithm is also used here. From [Pre86] we used routines for the spline integration, and routines for calculate integration points and weights for different Gauss integrations. A further SLATEC Common Mathematical Library routine is applied to calculate singular integrations.

- **Diffsolv.for**
  Solves the coupled-channel equations with a five-point Runge-Kutta algorithm.

The code has a modified version for the perturbation calculation. This code was partially developed by Christian Pfeiffer.

- **Sigma.for**
  Integrates the probabilities over the impact parameter to get the total cross section. For better accuracy a spline interpolation is used. This was partially written by C. Pfeiffer.

- **Kalss.for**
  A small program which projects the helium wave function onto another helium wave function built up from orthogonalised single particle wave functions to get the bound and single and double ionisation probabilities of a given state.

Bibliography

[Ada66] B. Adamczyk, A. J. H. Boerboom, B. L. Schram, J. Kistemaker: J. Chem. Phys. **44**, 4640, (1966)

[Abr70] M. Abramowitz and A. Stegun: Handbook of Mathematical Functions, Dover Publications Inc., New York 1972

[Ack95] J. Ackermann: Phys. Rev. A **52** 1968-1975 (1995)

[And86] L. H. Andersen, P. Hvelplund, H. Knudsen, S. P. Møller, A. H. Sorensen, K. Elsner, K. G. Rensfelt, E. Uggerhøj: Phys. Rev. Lett. **57**, 2147-2150, (1986)

[And87] L. H. Andersen, P. Hvelplund, H. Knudsen, S. P. Møller, A. H. Sorensen, K. Elsner, K. G. Rensfelt, E. Uggerhøj: Phys. Rev. A **40**, 7366, (1987)

[And90] L. H. Andersen, P. H. Hvelplund, H. Knudsen, S. P. Møller, J. O. P. Petersen, S. Tang-Petersen, E. Uggerhøj, K. Elsener, E. Morenzoni: Phys. Rev. A **41**, 6536, (1990)

[Bac91] H. Bachau, F. Martin, A. Riera, M. Yánez: Atomic Data and Nuclear Data Tables **48**, 167-212, (1991)

[Bal91] A. J. Baltz: Phys. Rev. A **44**, 5569-5585, (1991)

[Bap98] B. Bapat, R. Moshammer, S. Keller, W. Schmitt, A. Cassimi, L. Adoui, H. Kollmus, R. Dörner, Th. Weber, K. Khayyat, R. Mann, J. P. Grandin, J. Ullrich: J. Phys. B **32**, 1859-1872, (1998)

[Ber92a] H. E. Berg, J. Ullrich, E. Bernstein, M. Unverzagt, L. Spielberg, J. Euler, D. Schardt, O. Jagutzki, H. Schmidt-Böcking, R. Mann, P. H. Mokler, S. Hagmann, P. D. Fainstein: J. Phys. B. At. and Mol. Phys. **25**, 3655-3670, (1992)

[Ber92b] H. E. Berg, O. Jagutzki, R. Dörner, R. D. Dubois, C. Kelbach, H. Schmidt-Böcking, J. Ullrich, J. A. Tanis, A. S. Schlachter, L. Blumenfeld, B. d'Etat, S. Hagmann, A. Gonzales, T. Quinteros: Phys. Rev. A **46**, 5539-5544, (1992)

[Ber99] G. Bernardi: J. Phys. B**32**, L451, (1999)

[Bet57] H. A. Bethe and E. E. Salpeter: Quantum Mechanics of One- and Two-Electron Atoms, Springer Verlag 1957

[Bra83] B. H. Brandsen: Atomic Collision Theory, The Benjamin/Cummings Publishing Company INC. 1983

[Bra92] B. H. Brandsen and M. R. C. McDowell: Charge Exchange and the Thery of Ion-Atom Collisions Clarendon Press Oxford 1992

[Bus96] O. Busic: Diplomarbeit Universität, Gießen (1996)

[Byr66] F. W. Byron and C. J. Joachain: Phys. Rev. Lett. **16**, 1139, (1966)

[Che94] K. T. Cheng, M. H. Chen, W. R. Johnson, J. Sapirstein: Phys. Rev. A **50**, 247, (1994)

[Col98] F. D. Colavecchia, G. Gasaneo, C. R. Garibotti: Phys. Rev. A **58**, 2926, (1998)

[Cov81] Robert D. Cowan: The Theory of Atomic Structure and Spectra, University of California Press 1981

[Das97] T. Das and F. B. Malik: J. Phys. B. At. and Mol. Phys. **30**, 1223, (1997)

[Dor99] A. Dorn, R. Moshammer, C. D. Schröter, T. J. M. Zouros, W. Schmitt, H. Kollmus, R. Mann, J. Ullrich: Phys. Rev. Lett. **82**, 2496, (1999)

[Dra88] G. W. F. Drake: Can. J. Phys. **66**, 586, (1988)

[Edm63] A. R. Edmonds: Angular Momentum in Quantum Mechanics, Princeton, 1963

[Eic77] J. Eichler: Phys. Rev. A **15**, 1856, (1977)

[Eich90] J. Eichler and W. E. Meyerhof: Relativistic Atomic Collisions, Academic Press 1995

[Eic90] J. Eichler: Phys. Reports **193**, 165-277, (1990)

[For94] A. L. Ford, J. F. Reading: J. Phys. B **27**, 4215, (1994)

[For97] A. L. Ford, L. A. Wehrman, K. A. Hall and J. F. Reading: J. Phys. B **30**, 2889-2897, (1997)

[Fri89] W. Fritsch, C. D. Lin: Phys. Rev. A **41**, 4776, (1989)

[Gai01] Matthias Gail: Dissertation, Universität Gießen (2001)

[Gra81] I. S. Gradstein, I. M. Ryshik: Tables of series products, and integrals, Verlag Harri Deutsch 1981

[Gra89] K. Gramlich: Dissertation, Universität Gießen (1989)
K. Gramlich, N. Grün, W. Scheid: J. Phys. B. At. Mol. Phys. **22**, 2567-2579, (1989)

[Hau81] H. K. Haugen, L. H. Andersen, P. Hvelplund, H. Knudsen: Phys. Rev. A **26**, 1962, (1981)

[Haug82] H. K. Haugen, L. H. Andersen, P. Hvelplund and H. Knudsen: Phys. Rev. A **26**, 1950, (1982)

[Heb90] O. Heber, B. B. Bandong, G. Sampoll, R. L. Watson: Phys. Rev. Lett. **64**, 851, (1990)

[Hil90] R. Hildebrand: Diplomarbeit, Universität Gießen

[Hil94] R. Hildebrand: Dissertation, Universität Gießen

[Hil95] R. Hildebrand, N. Grün, W. Scheid: J. Phys. B: At. Mol. Phys. **28**, 4781-4798, (1995)

[Hip74] R. Hippler and K-H. Schartner J. Phys. B **7**, 618, (1974)

[Ho79] Y. K. Ho: J. Phys. B **12**, 387, (1979)

[Ho87] Y. K. Ho: Phys. Rev. A. **35**, 2035, (1987)

[Hof93] S. Hofstetter: Diplomarbeit, Universität Gießen (1994)

[Hof93] S. Hofstetter, N. Grün, W. Scheid: Z. Physik D **37**, 1-7, (1996)

[Hve94] P. Hvelplund, H. Knudsen, U. Mikkelsen, E. Morenzoni, S. P. Møller, T. Worm, E. Uggerhøj: J. Phys. B**27**, 925, (1994)

[Inok71] M. Inokuti: Rev. Mod. Phys. **42**, 297, (1971)

[Inok78] M. Inokuti: Rev. Mod. Phys. **50**, 23, (1971)

[Jac81] J. D. Jackson: Classical Electrodynamics, John Wiley & Sons (1975)

[Jan84] R. K. Janev, L. P. Presnyakov, V. P. Shevelko: Physics of Highly Charged Ions, Springer-Verlag 1984

[Lan68] L. D. Landau: Quantum Mechanics II 1968

[Lin93] C. D. Lin: Review of Fundamental Processes and Applications of Atoms and Ions, World Scientific (1993)

[Lip77]] L. Lipsky, A. Russell, M. J. Conneely: Atomic Data and Nuclear Data Tables **20**, 127-141, (1977)

[Khe99] A. Kheifets, I. Bray, A. Lahmam-Bennani, A. Duguet, I. Taouil: J. Phys. B **32**, 5047, (1999)

[Knu84] H. Knudsen, L. A. Andersen, P. Hvelplund, C. Astner, H. Cederquist, H. Danared, L. Liljeby, K-G Renfelt: J. Phys. B. At. Mol. Opt. Phys. **17**, 3545-3564, (1984)

[Knu92] H. Knudsen and J. F. Reading: Phys. Rep. 212(3&4), 107-222, (1992)

[McG82] J. H. McGuire: Phys. Rev. Lett. **49**, 1153-1157, (1982)

[McG84] J. H. McGuire, A. Müller, B. Schuch, W. Groth, E. Salzborn: Phys. Rev. A **35**, 2479, (1987)

[McG87] J. H. McGuire, A. Müller, B. Schuch, W. Groh, E. Salzborn: Phys. Rev. A **35**, 2479, (1987)

[McG97] J. H. McGuire: Electron Correlation Dynamics in Atomic Collisions, Cambridge University Press 1997

[McG00] C. Mc Grath, D. M. McSherry, M. B. Shah, S. F. C. O'Rourke, D. S. F. Crothers, G. Montgomery, H. B. Gilbody, C. Illescas, A. Riera: J. Phys. B **33**, 3693, (2000)

[Meh89] G. Mehler, G. Soff, K. Rumrich, W. Greiner: Zeitschrift für Phys. D **13**, 193-202, (1989)

[Mer97] V. Mergel Phys. Rev. Lett. **79**, 387, (1997)

[Moo71] C. E. Moore: Atomic Energy Levels 1971

[Mor91] K. Moribayashi, K. Hino, M. Matsuzawa, M. Kimura: Phys. Rev. A, **44**, 7234

[Mos94] R. Moshammer, J. Ullrich, M. Unverzagt, W. Schmidt, P. Jardin, R. E. Olson, R. Mann, R. Dörner, V. Mergel, U. Buck, H. Schmidt-Böcking: Phys. Rev. Lett. **73**, 3371-3374, (1994)

[Mos97] R. Moshammer: Phys. Rev. Letters **79**, 3621-3624, (1997)

[Nag80] P. Nagy, A. Skutlarz, V. Schmidt: J. Phys. B **13**, 1249, (1980)

[Ols77] R. E. Olson, A. Salop: Phys. Rev.A **16** , 531, (1977)

[Ols78] R. E. Olson, K. H. Berkner, W. G. Graham, R. V. Pyle, A. S. Schlachter, J. W. Stearns: Phys. Rev. Lett. **41**, 163, (1978)

[McK87] M. L. McKenzie, R. E. Olson: Phys. Rev A **35**, 2863, (1987)

[Pfe96] C. Pfeiffer: Diplomarbeit, Universität Gießen 1996

[Pfe99] C. Pfeiffer, N. Grün, W. Scheid: J. Phys. B. At. Mol. Opt. Phys. **32**, 53-64, (1999)

[Pre86] W. H. Press, B. P. Flannery, S. A. Teukolsky, W. T. Vetterling: Numerical Recipes-The Art of Scientific Computing, Cambridge University Press 1986

[Rea87] J. F. Reading, A. L. Ford J. Phys. B **20**, 3747-3769, (1987)

[Roes91] T. Rösel, C. Dupré, J. Röder, A. Duguet, K. Jung, A. Lahman-Bennani, H. Ehrhardt: J. Phys.B **24**, 3059, (1991)

[She77]] W. Shearer-Izumi: Atomic Data and Nuclear Data Tables **20**, 532, (1977)

[Sch66] B. L. Schram, A. J. H. Borboom, J. Kistenmaker: Physica **32**, 185-196, (1966)

[Sch86] H. R. Schwarz: Numerische Mathematik, B. G. Teubner Stuttgart (1993)

[Sch90] G. Schiwietz: Phys. Rev A **42**, 296,(1990)

[Sha85] M. B. Shah, H. B. Gilbody: J. Phys. B **18**, 899-913, (1985)

[Spi99] L. Spielberg, H. Bräuning, A. Muthig, J. Z. Tang, J. Wang, Y. Qiu, R. Dörner, O. Jagutzki, Th. Tschentscher, V. Honkimäki, V. Mergel, M. Achler, Th. Weber, Kh. Khayyat, J. Burgdörfer, J. McGuire, H. Schmidt-Böcking: Phys. Rev. A. **59**, 371, (1999)

[Ste80] K. Stephan, H. Helm, T. D. Märk: J. Chem. Phys. **73**, 3763-3778, (1980)

[Stol97] N. Stolterfoht, R. D. DuBois, R. D. Rivarola: Electron Emission in Heavy Ion Atom Collision, Berlin Springer Verlag (1997)

[Tir97] T. Das, F. B. Malik: J. Phys. B **30**, 1223,(1997)

[Tos94] N. Toshima: Phys. Rev. A **50**, 3940, (1994)

[Ull94a] J. Ullrich: Habilitationsschrift, Universität Frankfurt, GSI-Report 94-08

[Ull97] J. Ullrich, R. Moshammer, R. Dörner, O. Jagutzki, V. Mergel, H. Schmidt-Böcking, L. Spielberg: J. Phys. B **30**, 2917, (1997)

[Wil65] J. H. Wilkinson: The Algebraic Eigenvalue Problem, Claredon Press Oxford 1965

Acknowledgement

At first I thank Prof. Dr. W. Scheid for the chance to prepare my Phd. thesis at the Justus-Liebig Universität Gießen in his department and for the interesting research topic he assigned to me. In the second place thank to Prof. Dr. N. Grün for many numerical routines, the critical remarks and the support which helped me to reach my aim.

Further acknowledgements for all the colleagues in our Institute for the fruitful discussions, stimulating working climate and the valuable comments. I note M. Hölß for the smart local computer system and for all the technical helps he gave me. I also note C. Pfeiffer for further computer codes. I thank C. Müller and S. Zakowicz for the help they gave me correcting my Phd thesis. I thank Z. Harman for his general help in the last two years.

I am thankful to Dr. A. Voitkiv for his explanations to understand different problems.

At last but not least thank to my parents and my girlfriend for the continuous reassure in blind-alley situations.

Curriculum Vitae

Imre F. Barna
MSc. in Physics

Personal:

Born:	Nov. 13. 1972 Budapest
Nationality:	Hungarian
Foreign Languages:	English, German
Marital Status:	single

Studies:

Physics Student	1991-1997	Technical University of Budapest
Exchange Student:	1996	Justus-Liebig Universität Gießen, Tempus Grant
MSc. Exam:	1997	Technical University of Budapest
Research Assistant:	1998	Central Chemical research Institut in Budapest
PhD Student:	1998-2002	Justus-Liebig-Universtität Gießen

Research Activities: (past and *present*)

Nuclear Physics:
Localisation of nonlocal potentials
Atomic Physics:
Ionisation of helium in heavy-ion collisions

Scientific Publication:

I. F. Barna, B. Apagyi, W. Scheid
Localisation of nonlocal potentials by a Taylor expansion method
J. Phys. G. 26. (2000) 323-331